Chapter 15B. Analysis of Imaging Spectrometer Data for the Zarkashan Area of Interest

Contribution by Trude V.V. King and Michaela Johnson

Abstract

Computer analysis of the HyMap spectroscopic data of the Zarkashan area of interest (AOI) in the southeastern part of Afghanistan used spectrum matching techniques to identify the occurrence of selected materials at the surface based on characteristic absorption features (absorption bands) in the HyMap data compared with a library of spectral standards. The HyMap data have been used to better define the magnitude and extent of previously known mineral occurrences and identify potential areas of mineralization. HyMap data demonstrated the utility to serve as a highly effective tool, especially in the Zarkashan mine subarea, for detecting and mapping potential regions of mineralization in contact zones on the edges of intrusive bodies. In the Zarkashan mine subarea, well-defined contiguous areas of $Fe^{2+}Fe^{3+}$ Type 2 and epidote minerals delineate the boundary of the Zarkashan intrusion and are coincident with anomalous areas of reported high gold-concentration. The size and extent of the alteration shown in the HyMap data suggest that the distribution of copper and gold may be extensive. In the Bolo subarea, a linear trend of spectrally distinct pixels, primarily goethite and $Fe^{2+}Fe^{3+}$ Type 2, extends for 9 kilometers along the contact zone between Late Permian-age stratified rocks and the Late Cretaceous-Paleocene intrusion, which has been identified to be a potential region of deep gold-placer deposits.

15B.1 Introduction

Past studies of geologic data of Afghanistan revealed numerous areas with indications of potential mineral resources of various types (Peters and others, 2007; Abdullah and others, 1977). Several of these areas were selected for follow-up studies using hyperspectral (imaging spectroscopy) data to characterize surface materials. This report contains the results of the spectroscopic data analyses and identifies sites within the Zarkashan area of interest (AOI) that deserve further investigation, especially detailed geologic, geophysical, and geochemical investigations.

The Zarkashan AOI is approximately 240 kilometers (km) west and south of Kabul (fig. 15B–1) and is believed to host porphyry copper-gold, copper-gold skarn, polymetallic vein, tin-tungsten skarn, iron skarn, and lead-zinc skarn mineral deposits. In addition, placer gold and some tin and tungsten skarn occurrences are known to be present in the area (Peters and others, 2007; Abdullah and others, 1977).

15B.1.1 Hyperspectral Data Collection and Processing

In 2007, imaging spectrometer data were acquired over most of Afghanistan as part of the U.S. Geological Survey "Oil and Gas Resources Assessment of the Katawaz and Helmand Basins" project. The spectrometer data were collected to characterize surface materials in support of assessments of resources (coal, water, minerals, oil, and gas) and earthquake hazards in the country (King and others, 2010). Imaging spectrometers measure the reflectance of visible and near-infrared light from the Earth's surface in many narrow channels, producing a reflectance spectrum for each image pixel. These reflectance spectra can be interpreted to identify absorption features that result from specific chemical transitions and molecular bonds that provide compositional information about surface materials. Imaging spectrometer data can only be used to characterize the upper surface materials, and not

subsurface composition or structure. The results of subsurface processes, however, can be indicated by the distribution of surface materials that can be detected using hyperspectral (imaging spectroscopy) data.

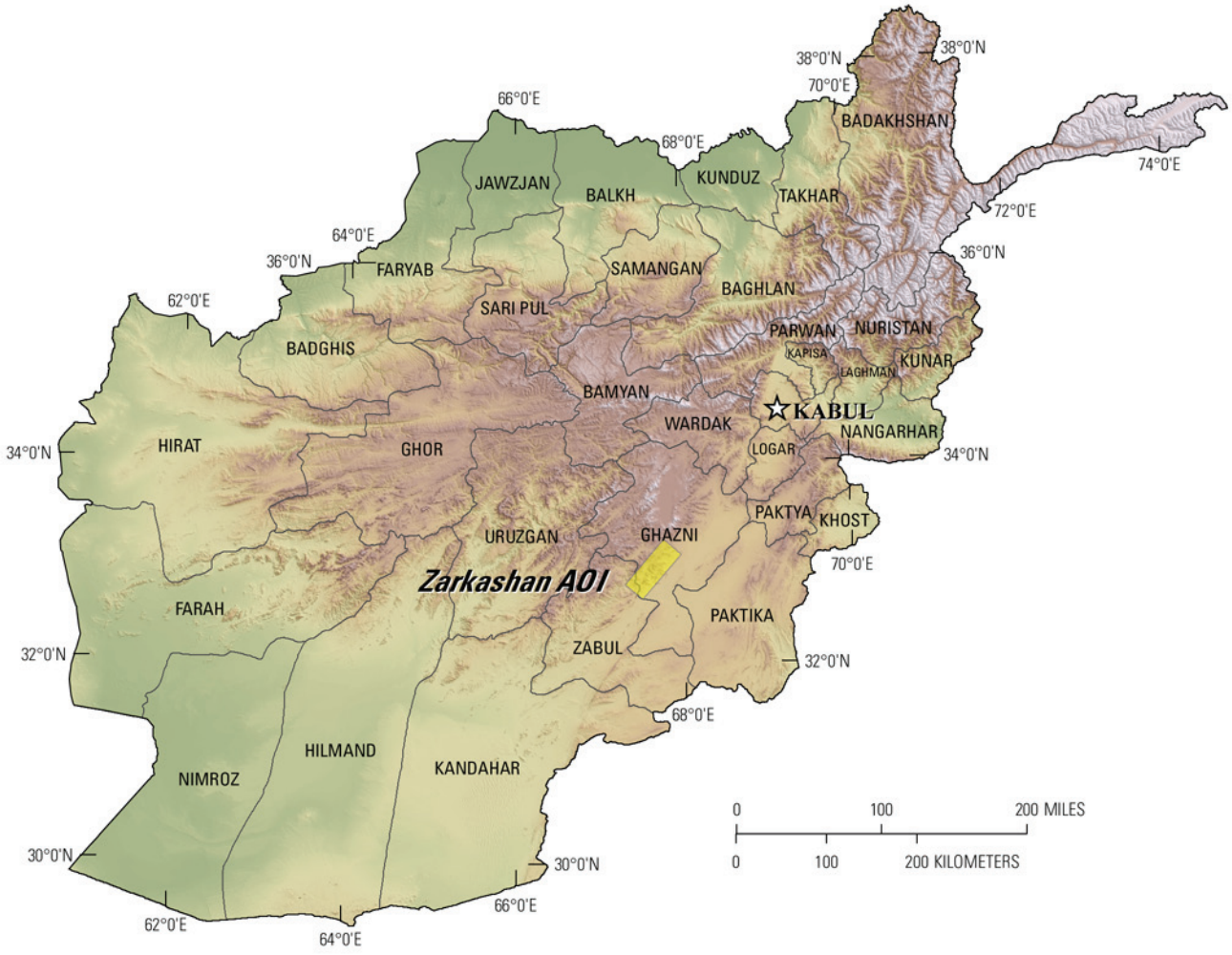

Figure 15B–1. The Zarkashan area of interest southwest of Kabul in the Ghazni and Zabul Provinces of Afghanistan.

15B.1.2 Collection of Imaging Spectrometer Data

The HyMap imaging spectrometer (Cocks and others, 1998) was flown over Afghanistan from August 22 to October 2, 2007 (Kokaly and others, 2008). HyMap has 512 cross-track pixels and covers the wavelength range from 0.43 to 2.48 microns in 128 channels. The imaging spectrometer was flown on a WB-57 high-altitude aircraft at 50,000 feet. There were 207 standard data flight lines and 11 cross-cutting calibration lines collected over the country of Afghanistan for a total of 218 flight lines, covering a surface area of 438,012 square kilometers (km^2) (Kokaly and others, 2008). Data were received in scaled-radiance format (calibrated to National Institute of Standards and Technology reference materials). Before processing, four channels that had low signal-to-noise ratios and (or) were in wavelength regions overlapped by adjacent detectors were removed from the image cubes. Each flight line was georeferenced to Landsat Thematic Mapper (TM) base imagery in Universal Transverse Mercator (UTM) projection (Davis, 2007).

15B.1.3 Calibration

To ensure the utility of the hyperspectral dataset, a rigorous calibration process to remove atmospheric absorptions and residual instrument artifacts was applied. Before the calibration process started, each flight line was georeferenced to Landsat base imagery in UTM projection (Davis, 2007). Because of the extreme topographic relief and restricted access to ground calibration sites, modifications to the traditional USGS calibration procedures were required to calibrate the 2007 Afghanistan HyMap dataset (Hoefen and others, 2010). Radiance data were converted to apparent surface reflectance using the radiative transfer correction program Atmospheric CORrection Now (ACORN; ImSpec LLC, Palmdale, Calif). The ACORN program was run multiple times for each flight line, using average elevations in 100 meter (m) increments, covering the range of minimum to maximum elevation within the flight line. A single atmospherically corrected dataset was assembled from the ACORN results in 100-m increments by determining the elevation of each pixel and selecting the atmospherically corrected pixel from the 100-m increment closest to the elevation of the pixel. The atmospherically corrected dataset was further empirically adjusted using ground-based reflectance measurements from the Kandahar Air Field, Bagram Air Base, and Mazar-e-Sharif Airport, as well as soil samples from two fallow fields. To improve the data quality, new calibration techniques were developed to address atmospheric differences within a flight line.

To refine data quality of ground-calibrated reflectance, a multiplier correction, computed by cross-calibrating north-south flight lines with a flight line that passed over a ground calibration site, was applied. For each north-south flight line, the pixels in overlapping regions of north-south and cross-cutting calibration lines, subject to slope, vegetation cover, and other restrictions, were used to develop these cross-calibration correction factors (Hoefen and others, 2010). The cross-calibration multiplier corrected any residual atmospheric contamination in the hyperspectral data that was not present in the spectra of the ground calibration site.

15B.1.4 Materials Maps and Presentation

HyMap reflectance data were processed using Material Identification and Characterization Algorithm (MICA), a module of the USGS Processing Routines in IDL for Spectroscopic Measurements (PRISM) software (Kokaly, 2011). The MICA module compared the reflectance spectrum of each pixel of HyMap data against entries in a spectral reference library of minerals, vegetation, water, and other materials. The library included 97 reference spectra of well-characterized mineral and material standards. The resulting maps of material distribution, resampled to a 23 × 23-square-meter (m^2) pixel grid, were used to prepare maps of mineral, vegetation, and other material occurrences.

HyMap data were analyzed twice. The MICA module was first run using the set of minerals with absorption features in the visible and near-infrared wavelength region, producing the 1-micrometer (μm) map of iron-bearing minerals and other materials (King, Kokaly, and others, 2011). MICA was run again using the minerals with absorption features in the shortwave infrared region, producing the 2-μm map of carbonates, phyllosilicates, sulfates, altered minerals, and other materials (Kokaly and others, 2011). For clarity of presentation, some individual classes in these two maps were bundled by combining selected specific mineral types (for example kaolinites, montmorillonites, and hematites) to reduce the number of mineral classes. In addition, iron-bearing minerals with different mineral compositions but similar spectral features are difficult to classify as specific mineral species. Thus, generic spectral classes, including several minerals with similar absorption features, such as Fe^{3+} Type 1 and Fe^{3+} Type 2, are depicted on the map. The carbonates, phyllosilicates, sulfates, and altered minerals map has 32 classes. Minerals with slightly different mineral compositions but similar spectral features are less easy to distinguish; therefore, some identified classes consist of several minerals with similar spectra, such as the "Chlorite or Epidote" class. When comparisons with reference spectra produced no viable match, a designation of "not classified" was assigned to a pixel.

Although the occurrence of certain minerals (pyrophyllite, buddingtonite, dickite, jarosite) may suggest that mineralization processes may have once operated in the area, many of the minerals that

were identified are also common rock-forming minerals. Consequently, knowledge about the distribution patterns of the identified minerals is essential to understanding the causes of mapped mineral occurrences and evaluating the possible potential for related mineral deposits.

15B.1.5 Data Limitations

Geographic registration between various data sets is not always possible because of differences in collection methods and resolution. The geographic accuracy and quality of each data set are limited by the original source. Significant efforts were made to ensure the geographic accuracy of the HyMap data (Kokaly and others, 2008; Hoefen and others, 2010). However, exact registration between previously published known mineral occurrences, fault traces, geologic units, and structural boundaries in comparison to the HyMap data, may not be ideal. To resolve additional details, the digital versions of these maps can be viewed at a higher spatial resolution than is possible for a single page printed map.

15B.2 Geologic Setting of the Zarkashan Area

The main Zarkashan AOI is located in the Ghazni and Zabul Provinces of Afghanistan (fig. 15B–1). The AOI covers approximately 1,692 km^2, and for the purposes of this investigation, includes three subareas, Bolo, Luman Tamaki, and Zarkashan mine, that are approximately 313 km^2, 356 km^2, and 214 km^2, respectively (fig. 15B–2). The elevation in the Zarkashan AOI ranges from 1,877 to 3,416 m (fig. 15B–2). The highest terrain occurs along the northwestern half and in the central portion of the AOI. Numerous faults and fractures of various orientations are present in the area (fig. 15B–3). A major tectonic feature separates the two high-terrain regions in the western part of the AOI. Landsat TM data are useful for understanding the general characteristics and distribution of surficial material, including rocks and soil, unconsolidated sediments, vegetation, and hydrologic features. The TM data for the area indicate that the rocks range in color from very light gray, to shades of green, red, and reddish-brown (fig. 15B–3).

Late Proterozoic metamorphic rocks, Lower Paleozoic rocks (limestone, dolomite and shale), and Carboniferous to Early Permian rocks (sandstone, siltstone, shale, and mafic volcanic rocks) occur in the AOI. These rocks are intruded by Oligocene-age rocks along the northwestern boundary of the AOI, and by Late Cretaceous-Paleocene age intrusive rock in the east-central region (fig. 15B–4). Intrusive rocks of Late Cretaceous to Paleocene age are present in the Bolo and Zarkashan mine subareas.

15B.2.1 Known Mineralization

Figure 15B–5 shows the locations of 40 areas where reconnaissance field geology and the geologic literature have identified probable mineralization. The locations of the mineral resources are also shown on the topical maps later in this report for the main Zarkashan AOI and three subareas (Bolo, Luman Tamaki, and Zarkashan mine) to illustrate how these mineralized prospects are reflected in the HyMap data. Mineralization within the AOI includes the following: (1) porphyry copper-gold; (2) copper-(gold) skarn; (3) polymetallic vein, (4) tin-tungsten skarn, (5) and lead-zinc skarn. In addition, placer gold occurrences are known to be present. Mineral prospects that occur in the Zarkashan AOI and are not included in one of the subareas include the Kharnay (skarn W), Tanghi (karst-type bauxite), Khinjak (unclassified), and an unnamed vein-W prospect. The known mineralization for the three subareas (Bolo, Luman Tamaki, and Zarkashan mine) are discussed next. The mineralogical characteristics for prospects in the AOI are summarized in table 15B–1.

15B.2.1.1 Bolo Subarea

The Bolo subarea was delineated to include a number of gold-rich occurrences adjacent to the eastern contact of a Cretaceous granite pluton. This tract contains the Bolo and Utkul gold occurrences and the Alaghzar, Belaw, and Anghuri copper prospects. According to Abdullah and others, 1977, the Bolo subarea contains Permian to Triassic-age calcareous rocks overlain by Cretaceous limestone and

sandstone, all of which are intruded by Late Cretaceous to Paleocene stocks and plutons. The Bolo gold prospect consists of mineralization in upper Permian-age rocks (Abdullah and others, 1977).

The Belaw copper-skarn occurrence (lat 32°57'50"N., long 67°33'20"E.) is confined to the contact zone between Late Cretaceous-Paleocene and Upper Permian age rocks. The Alaghzar copper occurrence is in Upper Permian and Devonian age rocks that have been intruded by rocks of Late Cretaceous-Paleocene age (Abdullah and others, 1977). The Anghuri copper prospect is in a mineralized zone that occurs in contact between Upper Permian and Late Cretaceous-Paleocene rocks; the Utkul gold occurrence (lat 32°55'50"N., long 67°33'40"E.) is in Late Permian age rocks.

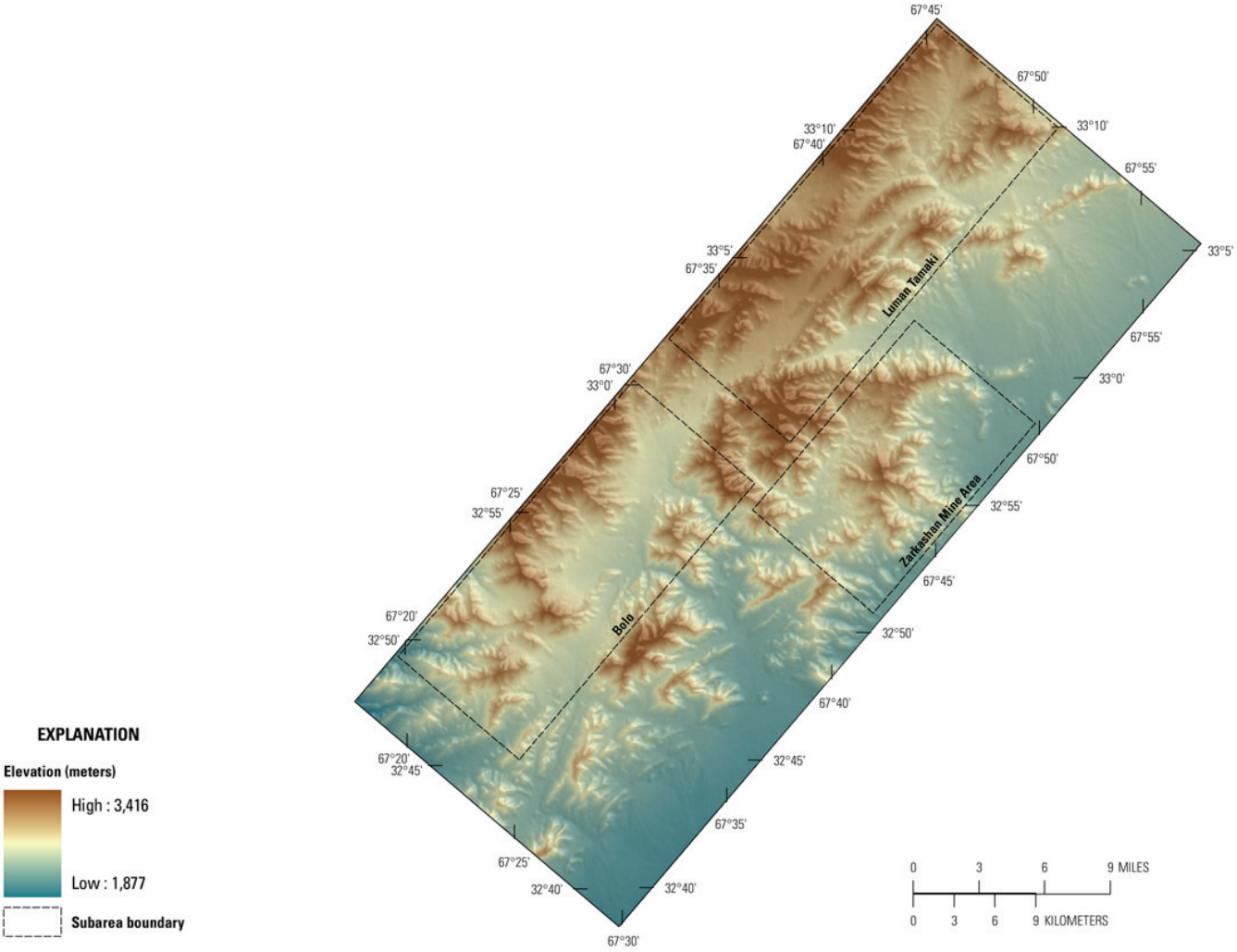

Figure 15B–2. Shaded relief map showing elevations of the Zarkashan area of interest, including the three subareas (Peters and others, 2007). Dark brown shading indicates higher elevations and blue shading indicates lower elevations.

15B.2.1.2 Luman Tamaki Subarea

The Luman Tamaki subarea occurs in a northeast-striking tectonic zone of Middle Paleozoic sedimentary rock encompassing gold, polymetallic vein, and copper skarn mineral occurrences (Peters and others, 2007). Previous remote sensing studies using Advanced Spaceborne Thermal Emission and Reflection Radiometer (ASTER) data identified zones of phyllic and argillic alteration (Mars and Rowan, 2007). According to Peters and others (this volume), the composition of the batholithic rocks is not highly favorable for mineralization, and the widespread exposure of mesozonal (?) batholithic rocks suggests that the area is relatively deeply eroded, and that much of the porphyry environment that may have once been present has been removed by erosion. Both the Tamaki and Luman are gold-rich

occurrences, and a number of unnamed precious base-metal vein and skarn prospects are also present within the subarea.

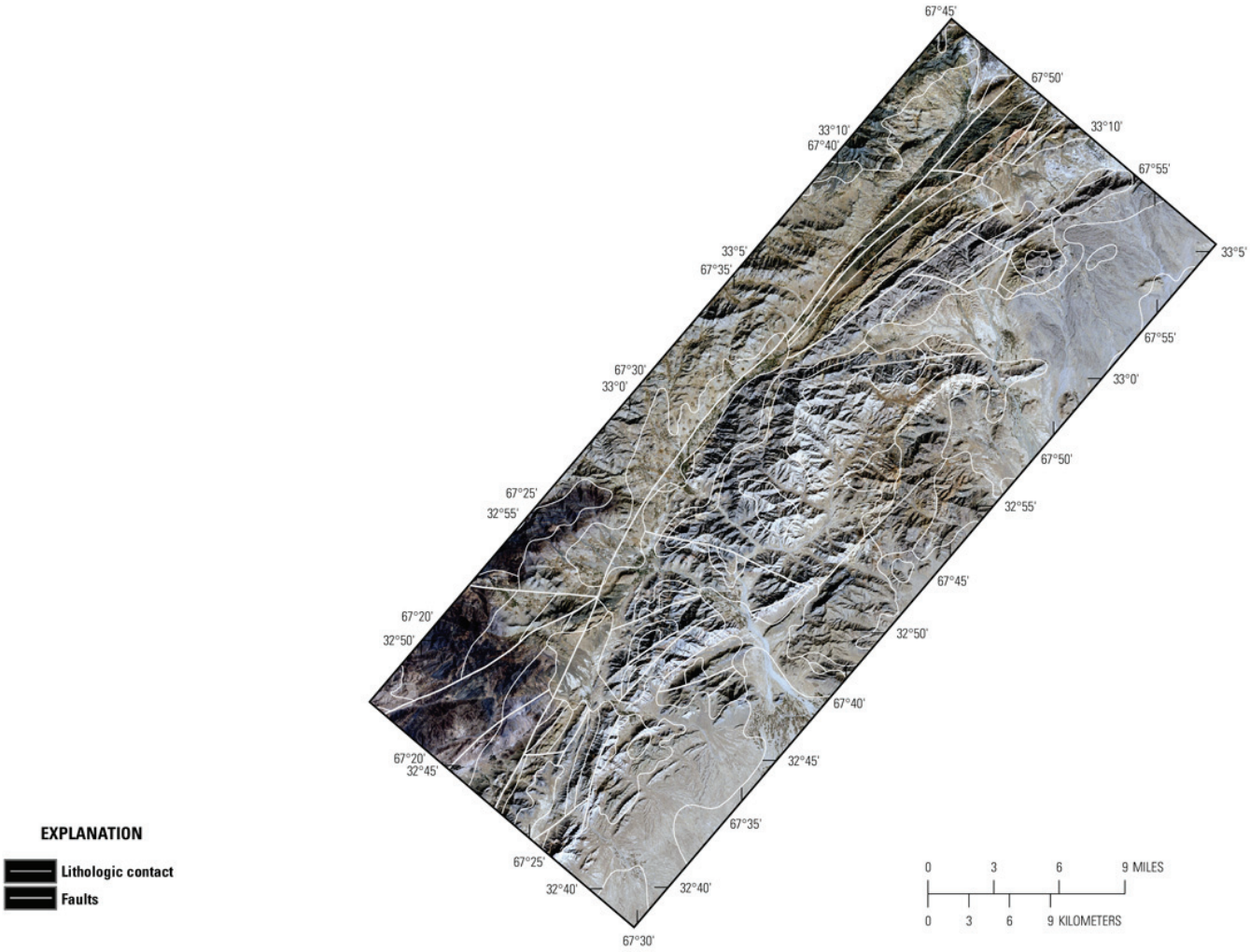

Figure 15B–3. Map showing faults and fractures within the Zarkashan area of interest (from Abdullah and Chmyriov, 1977, and Doebrich and others, 2006) superimposed on Landsat Enhanced Thematic Mapper data from Davis (2007).

15B.2.1.3 Zarkashan Mine Subarea

The Zarkashan copper-gold deposit as well as the Choh-i-Surkh, Dynamitic, and Sufi Kademi prospects contain gold and copper mineralization, within skarn and shattered zones altered by serpentinization, silicification and carbonatization (Peters and others, this volume).

The Choh-i-Surkh gold and copper prospect occurs in Middle Triassic age rocks and is characterized by the presence of hematite and limonite. The Dynamitic and Sufi Kademi gold and copper prospects lie in the northern part of the Zarkashan mine subarea. The Sufi Kademi occurrence is present along a bed of metasomatically altered conglomerate, largely composed of limestone pebbles, that occurs between Upper Jurassic-Lower Cretaceous age rocks (Peters and others, this volume). The Dynamitic prospect occurs in Middle Triassic age rocks along an easterly trending ridge north of the Zarkashan mines (Peters and others, this volume).

The Khinjaktu copper skarn prospect occurs on the southeastern side of the Zarkashan pluton along a north northwest-striking zone that penetrates the pluton from the south. The prospect contains gold mineralization in skarn at the contact between Upper Jurassic- Lower Cretaceous and Late Cretaceous-Paleocene age rocks (Peters and others, this volume). The Zardak gold prospect lies on the

southeastern side of the Zarkashan pluton in Upper Jurassic-Lower Cretaceous limestone, and the Gulyakhel gold prospect lies between Upper Jurassic to Lower Cretaceous and Late Cretaceous-Paleocene age rocks.

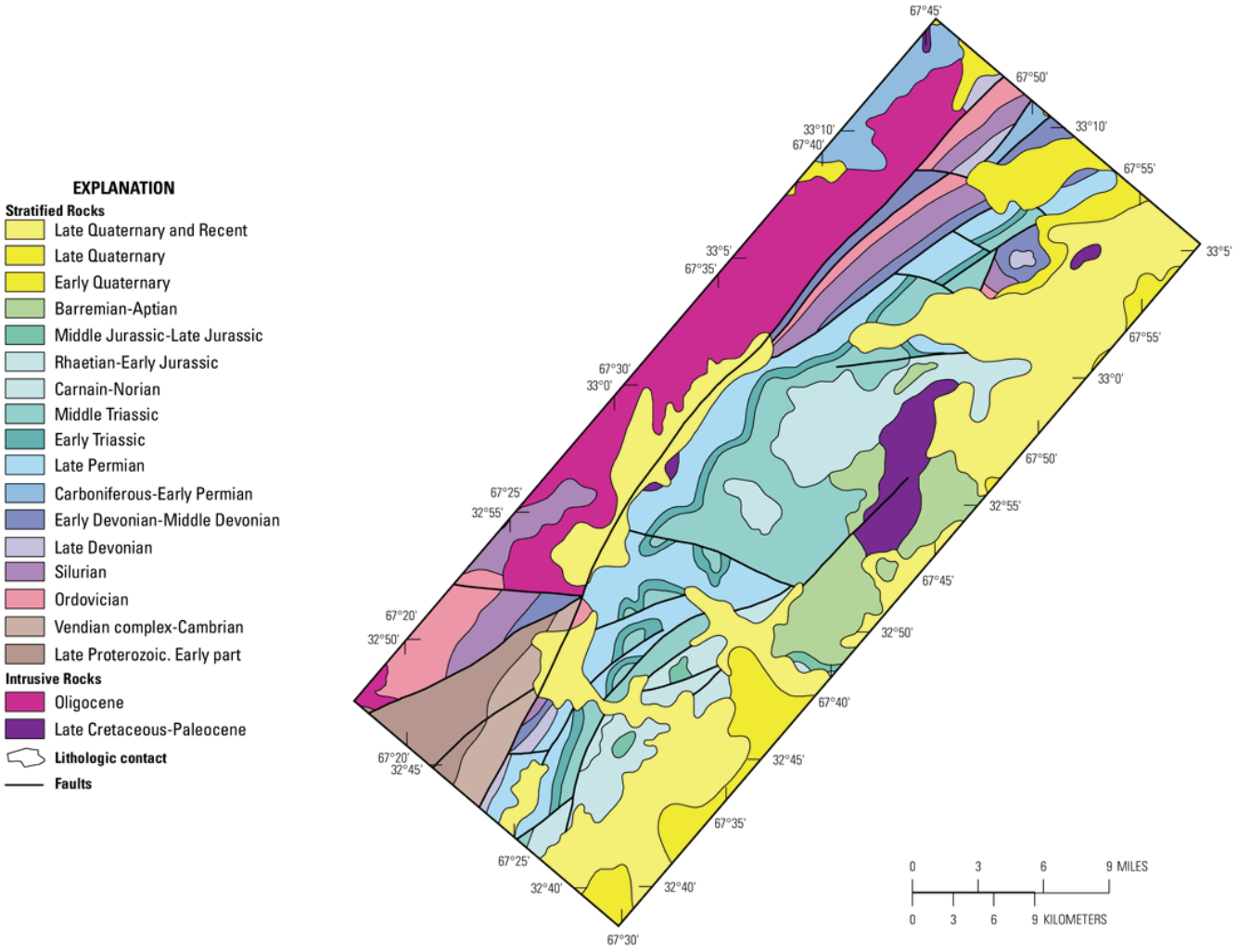

Figure 15B–4. Geologic map of the Zarkashan area of interest from the digital geologic map of Afghanistan (Abdullah and Chmyriov, 1977; Doebrich and others, 2006, Peters and others, 2007).

15B.3 Hyperspectral Mineral Maps of the Zarkashan Area of Interest

Computer analysis of the HyMap data of the Zarkashan AOI using spectral mapping techniques resulted in the identification of a variety of surficial minerals. These minerals have been identified on the presence and wavelength position of absorption features in the 0.45 to 2.48-µm wavelength region. Two general categories of minerals are recognized: (1) iron-bearing minerals that have characteristic spectral absorption features that occur at wavelengths near the 1-µm region, and (2) a wide variety of minerals, including carbonates, mica and clay minerals, and sulfates, that have diagnostic spectral absorptions near the 2-µm region. Although the occurrence of certain minerals may suggest mineralization processes may have operated in the area, many of the minerals identified and mapped are also common rock-forming minerals or minerals that can be derived from the weathering of a variety of rock types. Consequently, the distribution patterns of the identified minerals and the geologic context in which they occur are extremely important in understanding the causes of the mapped mineral occurrences, and in assessing the possible potential for related mineral deposits. A series of maps was produced for the entire Zarkashan AOI and the three subareas.

15B.3.1 Zarkashan Area

Figures 15B–6 and 15B–7 depict the distributions, respectively, of iron-bearing minerals (28 possible classes) and of carbonates, phyllosilicates, sulfates, altered minerals, and other materials (32 possible classes) for the entire Zarkashan AOI. The $Fe^{2+}Fe^{3+}$ Type 2 minerals dominate the map of iron-bearing minerals; the calcitic minerals and mineral groups are the most abundant mineral type in the carbonates, phyllosilicates, sulfates, altered minerals, and other materials map. Because of the large number of mineral classes represented and the subtleties of the distribution patterns in these image maps, it is instructive to display these results as a series of topical images, each depicting a group of minerals that are mineralogically related or commonly occur together in special geologic environments (figs. 15B–8-15B–13). Figure 15B–8 shows the distribution of carbonate minerals in the AOI, whereas figure 15B–9 shows where the clays and micas were mapped. The distribution of iron oxide and hydroxide minerals is shown in figure 15B–10. Secondary minerals are shown in figure 15B–11, and minerals commonly found in hydrothermally altered rocks are mapped in figure 15B–12.

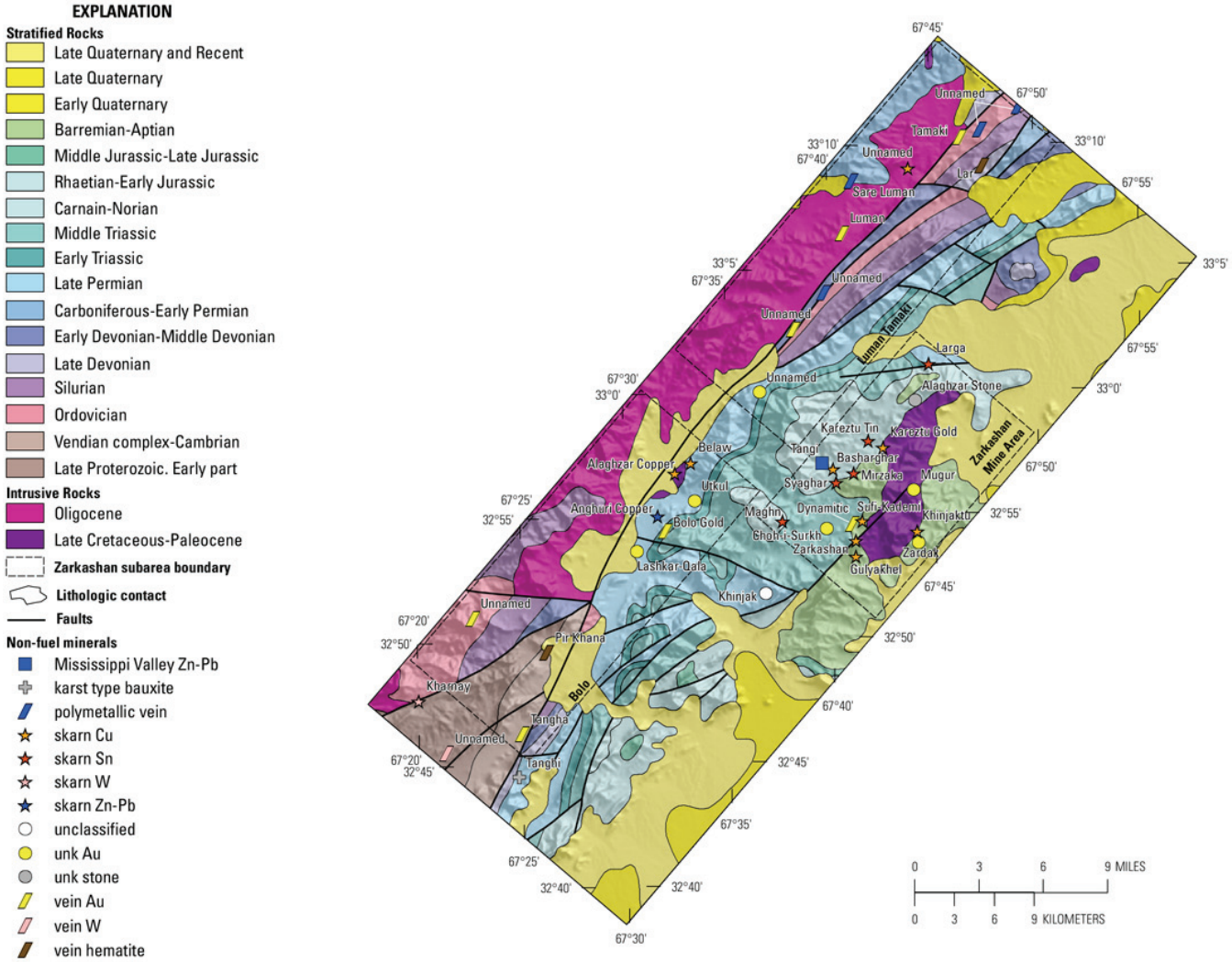

Figure 15B–5. Map showing the location of known mineral occurrences in the Zarkashan area of interest (AOI). The map consists of four data layers: a shaded relief base map; a transparency of the geologic map (from Abdullah and others, 1977, Doebrich and others, 2006, Peters and others, 2007); fault traces (from Abdullah and others, 1977, Doebrich and others, 2006, Peters and others, 2007); and known mineral occurrences (from Abdullah and Chmyriov, 1977, Doebrich and others, 2006, Peters and others, 2007). The map shows the overall AOI and three subareas: Bolo, Luman Tamaki and Zarkashan mine. unk, unknown.

Table 15B–1. List of known mineral occurrences in the Zarkashan area of interest.

[MV, Mississippi Valley; Au, gold; W, tungsten; Cu, copper; Sn, tin; unk, unknown; Zn-Pb, zinc-lead]

Name	Deposit type	Mineralogy	Gangue	Alteration
Tanghi	Karst type bauxite	Bauxite	No data	_
Tangha	Vein Au	Sulfides	Quartz	Silicification
Kharnay	Skarn W	Scheelite; chalcopyrite; molybdenite; beryl	Garnet; pyroxene; wollastonite; rhodonite; quartz	Skarn alteration\ quartz alteration
Pir Khana	Vein hematite	Limonite; martite	No data	Oxidation
Khinjak	Unclassified	Hematite; limonite	No data	Hematitization; limonitization
Gulyakhel	Skarn Cu	Chalcopyrite; magnetite; bornite; covellite; pyrite	No data	Skarn alteration
Lashkar-Qala	Unk Au	Pyrite; chalcopyrite; malachite; azurite; gold native	Dolomite	Dolomitization
Zardak	Unk Au	Pyrite; chalcopyrite; gold native	No data	_
Zarkashan	Skarn Cu	Chalcopyrite; pyrite; sphalerite; chalcocite; bornite; gold native	Garnet; diopside; phlogopite; epidote; wollastonite; serpentine	Skarn alteration/overprinting serpentine
Khinjaktu	Skarn Cu	No data	No data	Skarn alteration
Bolo gold	Vein Au	Limonite	No data	Limonitization
Choh-i-Surkh	Unk Au	Hematite; limonite	No data	Marmorization
Dynamitic	Vein Au	Limonite	No data	Limonitization
Maghn	Skarn Sn	secondary mineral of copper; secondary mineral of lead; secondary mineral of zinc	Garnet; epidote; tourmaline; calcite	Skarn alteration; Hematitization
Anghuri copper	Skarn Zn-Pb	Chalcopyrite; bornite; covellite	Garnet; pyroxene	Skarn alteration
Utkul	Unk Au	Sulfides	No data	Dolomitization; marmorization
Sufi-Kademi	Skarn Cu	No data	No data	Skarn alteration; hornfels
Syaghar	skarn Sn	Hematite; limonite; cassiterite; malachite; azurite; cerussite	No data	Skarn alteration; hematitization; Limonitization
Alaghzar copper	Skarn Cu	Sulfides	Garnet; pyroxene; serpentine	skarn alteration; overprinting serpentinization; Limonitization
Mirzaka	Skarn Sn	Magnetite; cerussite; pyromorphite; galena; scheelite; cassiterite; arsenopyrite; wulfenite	Quartz; serpentine	Silicification; overprinting serpentinization
Basharghar	Skarn Cu	Sulfides	Diopside; vesuvianite; garnet	Skarn alteration of diopside-vesuvianite facies
Belaw	Skarn Cu	Pyrite; chalcopyrite; gold native	Garnet; pyroxene; serpentine	Skarn alteration; overprinting serpentinization; Limonitization
Tangi	MV Zn-Pb	Goethite; limonite	No data	_
Kareztu tin	Skarn Sn	Sulfides	No data	Skarn alteration
Larga	Skarn Sn	Hematite; magnetite; limonite	Garnet; quartz; calcite;	Skarn alteration; silicification; calcite alteration;

Name	Deposit type	Mineralogy	Gangue	Alteration
				hematitization; limonitization
Luman	Vein Au	Sulfides	Quartz	Quartz alteration
Sare Luman	Polymetallic vein	Sulfides	Quartz	Silicification
Unnamed	Skarn Cu	Pyrite; chalcopyrite; sphalerite	Ludwigite; epidote; serpentine	Skarn alteration of ludwigite-epidote facies; overprinting serpentinization
Lar	Vein hematite	Hematite	No data	Marmorization
Tamaki	Vein Au	Chalcopyrite; galena	Quartz; sericite	Silicification; sericitization
Unnamed	Polymetallic vein	Galena; sphalerite; chalcopyrite; quartz	Quartz; sericite	Silicification; sericitization
Unnamed	Polymetallic vein	No data	Quartz; muscovite	Greisen alteration

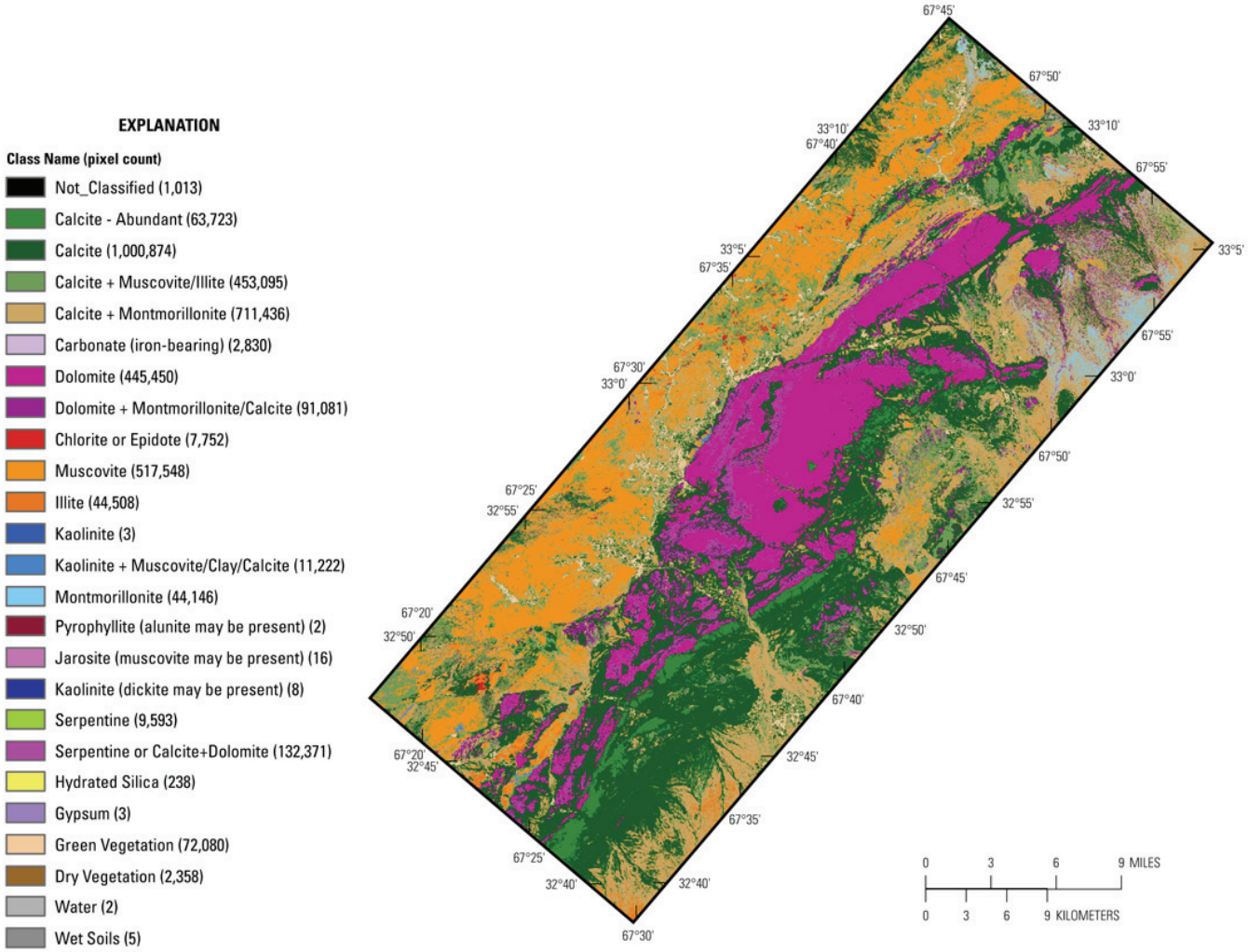

Figure 15B–6. Map showing the distribution of iron-bearing and other alteration minerals in the Zarkashan area of interest as detected in the HyMap data.

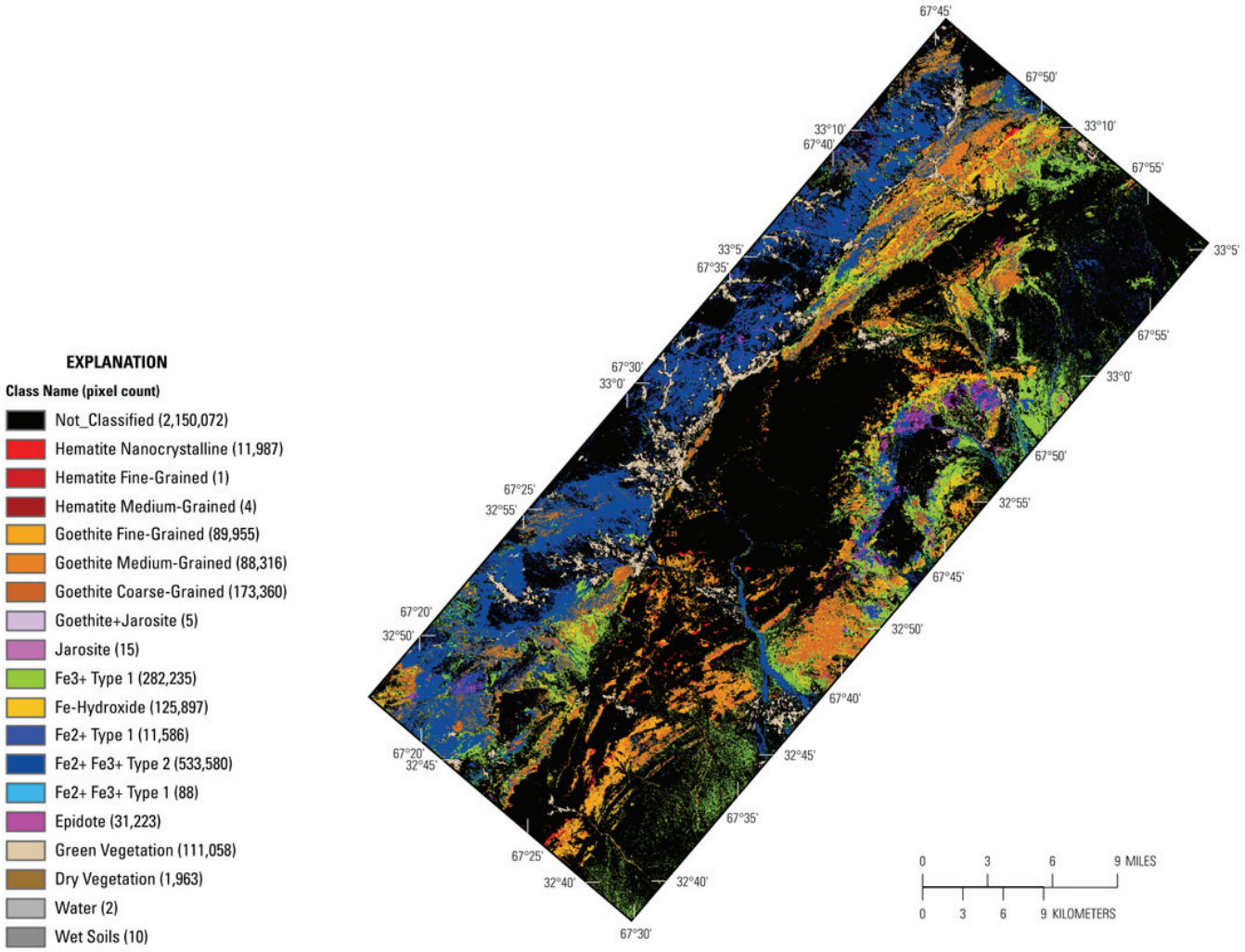

Figure 15B–7. Map showing the distribution of clays, carbonates, phyllosilicates, sulfates, and other alteration minerals detected in the HyMap data for the Zarkashan area of interest.

15B.3.1.1 Carbonate Minerals

The calcites, calcite and montmorillonite, and calcite and muscovite-illite groups are the dominant mapped materials, and are continuous across most geologic boundaries (fig. 15B–8). Dolomite and dolomitic mineral mixtures are present in the center of the AOI in Late Devonian to Carnain-Norian age rocks. The dolomitic and calcitic materials commonly occur in close proximity to one another.

15B.3.1.2 Clays and Micas

The phyllosilicates are the second most abundant mineral group mapped in the AOI (fig. 15B–9); muscovites and illites are the dominant minerals. The illites and muscovites most commonly occur together in subequal amounts (with muscovite predominant) on the western side of the large fault trace, with illite being more abundant than kaolinite in the Late Quaternary age rocks in the southeastern part of the AOI. Pixels of “chlorite or epidote” class minerals occur west of a large fault in the Oligocene age intrusive rocks and Late Proterozoic age rocks near lat 32°47'57.3"N., long 67°22'47"E. Montmorillonite is mapped in the Late Quaternary and Recent age rocks in the northeastern corner of the AOI. Small, but spatially distinct clusters of kaolinite and kaolinite group minerals are present in the western half of the AOI.

15B.3.1.3 Iron Oxides and Hydroxides

Figure 15B–10 shows the iron-bearing and other alteration minerals in the Zarkashan AOI. Goethite and iron hydroxides are the most abundant mineral groups, and are present in a number of stratified and intrusive geologic units. Epidote occurs in clusters in both the intrusive and stratified rocks. Hematitic minerals are mapped as small, spatially distinct pixel groups in the AOI.

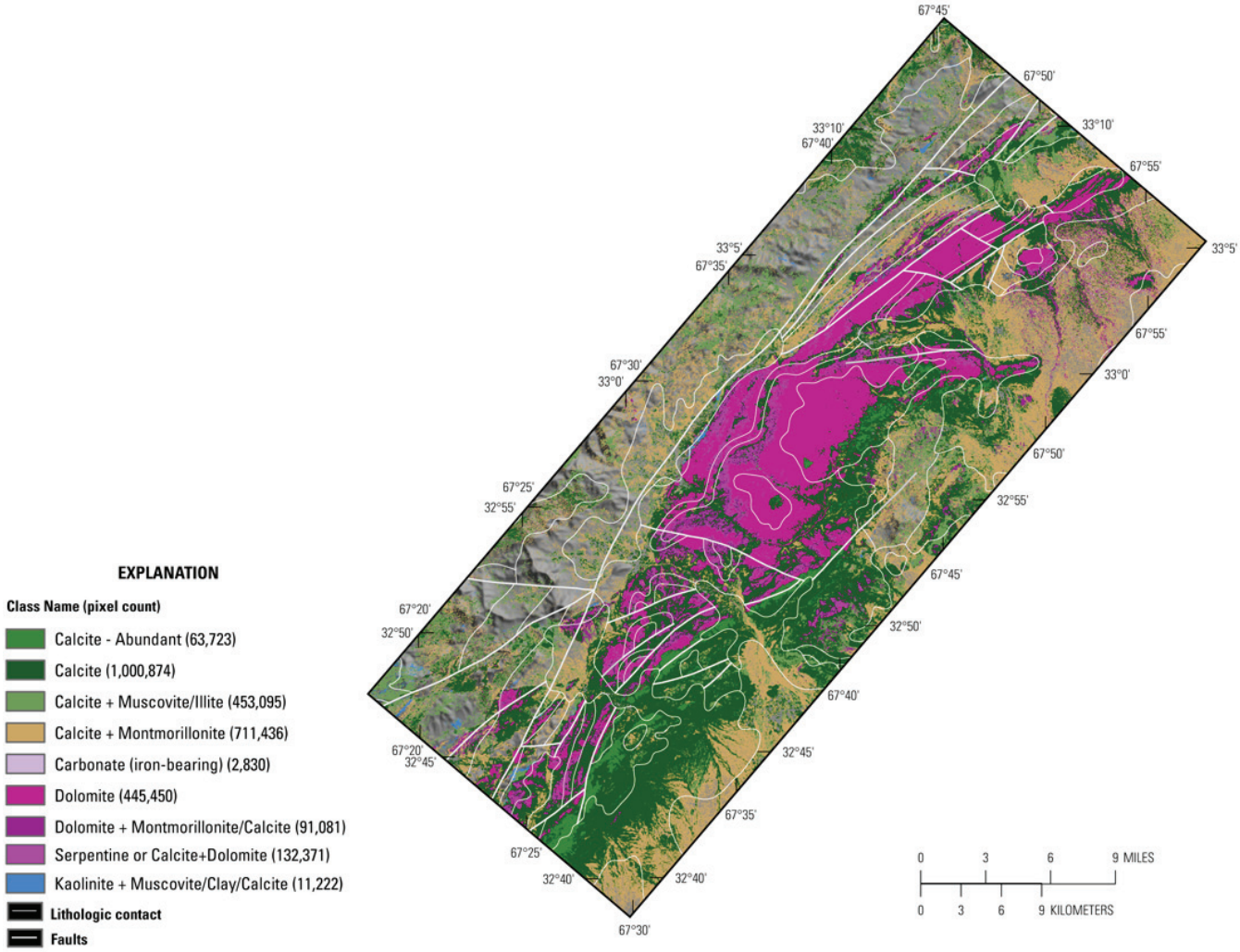

Figure 15B–8. Map showing the distribution of carbonate-bearing minerals detected by the HyMap data in the Zarkashan area of interest.

15B.3.1.4 Common Secondary Minerals

The occurrence and distribution of common secondary minerals in the AOI are shown in figure 15B–11. Serpentine and serpentine group minerals are the most abundant secondary minerals mapped, and are primarily within the central portion of the AOI in Middle Triassic, Carnain-Norian, and Barremian-Aptian age rocks. The chlorite or epidote group minerals occur in spatially distinct groups in both intrusive and stratified rocks.

15B.3.1.5 Common Alteration Minerals

Most of the minerals in this group are commonly present in hydrothermally altered rocks associated with epithermal processes. Consequently, where they occur in distinct clusters is of great interest in terms of potential mineral deposits. In the Zarkashan AOI, there are a limited number of spatially distinct pixels of common alteration minerals. Pixels of chlorite or epidote group minerals occur west of a large fault in the Oligocene age intrusive rocks and Late Proterozoic age rocks near

lat 32°47'57.3"N., long 67°22'47"E (fig 15B–12). Small, but well-defined clusters of kaolinite and kaolinite group minerals are present in the western and northern regions of the AOI. A few pixels of hydrated silica are mapped in the northwest corner of the AOI in Early Quaternary and Carboniferous-Early Permian age rocks (lat 33°13'11.12"N., long 67°46'0.96"E.).

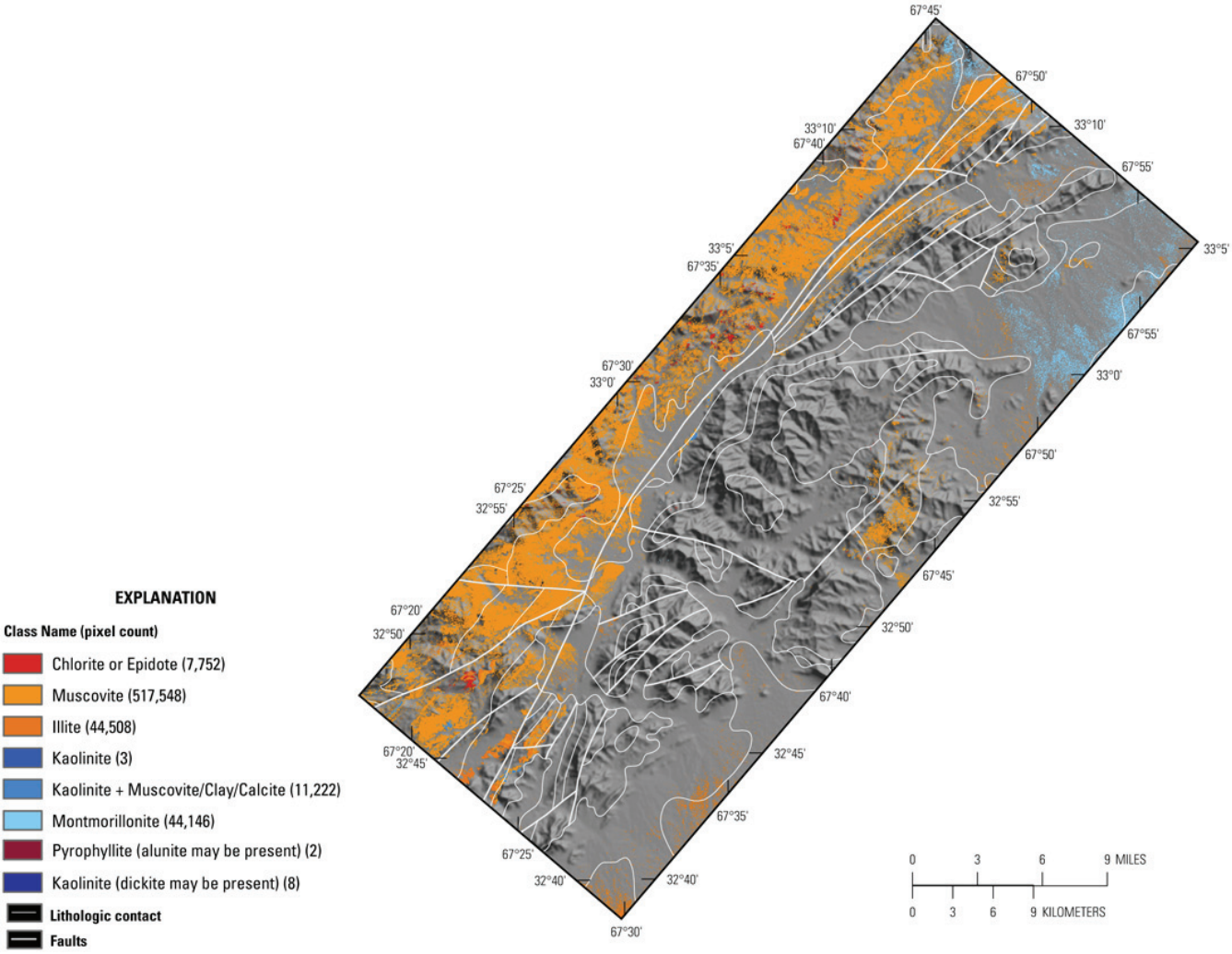

Figure 15B–9. Map showing the distribution of clays and micas identified in the HyMap data for the Zarkashan area of interest.

15B.3.2 Bolo Subarea

The known mineral occurrence map (a semi-transparent geologic map overlain on a shaded relief image) shows the position of nine known mineral prospects in the Bolo subarea (fig. 15B–13). The subarea is approximately 313 km^2 in size, and elevations range from 1,877 to 3, 15B–10368 m (fig. 15B–14).

Rocks in the TM data (fig. 15B–15) are light to dark gray, as well as shades of red, green, and blue. In general, rock color in the TM scene (Davis, 2007) does not correlate with the mapped geology (Dronov and others,1972; Doebrich and others, 2006, Peters and others, 2007). Numerous fault traces are present in the subarea. The geologic map of the area (fig. 15B–16) shows rocks ranging in age from Early Jurassic-Middle Jurassic to Late Quaternary. Early Cretaceous and Oligocene age intrusive rocks occur in the central part of the subarea.

Figures 15B–17 and 15B–18 show the distribution of Fe-bearing and carbonate, sulfate, phyllosilicate and other alteration minerals, respectively. The map of Fe-bearing minerals (fig. 15B–17) shows that the $Fe^{2+}Fe^{3+}$, Type 2 minerals are most abundant in the subarea, followed by goethitic,

Fe^{3+}, Type 1, and Fe-hydroxide minerals. Fewer occurrences of epidote, Fe^{2+}, Type 1, and hematite are mapped in the subarea.

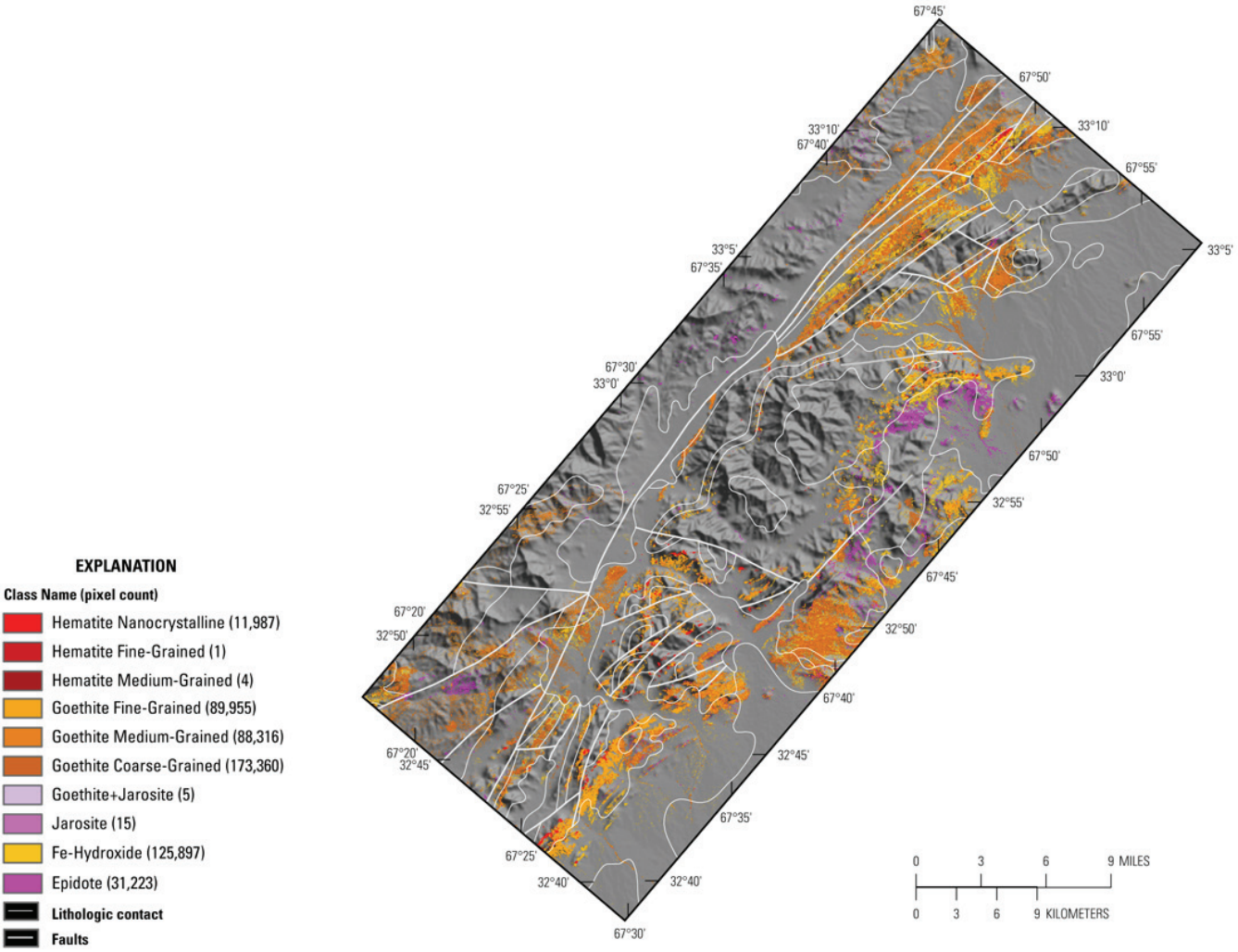

Figure 15B–10. Map showing the distribution of Fe-hydroxides and oxides mapped using the HyMap data for the Zarkashan area of interest.

Figure 15B–18 shows the distribution of carbonates, phyllosilicates, sulfates, altered minerals, and other materials (32 possible classes) in the subarea. Muscovite is the dominant mineral in the subarea, although smaller concentrations of chlorite or epidote group, dolomite group, and muscovite group minerals are also mapped.

15B.3.2.1 Bolo Subarea Carbonate Minerals

Calcite-rich rocks are widespread and occur over the entire subarea (fig.15B–19). A lesser number of pixels mapped as dolomite and dolomitic mineral mixtures are distributed over much of the eastern and southern portions of the subarea. Calcite shows a strong correlation with dolomite and dolomite+montmorillonite/calcite group minerals. Spatially less abundant, but mineralogically significant, are the kaolinite group minerals near lat 32°57'45.37"N., long 67°33'39.9"E.

The Belaw (copper-skarn) and Bolo (gold) prospects occur in regions mapped as dolomitic material; the Utkul (gold), Tangha (vein gold), and Pir Khana (vein hematite) occurrences are in calcite rich-areas; the Alaghzar (copper), Anghuri (copper), and Lashkar-Qala (gold) occurrences and an unnamed vein gold prospect are in rocks mapped as calcite/clay.

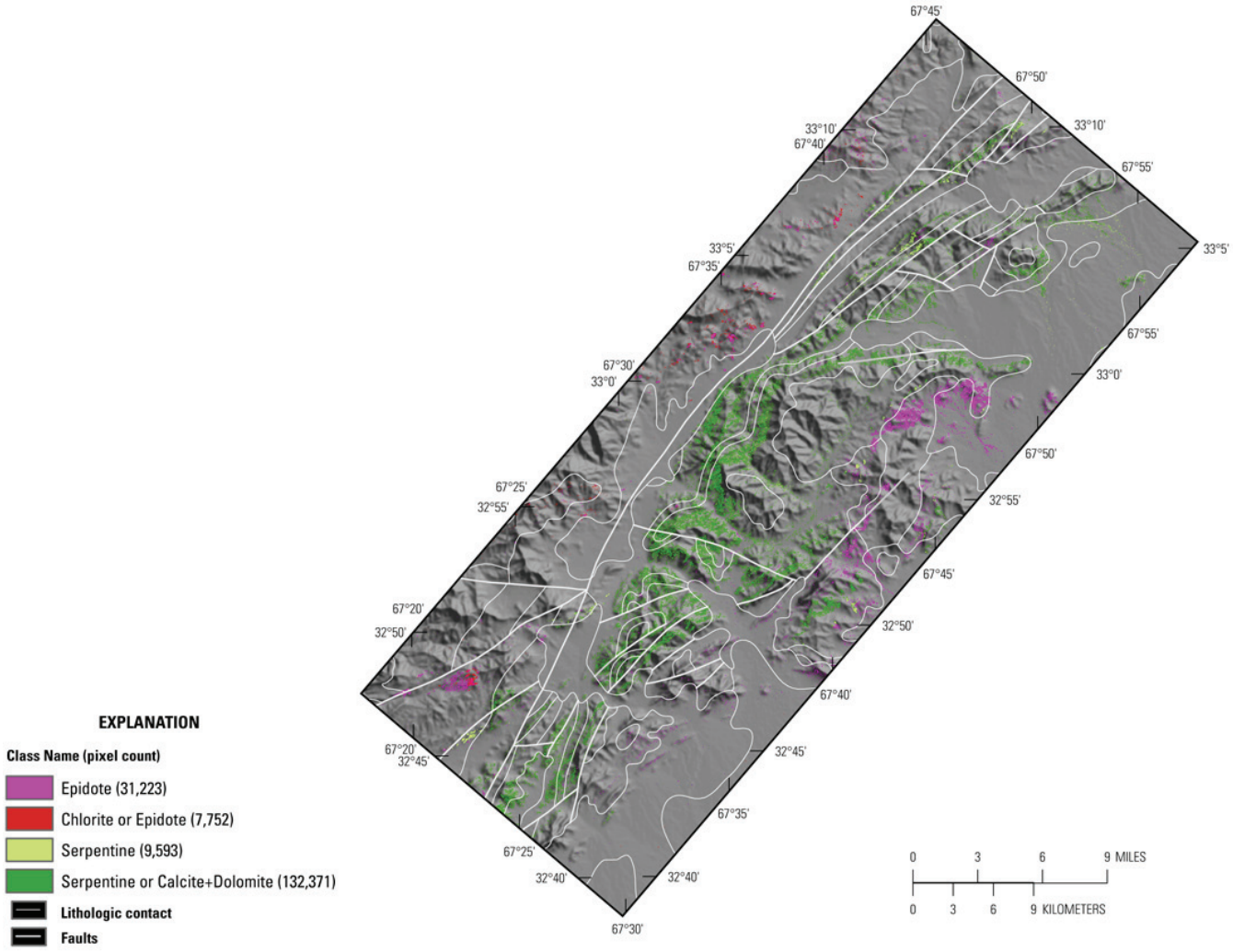

Figure 15B–11. Map showing the occurrence and distribution of common secondary minerals detected in the HyMap data for the Zarkashan area of interest.

15B.3.2.2 Bolo Subarea Clays and Micas

The HyMap data (fig. 15B–20) show the enrichment of clays and micas in the Bolo subarea. Muscovites and illites are the spatially dominant mineral groups. The largest percentages of these minerals occur on the western side of the large fault on the western side of the AOI.

The chlorite or epidote group minerals are most predominant in the Late Proterozoic age rocks (lat 32°48'2.1"N., long 67°22'49.1"E.). Clusters of kaolinite-rich material occur along the contact of the Late Permian and Late Quaternary and Recent age rocks (lat 32°57'45.0"N., long 67°33'40.7"E.), and in the stratified Ordovician age rocks near the center of the subarea.

The Belaw, Alaghzar, and Lashkar-Qala prospects as well as the unnamed mineral prospects occur in areas mapped as muscovites and kaolinite group minerals in the HyMap data.

15B.3.2.3 Bolo Subarea Iron Oxide and Hydroxide Minerals

Figure 15B–21 shows the distribution of iron oxides and hydroxides in the Bolo subarea. The goethite mineral group is spatially dominant; consistent patterns of goethitic minerals are distributed across the subarea. Tight spatial clustering of goethitic materials occurs in and near contact boundaries of Late Permian age rocks east of the major fault. Spatially well-defined zones of goethitic minerals occur in a topographically low area in Late Permian age rocks near lat 32°52'21.50"N., long 67°29'29.85"E., and in a linear trend centered near lat 32°52'12.58"N., long 67°33'03.37"E. Hematite

occurs with the goethite in the Late Permian through Middle Triassic age rocks in the eastern half of the subarea.

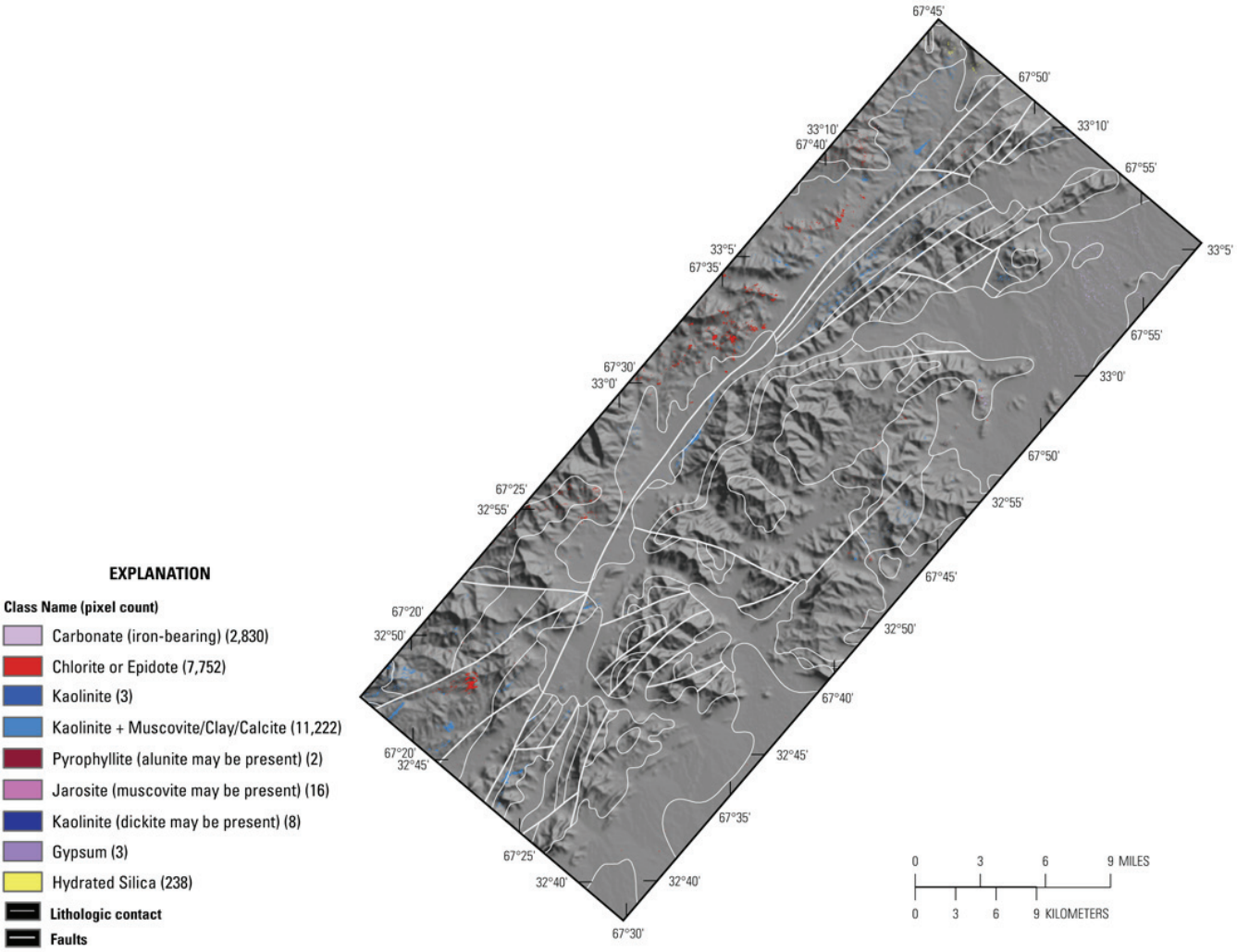

Figure 15B–12. Map showing the distribution of common alteration minerals in the Zarkashan area of interest based on the HyMap data.

A spatially distinct pattern of epidote occurs in Late Proterozoic age rocks (lat 32°48'3.0"N., long 67°22'16.13"E.), and iron hydroxides are common in the subarea.

Only the Pir Khana and Bolo gold mineral prospects show correlation with the iron-hydroxides and oxides detected in the HyMap data.

15B.3.2.4 Bolo Subarea Common Secondary Minerals

The serpentine mineral groups are the most abundant secondary minerals (fig.15B–22) in the subarea. The serpentine minerals are most common in the Late Permian, Early Triassic, and Middle Triassic age rocks on the eastern side of the subarea. “Chlorite or Epidote” group and epidote minerals form a spatially distinct pattern near lat 32°48'3.0"N., long 67°22'16.13"E. Minor amounts of epidote and chlorite group minerals and epidote also occur in other parts of the subarea.

None of the known mineral prospects in the subarea show a strong correlation with the secondary minerals detected in the HyMap data.

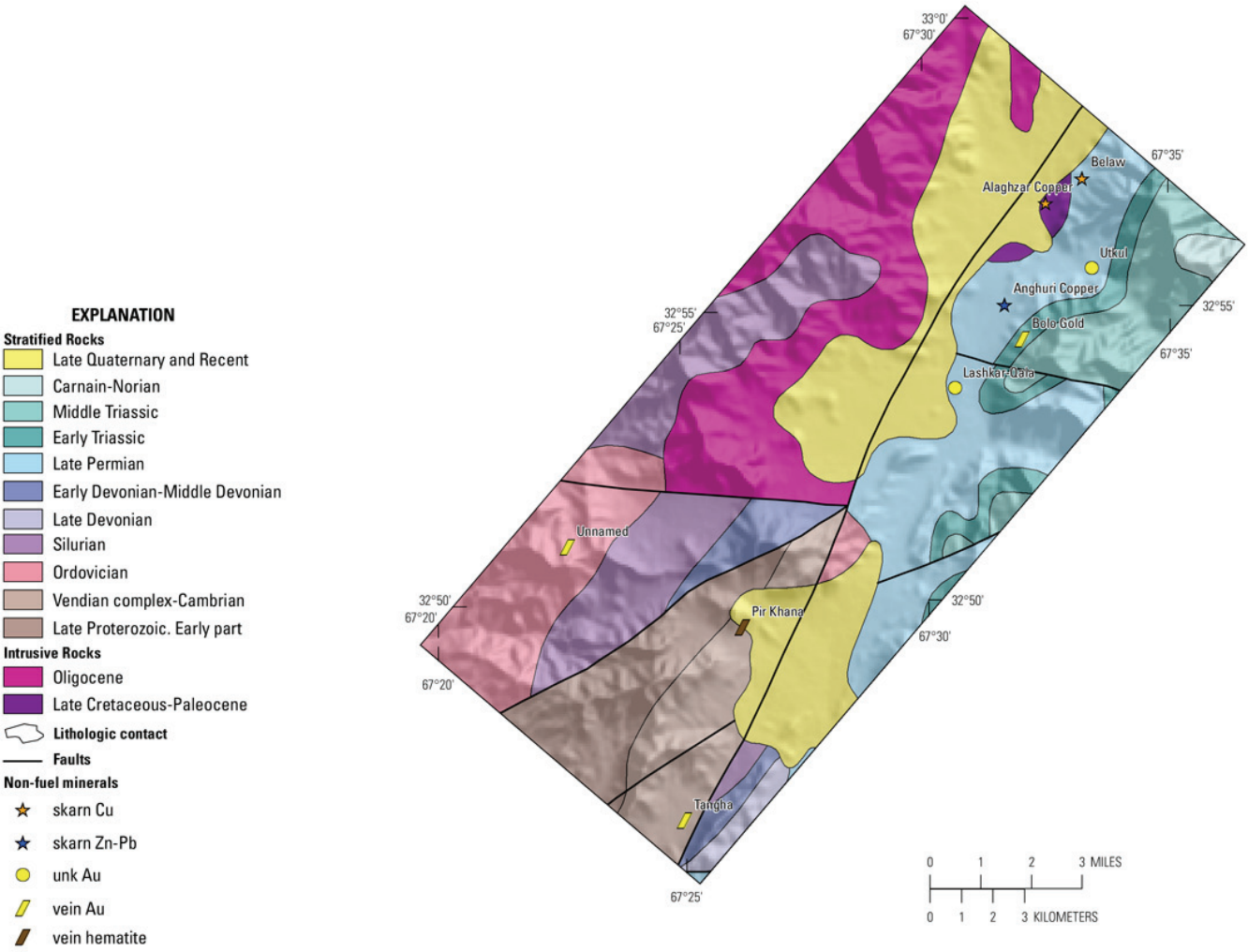

Figure 15B–13. Map showing known mineral occurrences in the Bolo subarea (from Abdullah and Chmyriov, 1977, and Doebrich and others, 2006, Peters and others, 2007). unk, unknown.

15B.3.2.5 Bolo Subarea Common Alteration Minerals

Kaolinite group minerals are the most abundant and common alteration products detected in the HyMap data (fig. 15B–23). Spatially distinct areas of kaolinite occur along a linear trend near lat 32°57'45.0"N., long 67°33'40.7"E., as well as in Silurian age rocks near lat 32°51'2.17"N, long 67°28'26.14"E. The largest contiguous pattern of chlorite or epidote group minerals occurs in the Late Proterozoic age rocks near the southern boundary of the subarea. A few pixels of jarositic minerals are mapped in the Silurian age rocks near the western boundary of the subarea.

Belaw and Alaghzar are the only mineral prospects near the hydrothermal alteration minerals mapped in the HyMap data.

15B.3.3 Luman Tamaki Subarea

The known mineral occurrence map shows the locations of the nine reported sites of mineralization in the Luman Tamaki subarea (fig. 15B–24). Most of the prospects in this subarea are not associated with minerals or mineral assemblages detected in the HyMap data. The elevation in the area ranges from 2,314 to 3,380 meters (fig. 15B–25). Stratified rocks in the subarea range in age from Ordovician to Late Quaternary and Recent; Late Cretaceous-Paleocene and Oligocene intrusive rocks are also present (fig. 15B–26).

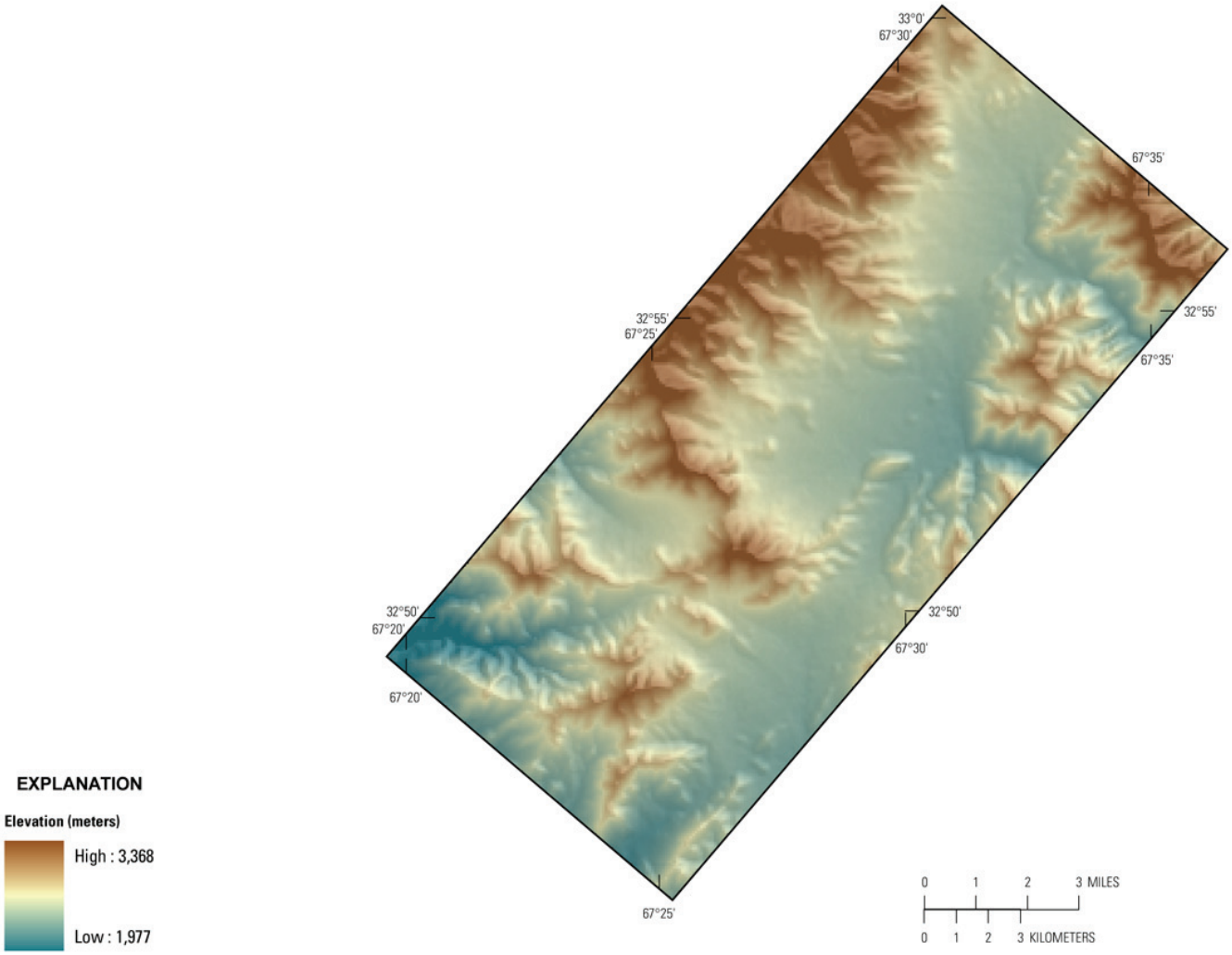

Figure 15B–14. Shaded relief map showing elevations in the Bolo subarea. Dark brown shading indicates higher elevations and lower elevations are represented by blue shading.

Landsat TM data from Davis (2007) indicate that the rocks in the subarea range in color from light gray to greenish, shades of brown, and dark gray (fig.15B–27). The extensive fault trace that bisects the subarea delineates a color difference between the Oligocene age intrusive rocks (light brown) on the west side of the fault trace, and the Ordovician and Early Devonian-Middle Devonian age stratified rocks (greenish) on the east side of the fault trace.

The hyperspectral data for the subarea (figs. 15B–28 and 15B–29) show the distribution of Fe-bearing minerals, and carbonate, phyllosilicate, sulfate and other alteration minerals, respectively. The $Fe^{2+}Fe^{3+}$, Type 2 and goethitic minerals are the dominant Fe-bearing minerals in the Luman Tamaki subarea. Muscovites and dolomite group minerals are the primary mineral phases detected in the HyMap data for carbonates, phyllosilicates, sulfates, altered minerals, and other materials in the subarea (fig. 15B–29).

15B.3.3.1 Luman Tamaki Subarea Carbonate Minerals

Figure 15B–30 shows the spatial distribution of carbonate-rich rocks that cover much of the subarea. Calcite and calcite group mineral mixtures occur over much of the subarea, with a large area of spatially distinct dolomite group minerals in the southeastern portion of the subarea in Late Permian, Early Triassic, Middle Triassic and Carnain-Norian age rocks.

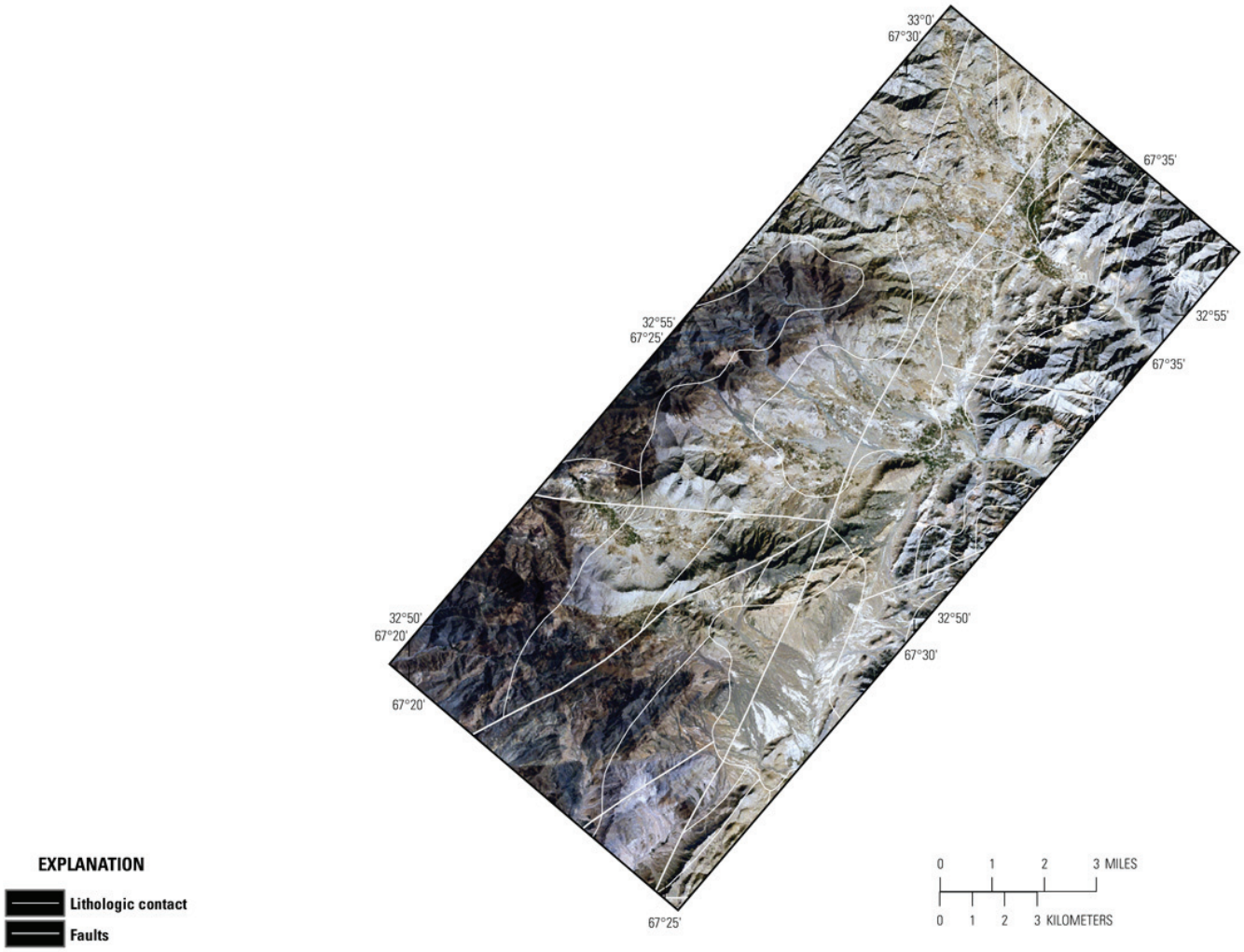

Figure 15B–15. Map showing faults and fractures in the Bolo subarea (from Abdullah and others, 1977, and Doebrich and others, 2006, Peters and others, 2007) superimposed on Landsat Enhanced Thematic Mapper (TM) data from Davis (2007).

Dolomites and dolomite group minerals are also present as linear features in the Silurian through Middle Devonian age rocks east of the major fault trace. Phyllosilicate and kaolinite group minerals are spatially distributed over the subarea with a well-defined cluster near lat 33°9'16.55"N., long 67°44'17.94"E.

The unnamed gold, unnamed polymetallic vein, and unnamed copper-skarn prospects occur in or near areas mapped as dolomite or dolomite group minerals based on the HyMap data.

15B.3.3.2 Luman Tamaki Subarea Clays and Micas

Figure 15B–31 shows the enrichment of phyllosilicate minerals in the Luman Tamaki subarea. Muscovite is the most abundant mineral in the subarea, and is primarily associated with the Oligocene age intrusive rocks, and to a lesser extent, Ordovician and Early Devonian-Middle Devonian age rocks. The muscovites are commonly associated with lesser amounts of illite.

The chlorite or epidote group minerals primarily occur in association with Ordovician-age intrusive rocks, and show a spatially distinct occurrence near lat 33°1'45.58"N., long 67°35'27.11"E. Montmorillonite is present along the northern boundary of the subarea. Kaolinite and kaolinite group

minerals are mostly present in areas of Ordovician-age intrusive rocks, with lesser amounts in Silurian and Early Devonian-Middle Devonian stratified rocks east of the major fault trace.

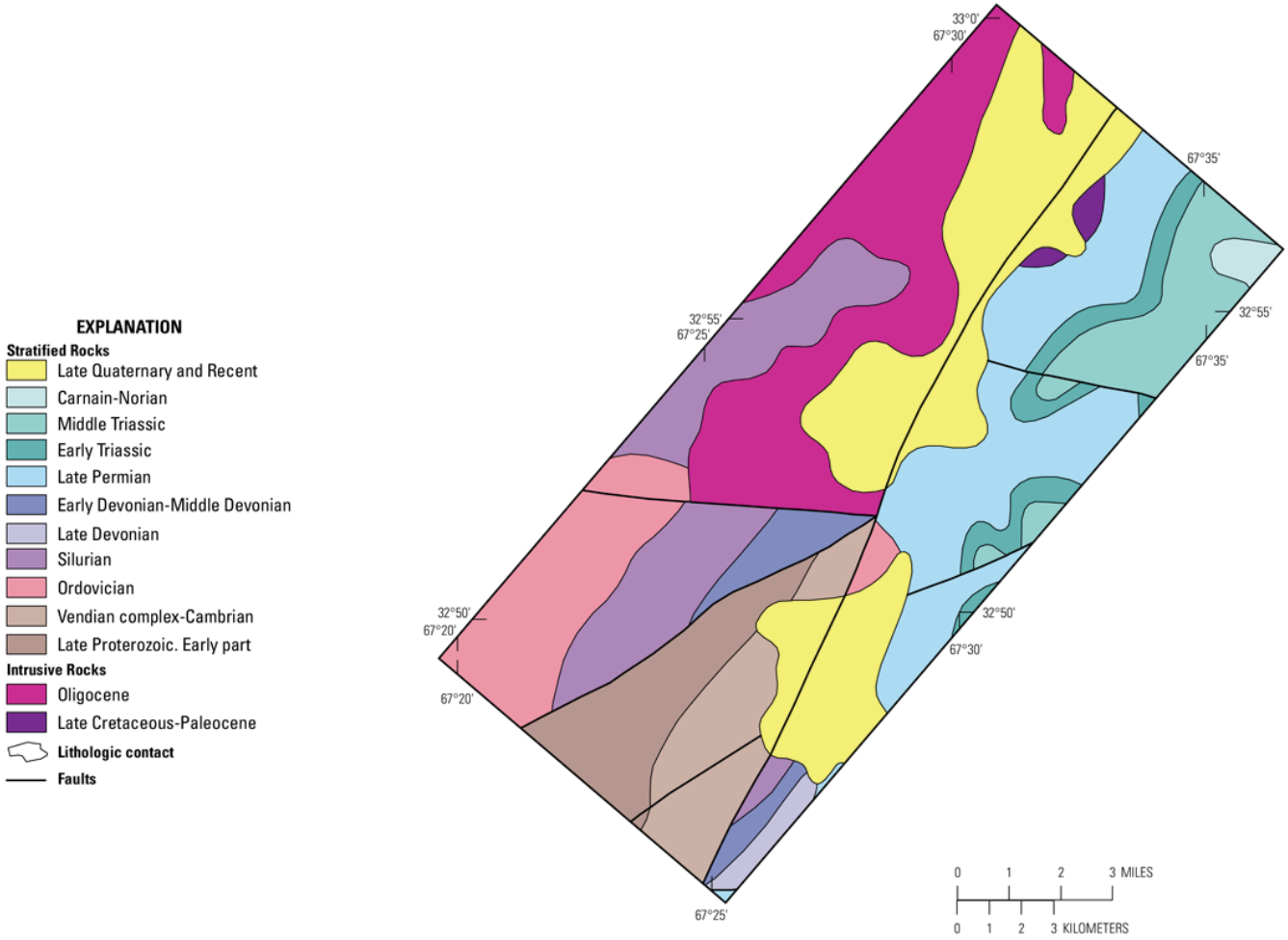

Figure 15B–16. Geologic map of the Bolo subarea from the digital geologic map of Afghanistan (Abdullah and others, 1977; Doebrich and others, 2006, Peters and others 2007).

The Luman prospect is in an area with spatially distinct pixels mapped as chlorite or epidote, $Fe^{2+}Fe^{3+}$, Type 2 and muscovite. The Tamaki prospect is characterized by spatially distinct $Fe^{2+}Fe^{3+}$, Type 2, goethitic minerals, and chlorite or epidote group minerals.

15B.3.3.3 Luman Tamaki Subarea Iron Oxides and Hydroxides

The distribution of Fe-oxides and hydroxides is shown in Figure 15B–32. Goethites and Fe-hydroxide minerals are the dominant mineral groups in the subarea. These groups primarily occur in Ordovician, Silurian, and Early Devonian-Middle Devonian age stratified rocks, and occur in lesser amounts in Late Devonian, Carboniferous-Early Permian, Late Permian, and Early Quaternary age rocks. Hematite is present in spatially distinct patterns in the Late Devonian age rocks near lat 33°9'54.5"N., long 67°48'42.07"E. Epidote is mapped in Oligocene age intrusive rocks and the Carboniferous-Early Permian age rocks west of the dominant fault trace, and in Silurian and Carboniferous-Early Permian age stratified rocks east of the fault.

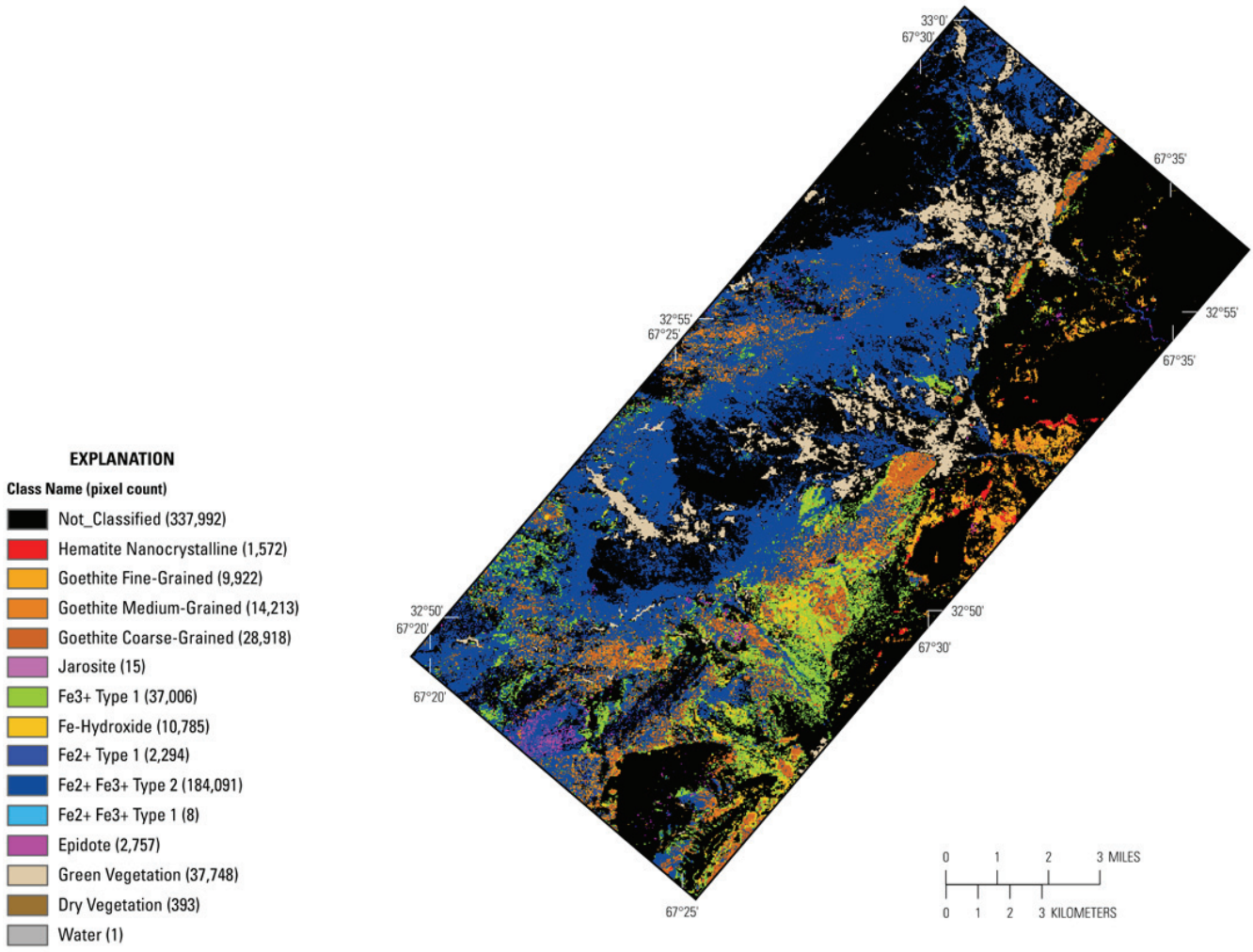

Figure 15B–17. Map showing iron-bearing and other alteration minerals detected in HyMap data for the Bolo subarea.

All of the mineral prospects in the subarea, with the exception of the unnamed gold prospect, are in the general vicinity of one of the iron oxides or hydroxides group minerals detected in the HyMap data. The Lar vein hematite prospect is near a contiguous area mapped as hematite in the HyMap data.

15B.3.3.4 Luman Tamaki Subarea Common Secondary Minerals

Serpentine and serpentine group minerals are the widely distributed common secondary minerals in the Luman Tamaki subarea (fig.15B–33). The serpentine minerals primarily occur in stratified rocks east of the dominant fault trace. However, a small, distinct cluster of chlorite or epidote group and epidote occurs near lat 33°1'46.52"N., long 67°35'24.14"E., in the Ordovician age intrusive rocks.

15B.3.3.5 Luman Tamaki Subarea Common Alteration Minerals

The kaolinite group minerals are the most abundant of the common alteration minerals in the subarea, and are primarily mapped in Ordovician-age intrusive rocks with lesser amounts in Silurian and Early Devonian-Middle Devonian stratified rocks east of the dominant fault (fig.15B–34). Spatially distinct kaolinite group minerals occur near lat 33°9'13.39"N., long 67°44'27.96"E., in the Oligocene age intrusive rocks. A small, distinct cluster of the chlorite or epidote group and epidote occurs near lat 33°1'46.52"N., long 67°35'24.14"E. in the Ordovician-age intrusive rocks and is in close proximity to

iron carbonates and kaolinite group minerals. A contiguous area of the chlorite or epidote group and epidote occurs near the Luman prospect.

A small cluster of hydrated silica is mapped in the northernmost part of the subarea in Early Quaternary and Carboniferous-Early Permian age rocks.

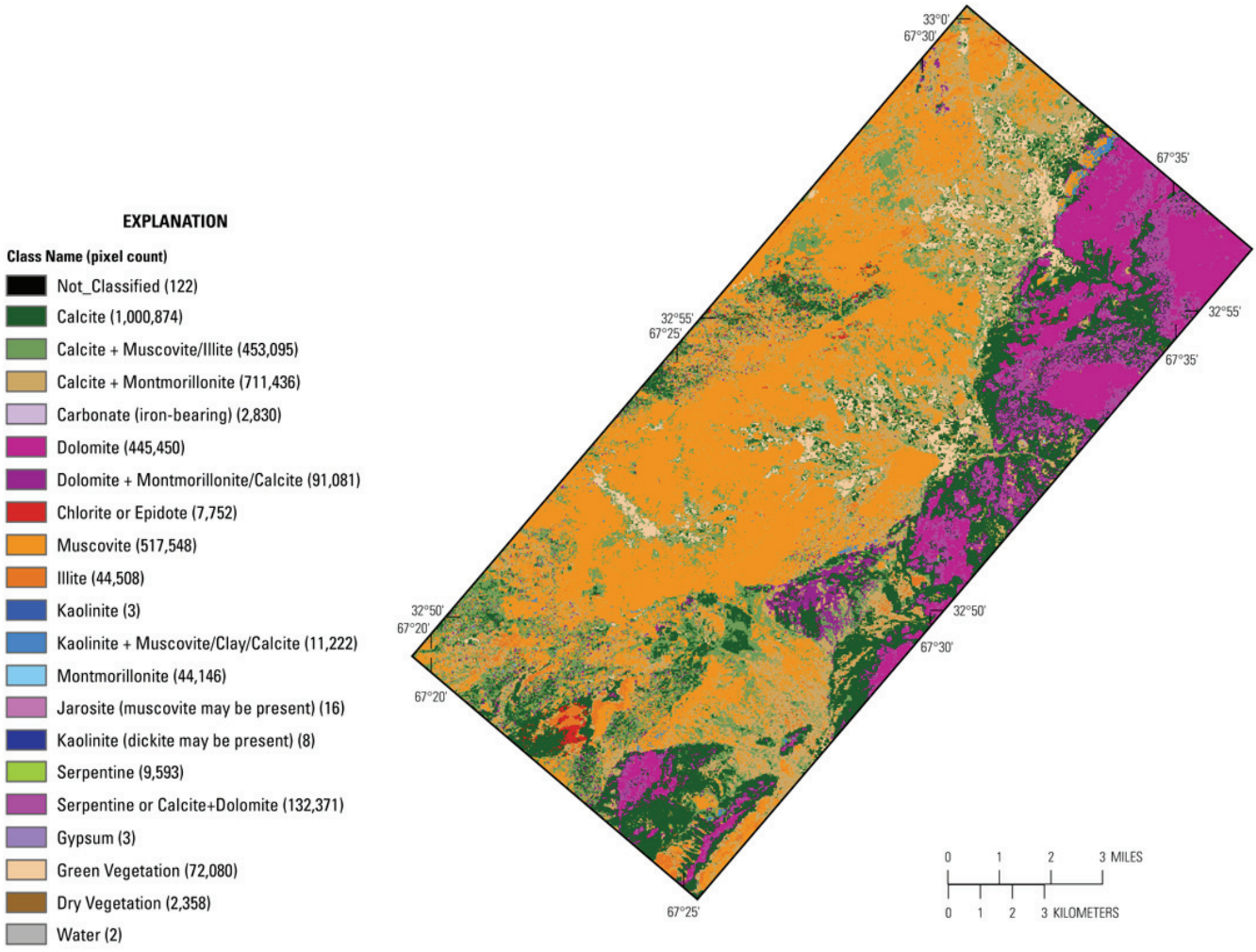

Figure 15B–18. Map showing the distribution of clays, carbonates, phyllosilicates, sulfates, and other alteration minerals for the Bolo subarea based on HyMap data.

15B.3.4 Zarkashan Mine Subarea

The known mineral occurrence map (fig. 15B–35) shows the position of reported mineral occurrences in the Zarkashan mine subarea (Abdullah and others, 1977, Doebrich and others, 2006, Peters and others, 2007). The subarea is approximately 214 km^2 in extent, and elevations range from 2,086 to 2,979 m (fig. 15B–36).

A geologic map of the area (fig. 15B–37) shows rocks ranging in age from Late Permian to Late Quaternary and Recent. Late Cretaceous-Paleocene age intrusive rocks occur in the central part of the subarea. The rocks in the TM data (fig. 15B–38) range in color from light to dark gray, and also include shades of reddish-brown. In general, the colors of the rock in the TM imagery do not correlate with the mapped geology (Abdullah and others, 1977; Doebrich and others, 2006, Peters and others, 2007). Two fault traces occur in the subarea.

Figures 15B–39 and 15B–40 show the distribution of Fe-bearing, and carbonate, sulfate, phyllosilicate and other alteration minerals, respectively (28 possible classes). The map of Fe-bearing

minerals (fig. 15B–39) shows that $Fe^{2+}Fe^{3+}$, Type 2 minerals are most abundant in the subarea, followed by Fe-hydroxides, goethitic, and Fe^{3+}, Type 1. Epidote and hematite are less common in the subarea.

Figure 15B–40 shows the distribution of carbonates, phyllosilicates, sulfates, altered minerals, and other materials (32 possible classes) for the subarea. Pixels mapped as calcite and calcite mineral mixtures are dominant in the area, although spatially distinct pixels of dolomite group minerals, serpentines, and muscovite and illite are also present.

15B.3.4.1 Zarkashan Mine Subarea Carbonate Minerals

Calcite-rich rocks are widespread and occur over most of the subarea (fig.15B–41). Large contiguous areas mapped as dolomitic group minerals are present in the Early Triassic, Middle Triassic, and Carnain-Norian age rocks in the western part of the subarea. A spatially distinct, but small, group of iron-bearing carbonates are mapped in the Carnain-Norian age rocks (lat 35°59'2.49"N., long 67°47'22.22"E.) near the northern boundary of the subarea.

Figure 15B–19. Map showing the distribution of carbonate-bearing minerals in the Bolo subarea detected by the HyMap data. unk, unknown.

The Dynamitic and Choh-i-Surkh gold prospects and the Sufi Kademi copper prospect, are mapped in areas primarily mapped as calcite in the HyMap data.

15B.3.4.2 Zarkashan Mine Subarea Clays and Micas

The HyMap data (fig. 15B–42) show the enrichment of clays and micas in the Zarkashan mine subarea. Muscovites and illites are the spatially dominant mineral groups. Both groups mostly occur in the Late Cretaceous-Paleocene age intrusive rocks, but are also present to a lesser extent in stratified rocks.

Small clusters or individual pixels of montmorillonite and kaolinite group minerals are present throughout most of the subarea. The largest spatially coherent pattern of kaolinite group and montmorillonite in the subarea occurs along the contact (lat 32°56'11.92"N., long 67°42'34.68"E.) of the Late Cretaceous-Paleocene age intrusive rocks and Barremian-Aptian age stratified rocks. The chlorite or epidote group minerals do not form a spatially contiguous group of significant size in the subarea.

15B.3.4.3 Zarkashan Mine Subarea Iron Oxide and Hydroxide Minerals

Figure 15B–43 shows the distribution of Fe-oxides and hydroxides in the Zarkashan mine subarea. The Fe-hydroxide mineral group is spatially dominant within the subarea, and is commonly associated with goethitic minerals. The goethitic and Fe-hydroxide minerals are dispersed across the subarea and commonly form small spatially coherent patterns. Three spatially distinct, tightly spaced groups of coarse grained goethite occur near the Khinjaktu prospect (lat 32°54'42.64"N., long 67°43'44.4"E.).

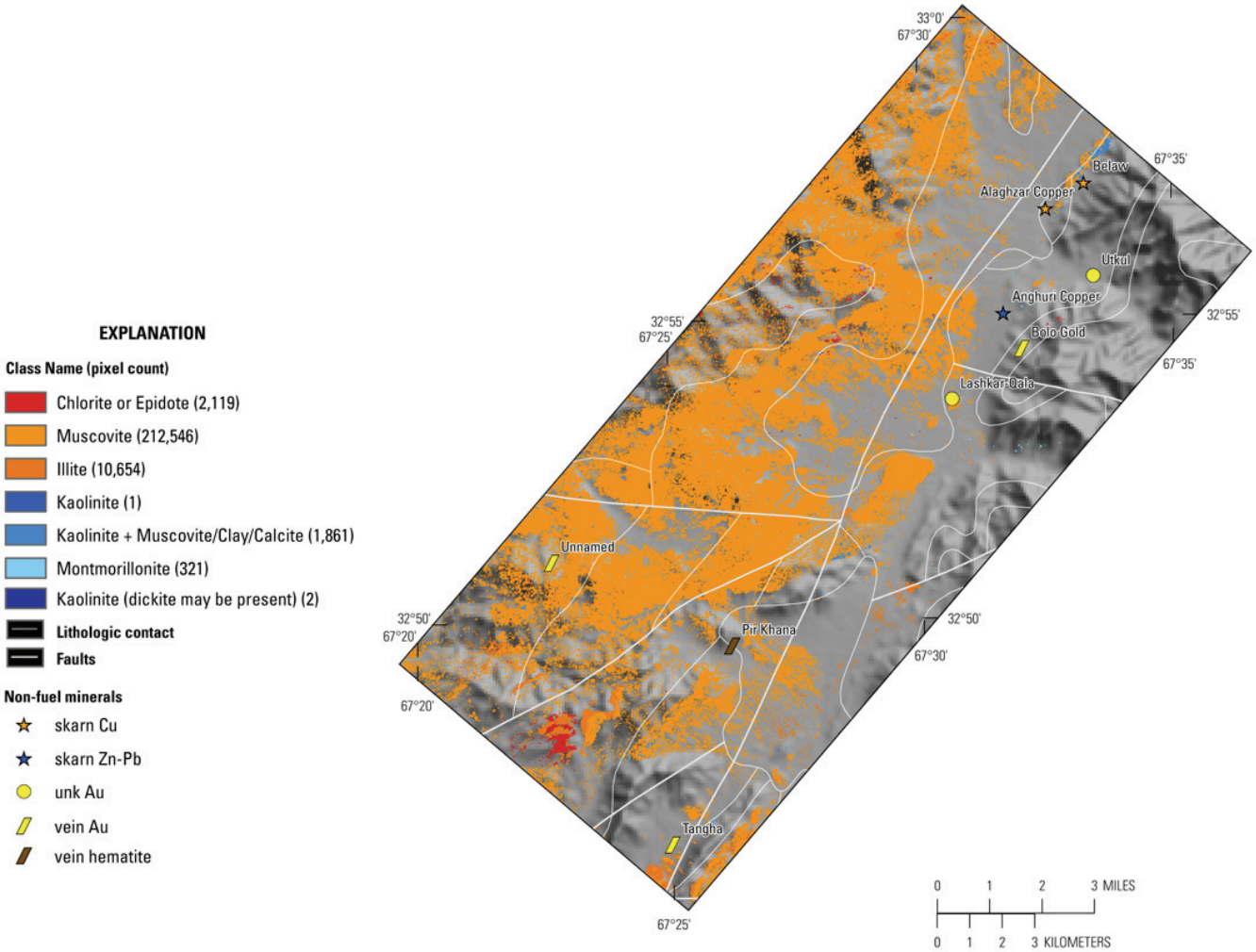

Figure 15B–20. Map showing the distribution of clays and micas detected using the HyMap data in the Bolo subarea. unk, unknown.

Epidote also occurs in spatially distinct patterns, primarily in the Carnain-Norian and Barremian-Aptian age stratified rocks and the Late Cretaceous-Paleocene age intrusive rocks. Hematites are mostly in the northwestern corner of the subarea.

15B.3.4.4 Zarkashan Mine Subarea Common Secondary Minerals

The epidote and chlorite mineral group or epidote are the most abundant secondary minerals (fig.15B–44) in the subarea and are associated with both stratified and intrusive rocks. Serpentine and serpentine group mineral mixtures occur in small concentrations in all ages of stratified rocks, but are not mapped in the Late-Cretaceous-Paleocene age intrusive body.

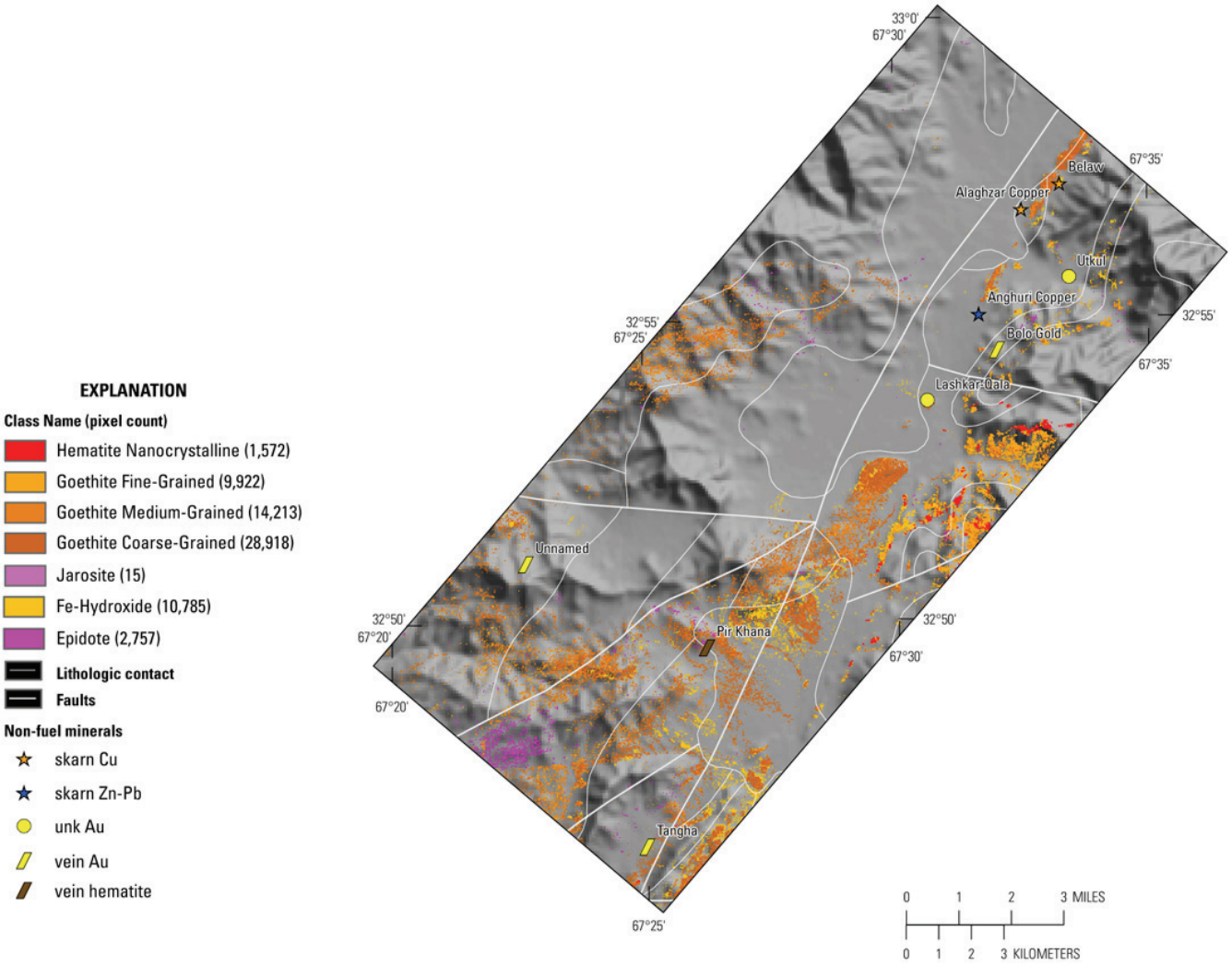

Figure 15B–21. Map showing the distribution of iron oxides and hydroxides in the Bolo subarea based on the HyMap data. unk, unknown.

15B.3.4.5 Zarkashan Mine Subarea Common Alteration Minerals

There are relatively few pixels of mapped common alteration minerals in the subarea (fig. 15B–45). The most significant grouping is a small cluster of Fe-bearing carbonates that are mapped in the Carnain-Norian age rocks (lat 32°59'2.49"N., long 67°47'22.22"E.) near the northeastern boundary of the subarea. The largest spatially coherent pattern of kaolinite group and montmorillonite in the subarea occurs along the contact (lat 32°56'11.92"N., long 67°42'34.68"E.) between Late Cretaceous-Paleocene age intrusive rocks and Barremian-Aptian age stratified rocks. The chlorite or epidote mineral group minerals do not form spatially coherent groupings of significant size in the subarea.

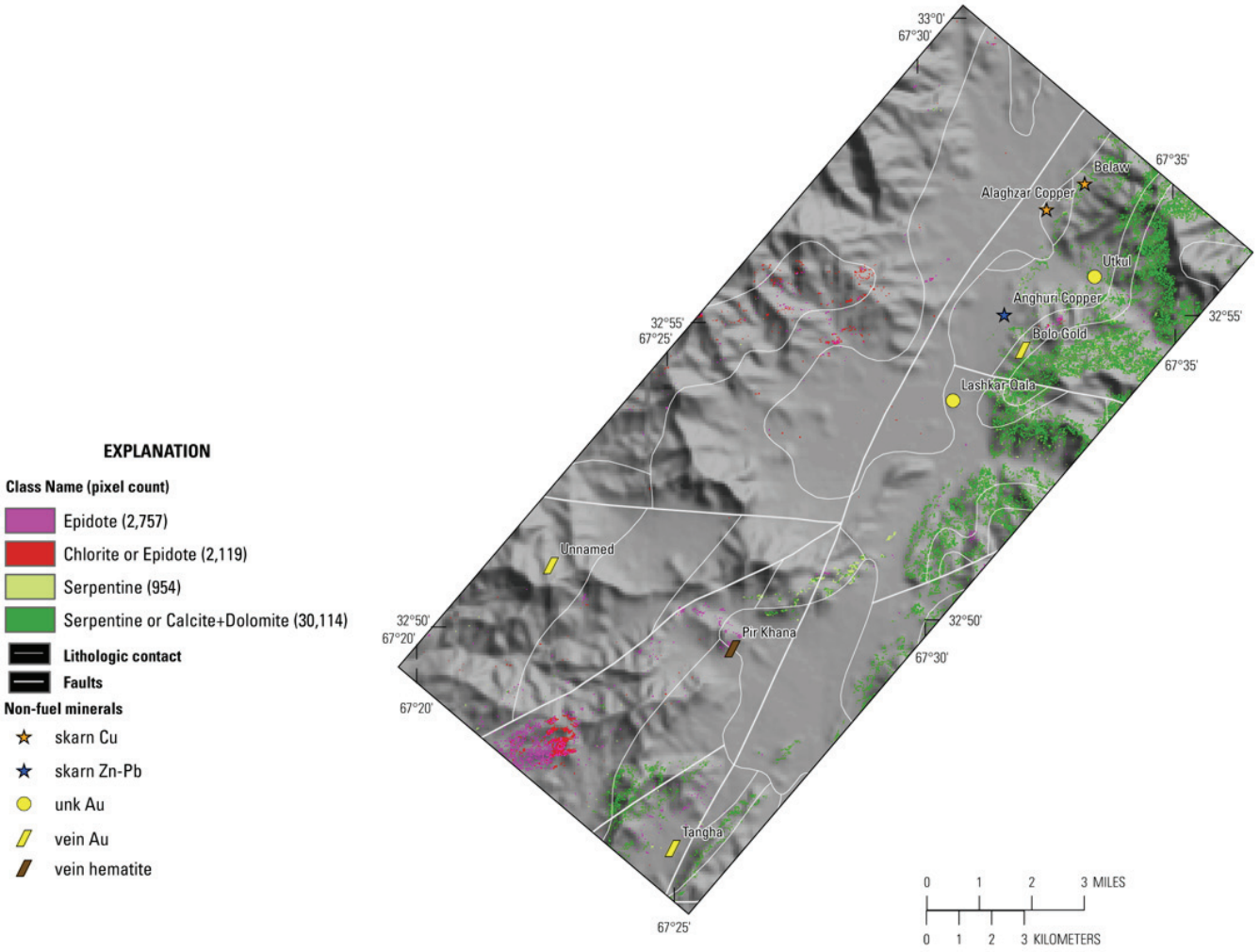

Figure 15B–22. Map showing the distribution of common secondary minerals detected in the HyMap data for the Bolo subarea. unk, unknown.

15B.4 Summary and Conclusions

The Zarkashan AOI and subareas (Bolo, Luman Tamaki, and Zarkashan mine) were thought to be favorable regions for near-term development of mineral production based on previous studies by geologists from the Union of Soviet Socialist Republics (USSR) and its Eastern European allies between the early 1950s and about 1985 (Peters and others, 2007). Recent geophysical data collected by the USGS (Sweeney and others, 2006), and joint field sampling and analysis activities completed by the USGS in collaboration with the Task Force for Business and Stability Operations (TFBSO) of the Department of Defense, and the Afghanistan Geological Survey (AGS) of the Ministry of Mines of Afghanistan between 2009 and 2011, have provided valuable new data that substantially increases the understanding of the extent and value of the potential mineralization. The HyMap imaging spectroscopy data for the Zarkashan AOI further support this conclusion.

Several gold target zones occur in the Zarkashan AOI; two primary regions are the Bolo and Zarkashan mine subareas (Peters and others, this volume). Although these areas require additional detailed mapping and sampling, the studies by the USGS and TFBSO during FY 2010 have substantiated much of the previous Soviet findings and confirmed the presence of copper and gold in economically profitable concentrations. HyMap and ASTER data suggest that the distribution of the copper and gold may be extensive, and that a number of previously unknown medium- to large-size

areas of gold- and copper-rich mineralization are probable in the area (King, Johnson, and others, 2011). According to Peters and others (this volume) the Zarkashan copper-gold deposits would be amenable in the early stages of exploitation to simple metallurgy, and this would result in short lead times and short payback periods for mining of medium to large sized gold-copper ores.

Because of the nearly complete inclusion of the AOI within the boundaries of the three subareas, the discussion of the hyperspectral data for the AOI will be addressed by subareas. However, one mineralogical anomaly near lat 33°3'59.92"N., long 67°48'15.77"E., that is not included in a subarea is included in King, Johnson, and others (2011).

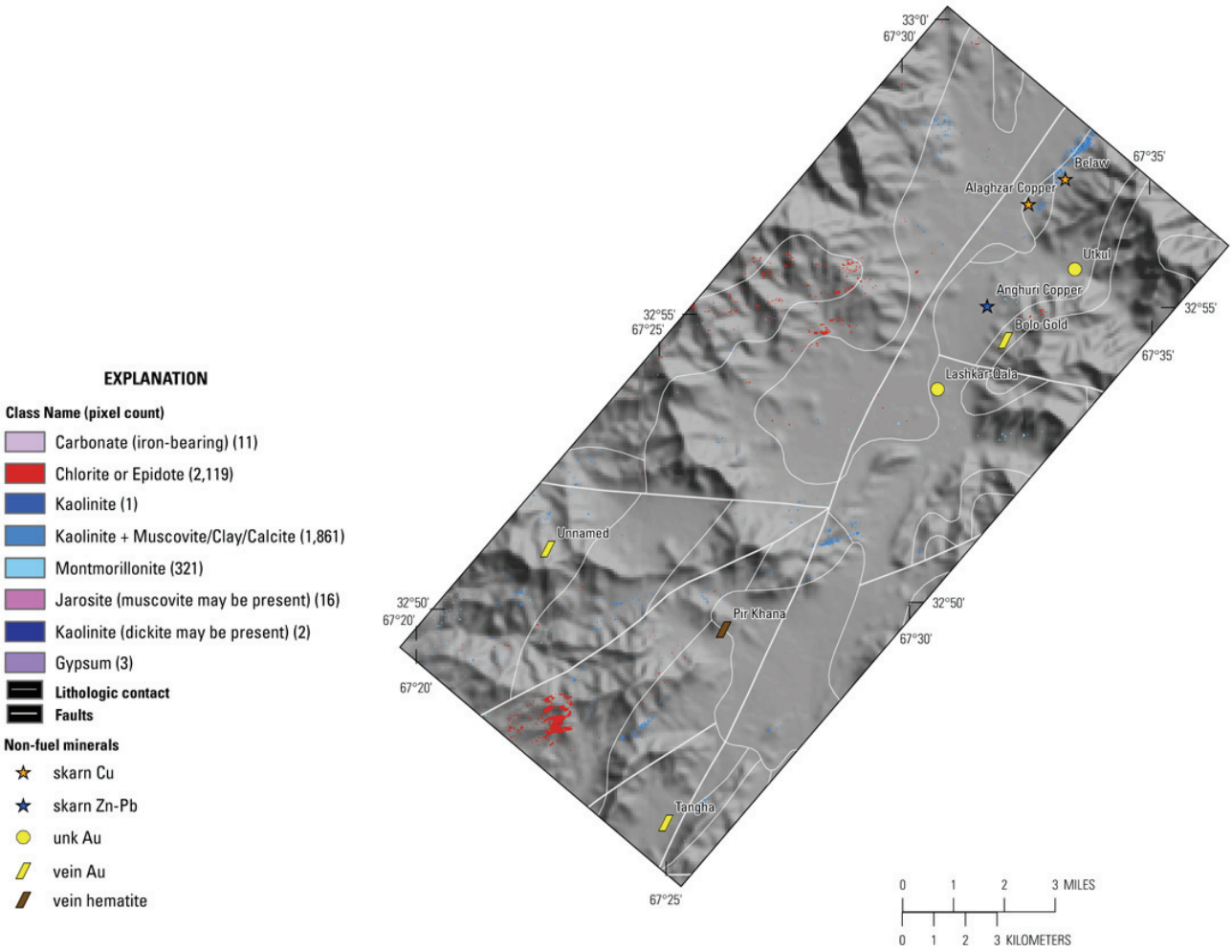

Figure 15B–23. Map showing common alteration materials detected in the HyMap data for the Bolo subarea. unk, unknown.

15B.4.1 Bolo Subarea

The Bolo subarea includes a number of gold-rich occurrences adjacent to the eastern boundary of a Cretaceous age granitic pluton. The tract contains the Bolo and Utkul gold occurrences, as well as the Alaghzar, Belaw, and Anghuri copper prospects. Additional evaluations and analysis are needed because recent stream sediment field sampling completed by the USGS and TFBSO in 2010 did not include the sampling of prospective horizons in the streambed and, therefore, the sampled sediments are not considered representative of potential mineralization in the subarea

A linear trend of goethite, $Fe^{2+}Fe^{3+}$, Type 2, kaolinite, muscovite and lesser amounts of Fe^{3+}, Type 1, (figs. 15B–6 and 15B–7) extends from near lat 32°59'33.37"N., long 67°34'31"E., to near lat 32°55'16.60"N., long 67°31'42.48"E., in a contact zone between Late Permian age stratified rocks and the Late Cretaceous-Paleocene intrusion, and includes the Belaw prospect (fig. 15B–46). The area

should be examined by additional fieldwork and supporting chemical analysis (King, Johnson, and others, 2011).

Another region of potential mineralization occurs near lat 32°50’20.43”N., long 67°27’44.03”E., in a contact zone between Ordovician, Early Devonian-Middle Devonian, and Late Quaternary-Recent age rocks. The HyMap data for the area show that this region contains dolomitic, goethitic, and calcitic group minerals and $Fe^{2+}Fe^{3+}$, Type 2,and Fe^{3+}, Type 1, with lesser amounts of serpentine and kaolinite group minerals, and has a similar compositional pattern to the mineralization mapped near the Belaw occurrence (figs. 15B–6 and 15B–7).

In the southern part of the subarea near lat 32°43'3.53"N., long 67°22'54.02"E. in Late Proterozoic age rocks, a spatially coherent group, roughly circular in shape, of epidote, muscovite, chlorite, and $Fe^{2+}Fe^{3+}$, Type 2 minerals are mapped in the HyMap data.

HyMap data show that potential mineralization in this subarea differs in character from that of the Zarkashan mine subarea, presumably because of differences in the age and composition of the host rocks as well as the age and type of mineralization processes.

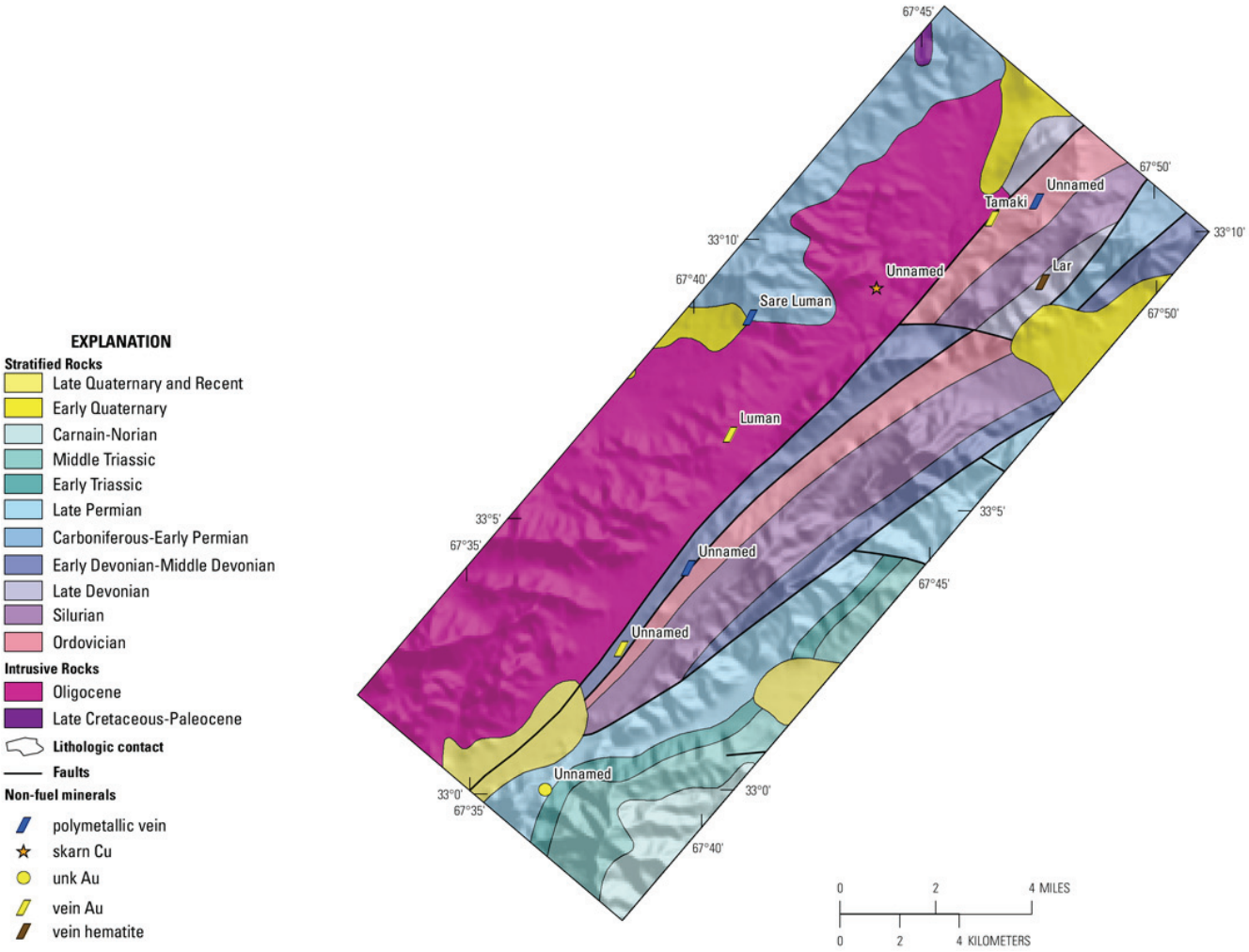

Figure 15B–24. Map showing known mineral occurrences in the Luman Tamaki subarea (Abdullah and Chmyriov, 1977, Doebrich and others, 2006, Peters and others, 2007). unk, unknown.

15B.4.2 Luman Tamaki Subarea

The Luman Tamaki subarea lies within a northeast-striking tectonic zone of Middle Paleozoic sedimentary rock encompassing gold, polymetallic vein, and copper skarn mineral occurrences. Previous remote sensing studies using ASTER data identified zones of phyllic and argillic alteration. The mineral

alteration patterns appear to be related to regional fractures within the batholith, and do not correlate well spatially with the known mineral prospects.

Both the Tamaki and Luman occurrences are reported to be gold-rich, and a number of unnamed precious- base metal-vein and skarn occurrences are also present within the subarea. The Luman prospect occurs in an area mapped as epidote, $Fe^{2+}Fe^{3+}$, Type 2, and muscovite (figs. 15B–28 and 15B–29). The Tamaki prospect is characterized by spatially distinct $Fe^{2+}Fe^{3+}$, Type 2, goethitic minerals, and muscovite and minor amounts of calcitic group minerals and epidote.

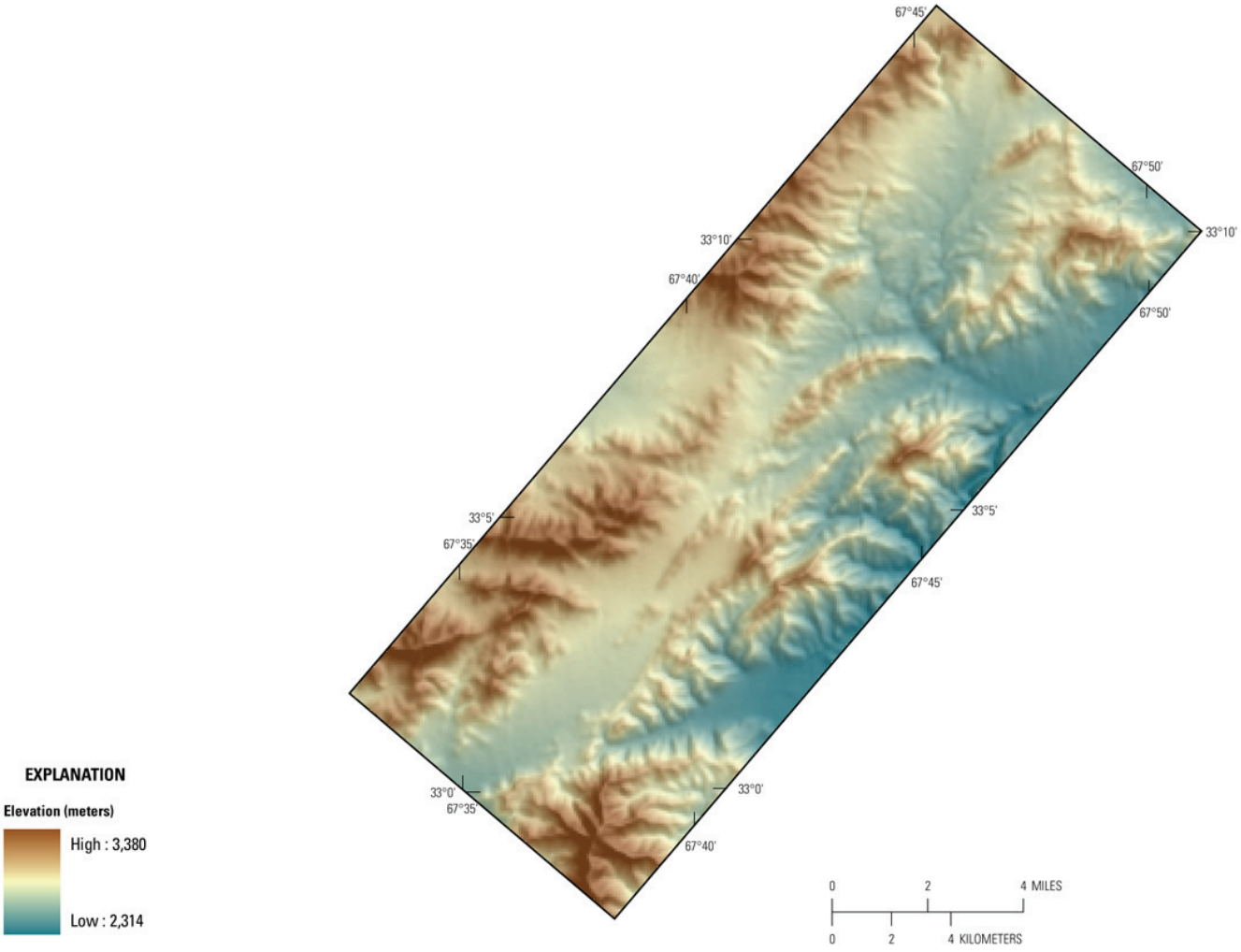

Figure 15B–25. Shaded relief map showing the elevations within the Luman Tamaki subarea. Dark brown shading indicates the higher elevations and the lower elevations are represented by blue shading.

The Lar vein hematite prospect occurs in Late Devonian age rocks that are primarily dolomitic, calcitic, and Fe-Hydroxide group minerals with minor amounts of serpentine. A small cluster of hematite is mapped nearby.

15B.4.3 Zarkashan Mine Subarea

Calcite and calcite mineral mixtures are the most dominant minerals in the Zarkashan mine subarea (fig. 15B–40), although spatially distinct pixels of dolomite group minerals, serpentines, muscovite and illite are also mapped. The calcite group minerals (calcite + muscovite/illite and calcite + montmorillonite), mixed with lesser amounts of dolomitic group minerals and scattered occurrences of calcite group minerals, are mapped in the main Late Cretaceous-Paleocene age intrusive body. Spatially distinct clusters of dolomitic group minerals and serpentines occur along the margins of the intrusion.

Calcite group minerals occur in the Carnain-Norian and Barremian-Aptian age rocks on the periphery of the intrusion.

$Fe^{2+}Fe^{3+}$, Type 2 minerals are most abundant and spatially distinct Fe-bearing minerals in the subarea, although Fe-hydroxides, goethitic, and Fe^{3+}, Type 1 minerals are also mapped (fig. 15B–39). Fewer pixels of spatially well-defined epidote and hematite are mapped in the subarea. Mixed $Fe^{2+}Fe^{3+}$, Type 2 and epidote pixels commonly occur and surround the main Late Cretaceous-Paleocene age intrusive rocks (fig. 15B–47). Smaller, spatially coherent patterns of goethitic and Fe^{3+}, Type 1 minerals are also present along the margins of the intrusions in low topographic areas. The contact zone mineral assemblages detected in the HyMap data correspond to the aeromagmetic anomalies reported by Sweeney and others (2006). On the basis of field investigations and sampling during the 2010 reconnaissance missions and subsequent chemical analysis, Peters and others (this volume) confirmed that the spatially distinct distribution of $Fe^{2+}Fe^{3+}$, Type 2 and epidote minerals in the HyMap data redefined the extent and target zones around the main Late Cretaceous-Paleocene age intrusion that are likely to contain ore-grade copper and gold, which suggests the HyMap data are an effective mineral exploration tool.

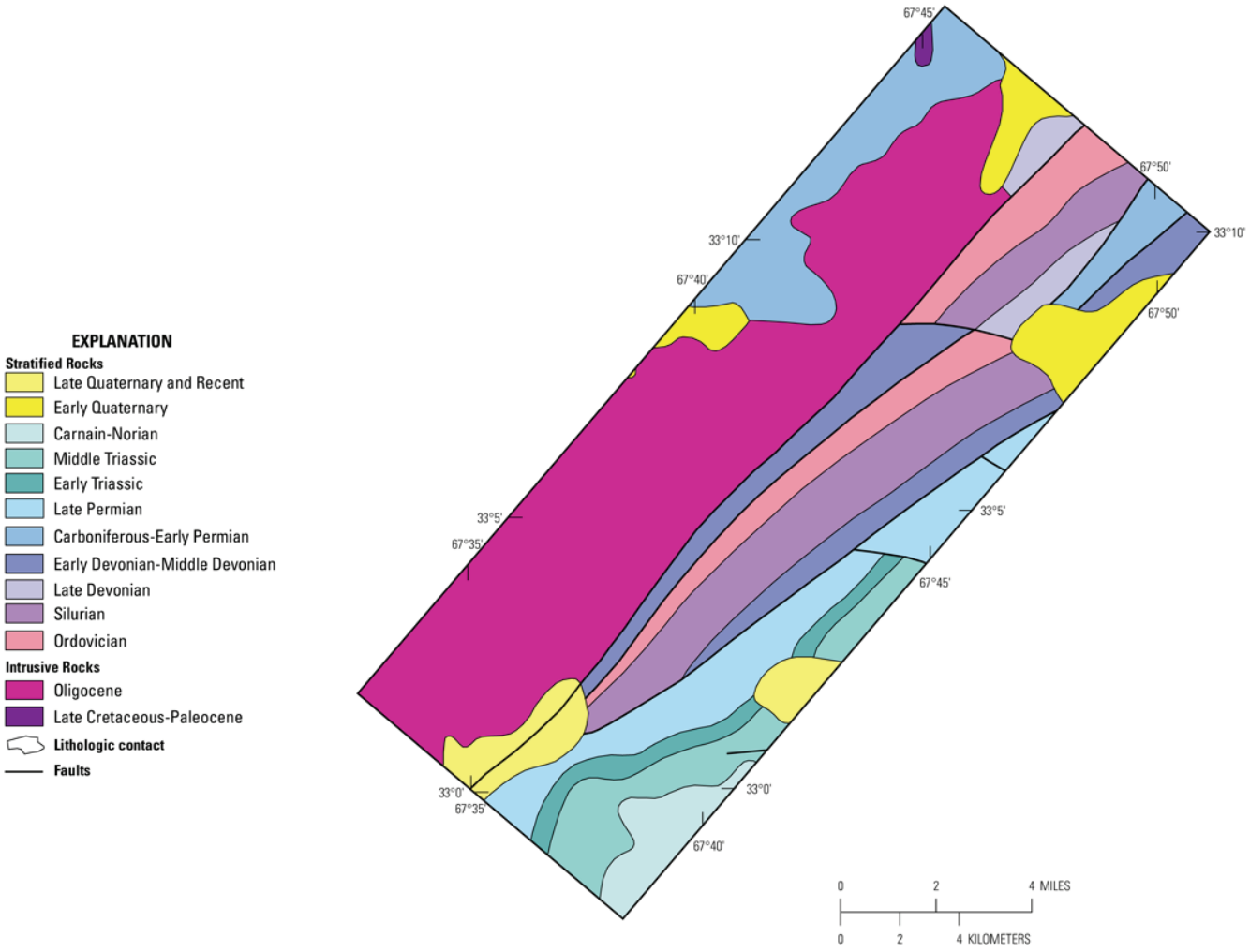

Figure 15B–26. Geologic map of the Luman Tamaki subarea from the digital geologic map of Afghanistan (Abdullah and others, 1977; Doebrich and others, 2006, Peters and others, 2007).

Fe^{2+} Fe^{3+} Type 2 and epidote minerals, with similar types of spatial relations as those adjacent to the margin of the Late Cretaceous-Paleocene age intrusive, are present in the Carnain-Norian and Late Quaternary-Recent age rocks in the northeastern part of the subarea (lat 32°59'20.50"N., long 67°47'5.15"E.). The presence of these minerals is also associated with spatially related and distinct

patterns of goethitic and Fe^{3+} Type 1 minerals, similar to the peripheral area of the primary intrusion in the subarea (King, Johnson, and others, 2011).

An east-west trend of spatially distinct pixels of hematite spans geologic boundaries in Carnain-Norian and Barremian-Aptian age rocks, south of the east-west fault trace in the northwestern corner of the subarea, which is suggestive of fault-controlled mineralization (fig. 15B–39).

The Zarkashan copper-gold deposit and Zardak mineral prospects occur in areas primarily mapped spatially as distinct patterns of $Fe^{2+}Fe^{3+}$, Type 2 and epidote minerals, with minor amounts of serpentine; both sites have been confirmed to contain gold (Peters and others, this volume). The Gulyakhel prospect, which lies within in Upper Jurassic-Lower Cretaceous (Barremian-Aptian) age rocks, is also mapped in association with $Fe^{2+}Fe^{3+}$, Type 2, and epidote, with minor amounts of serpentine. On the basis of similarities in respective HyMap data, the Gulyakhel prospect may have a high potential for economic mineralization comparable to that of the Zarkashan and Zardak prospects.

The Dynamitic, Sufi Kademi and Choh-i-Surkh prospects host gold and copper mineralization, and occur in materials mapped in the HyMap data as primarily Fe^{3+} Type 1 and carbonate minerals.

The Khinjaktu copper skarn prospect occurs on the eastern side of the main intrusion along a north northwest-trending zone that penetrates the pluton from the south, and contains gold mineralization in skarn at the contact between Upper Jurassic-Lower Cretaceous (Barremian-Aptian) and Late Cretaceous-Paleocene age intrusive rocks (Peters and others, this volume). The HyMap data show the prospect occurring in a spatially distinct zone of muscovite and coarse grained goethite that is lower in elevation than the surface exposure of the pluton.

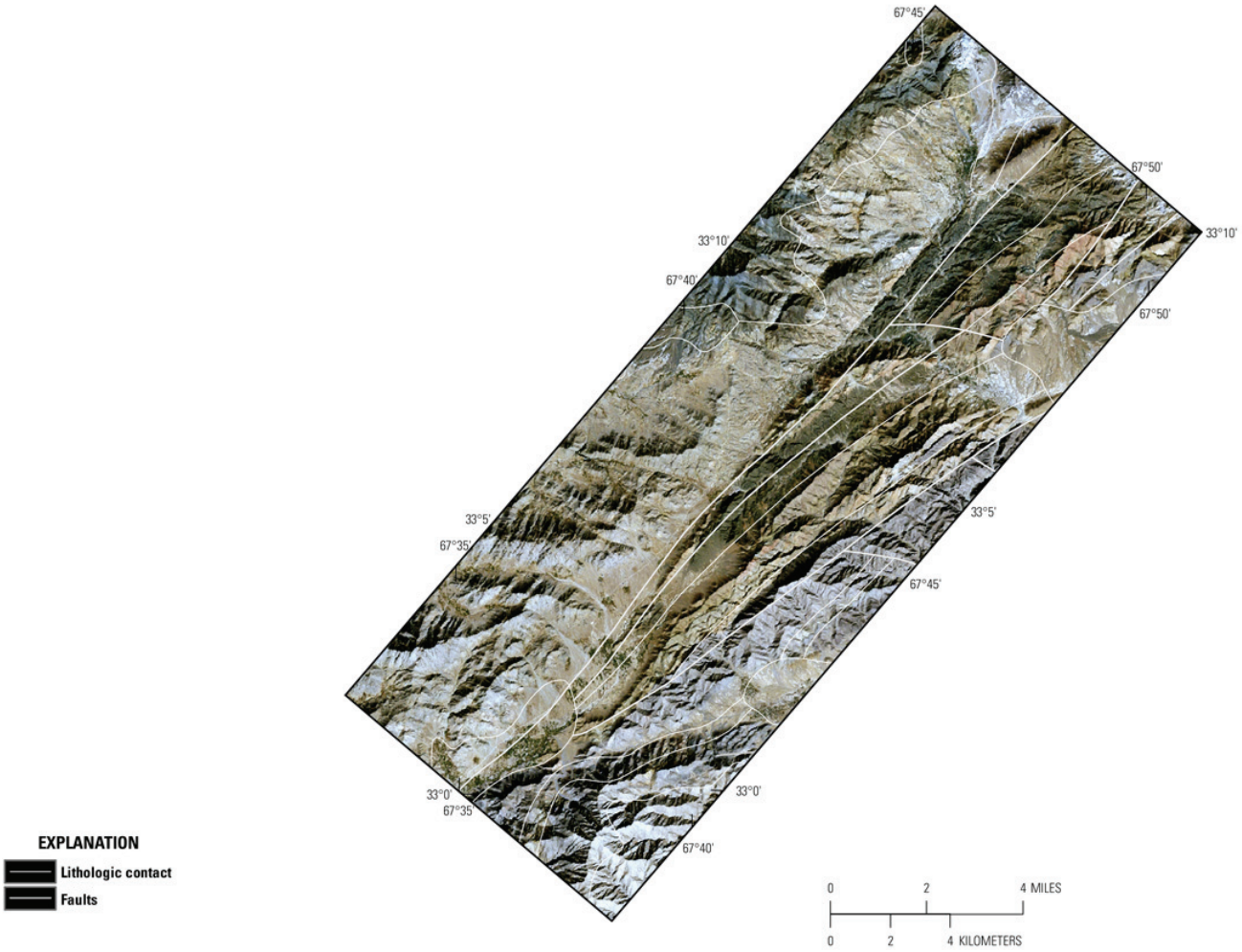

Figure 15B–27. Map showing the Landsat Thematic Mapper (TM) data for the Luman Tamaki subarea (from Davis, 2007).

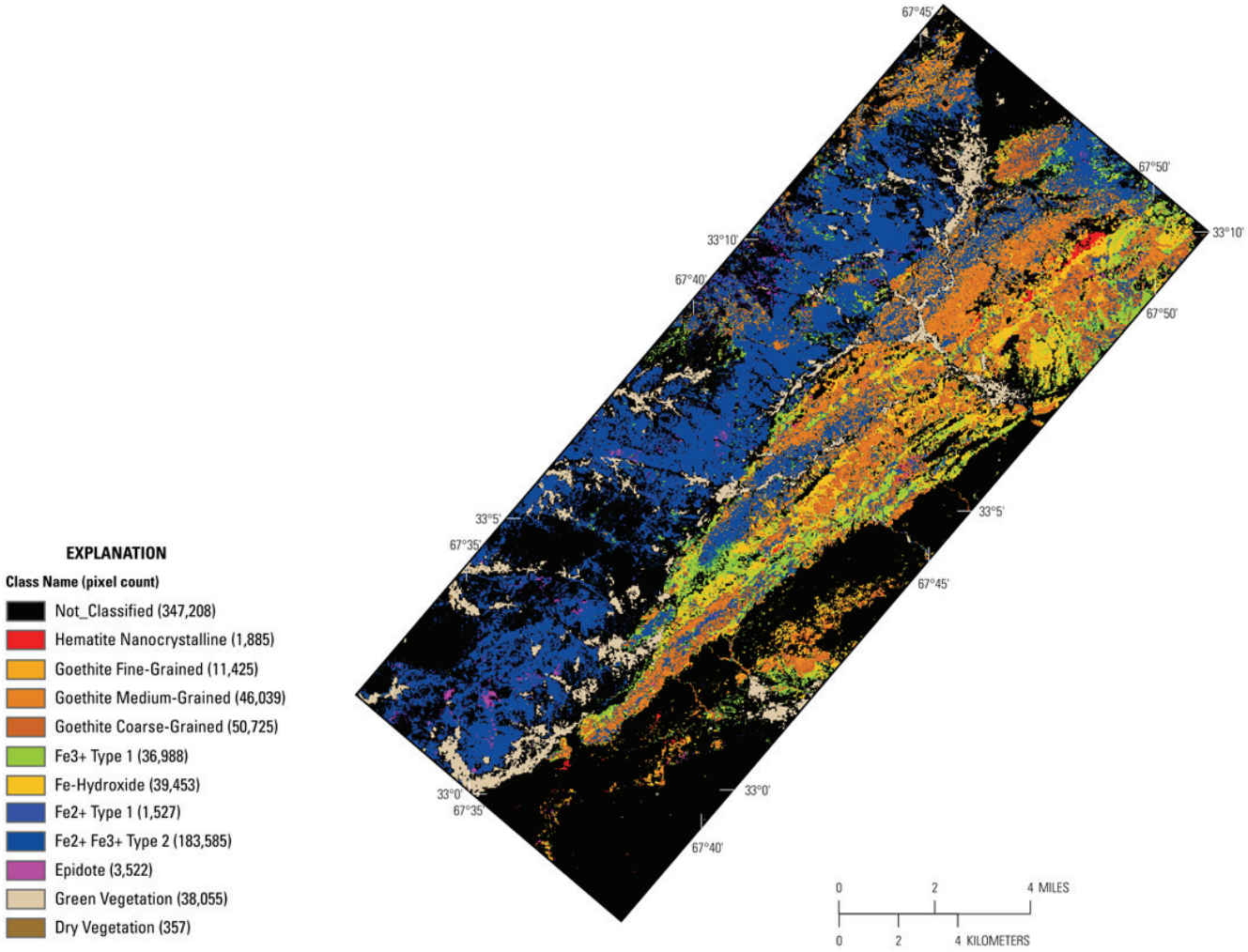

Figure 15B–28. Map showing iron-bearing and other alteration minerals detected in the HyMap data of the Luman Tamaki subarea.

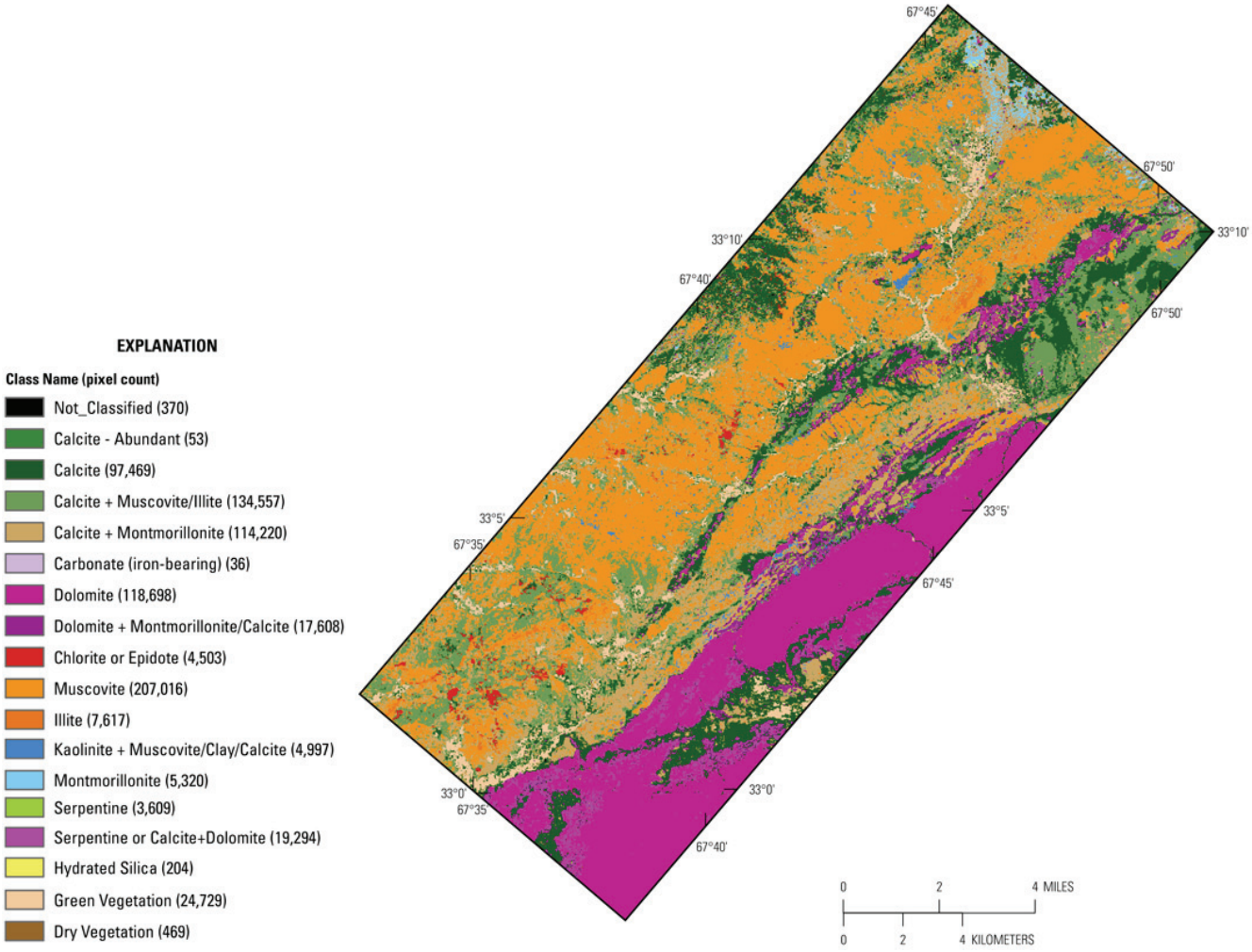

Figure 15B–29. Map showing the distribution of clays, carbonates, phyllosilicates, sulfates, and other alteration minerals in the Luman Tamaki subarea based on the HyMap data.

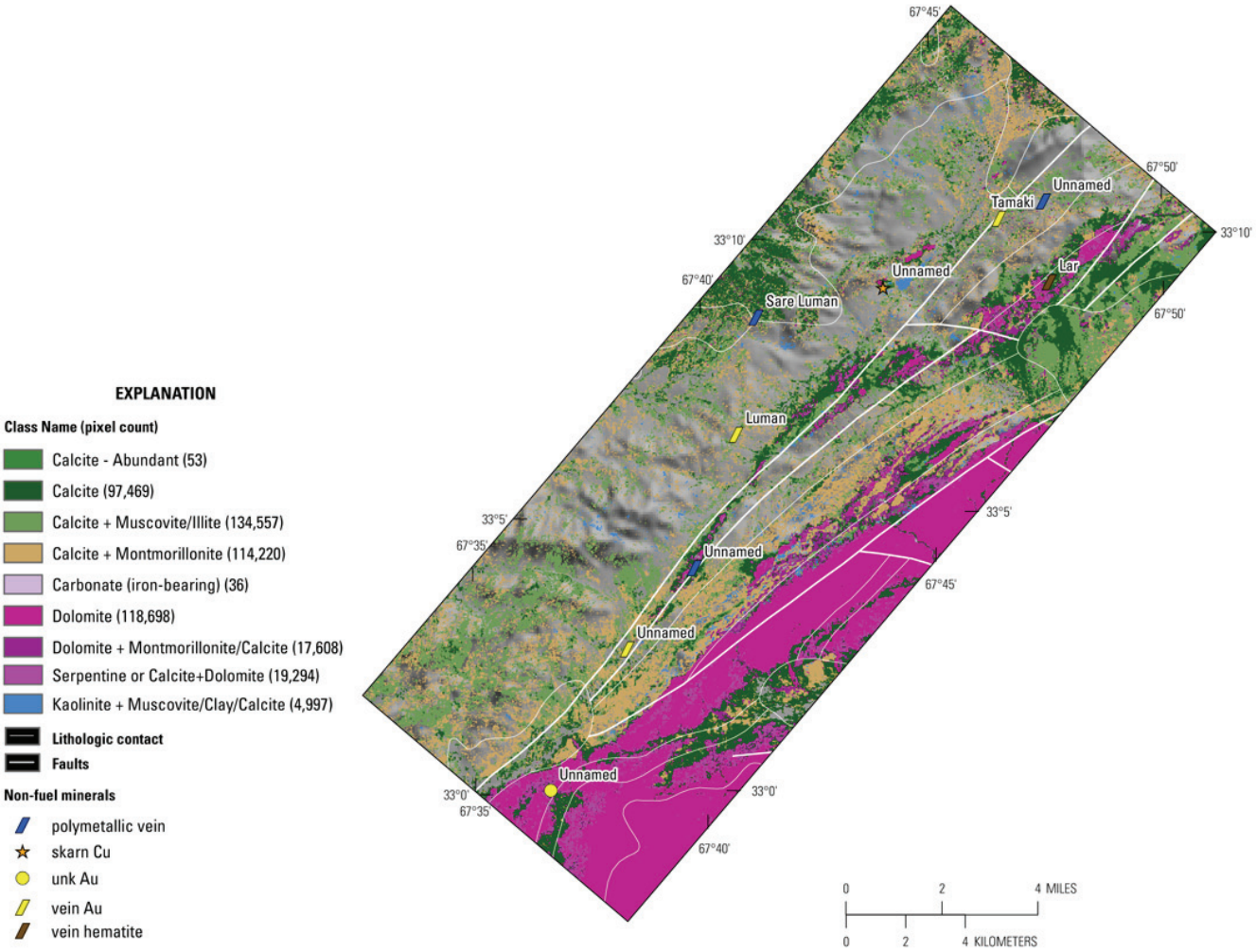

Figure 15B–30. Map showing the distribution of carbonate-bearing minerals in Luman Tamaki subarea detected in the HyMap data. unk, unknown.

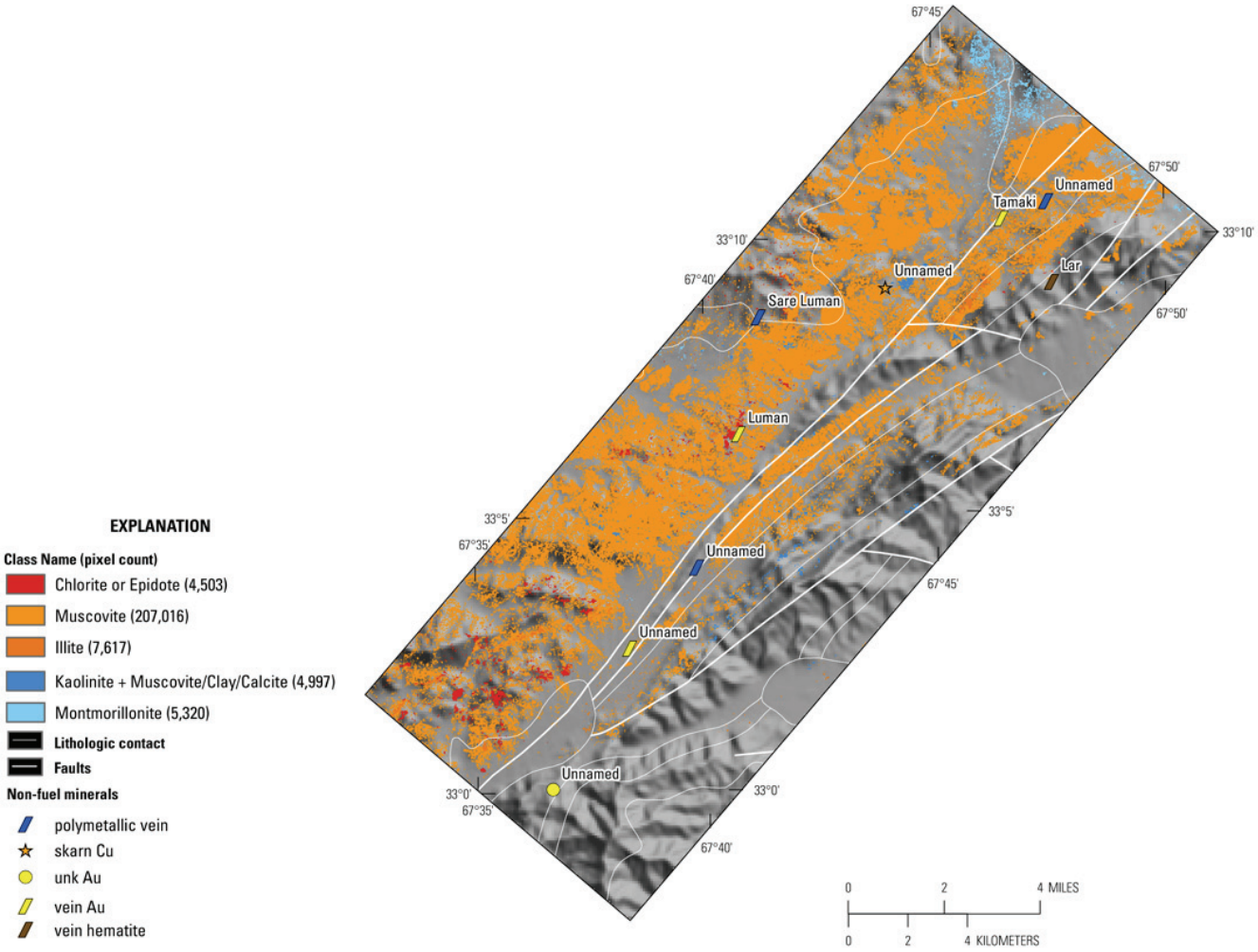

Figure 15B–31. Map showing distribution of clays and micas in the Luman Tamaki subarea based on HyMap data. unk, unknown.

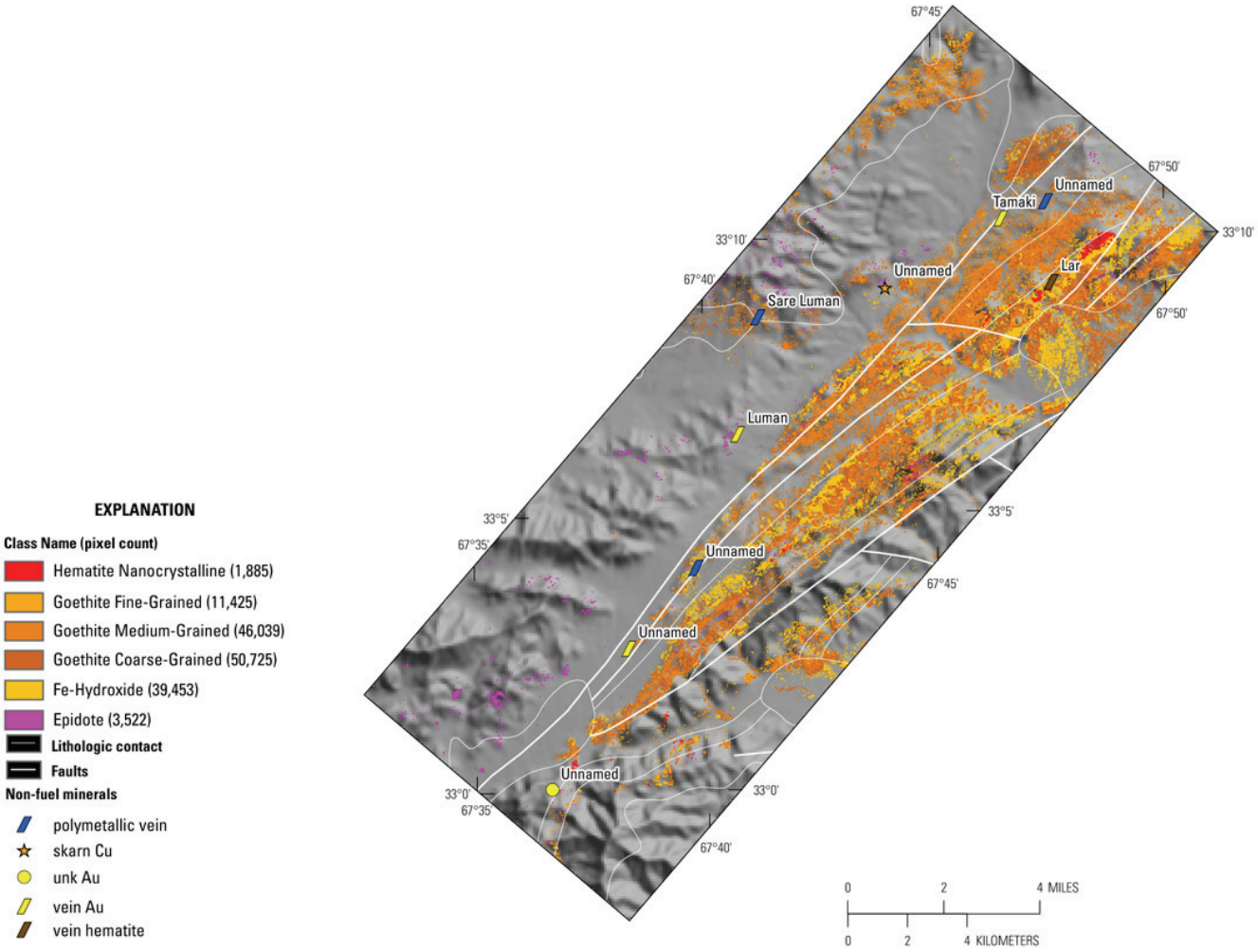

Figure 15B–32. Map showing the distribution of Fe-hydroxides and oxides in the Luman Tamaki subarea based on HyMap data. unk, unknown.

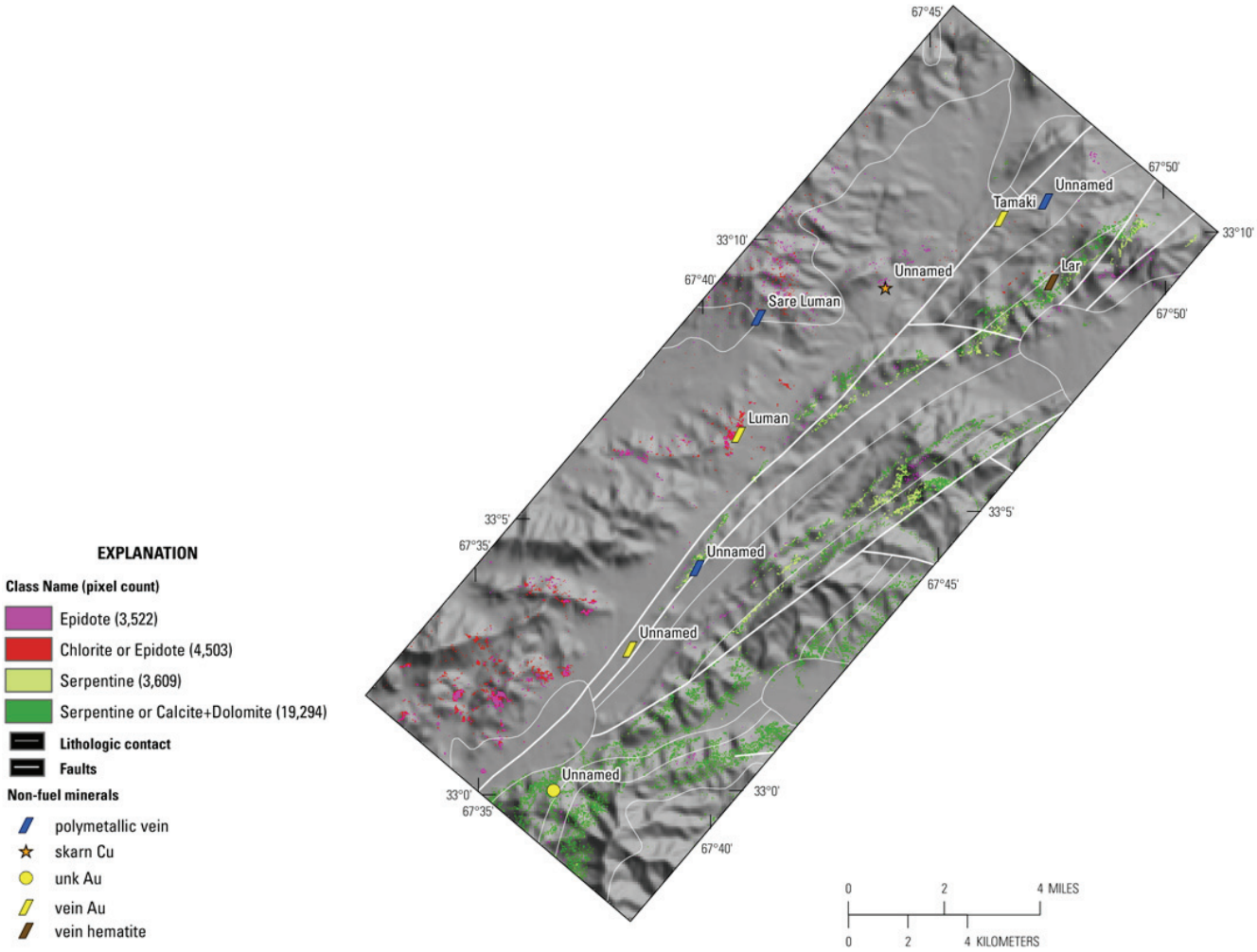

Figure 15B–33. Map showing the occurrence and distribution of common secondary minerals detected in the HyMap data for the Luman Tamaki subarea. unk, unknown.

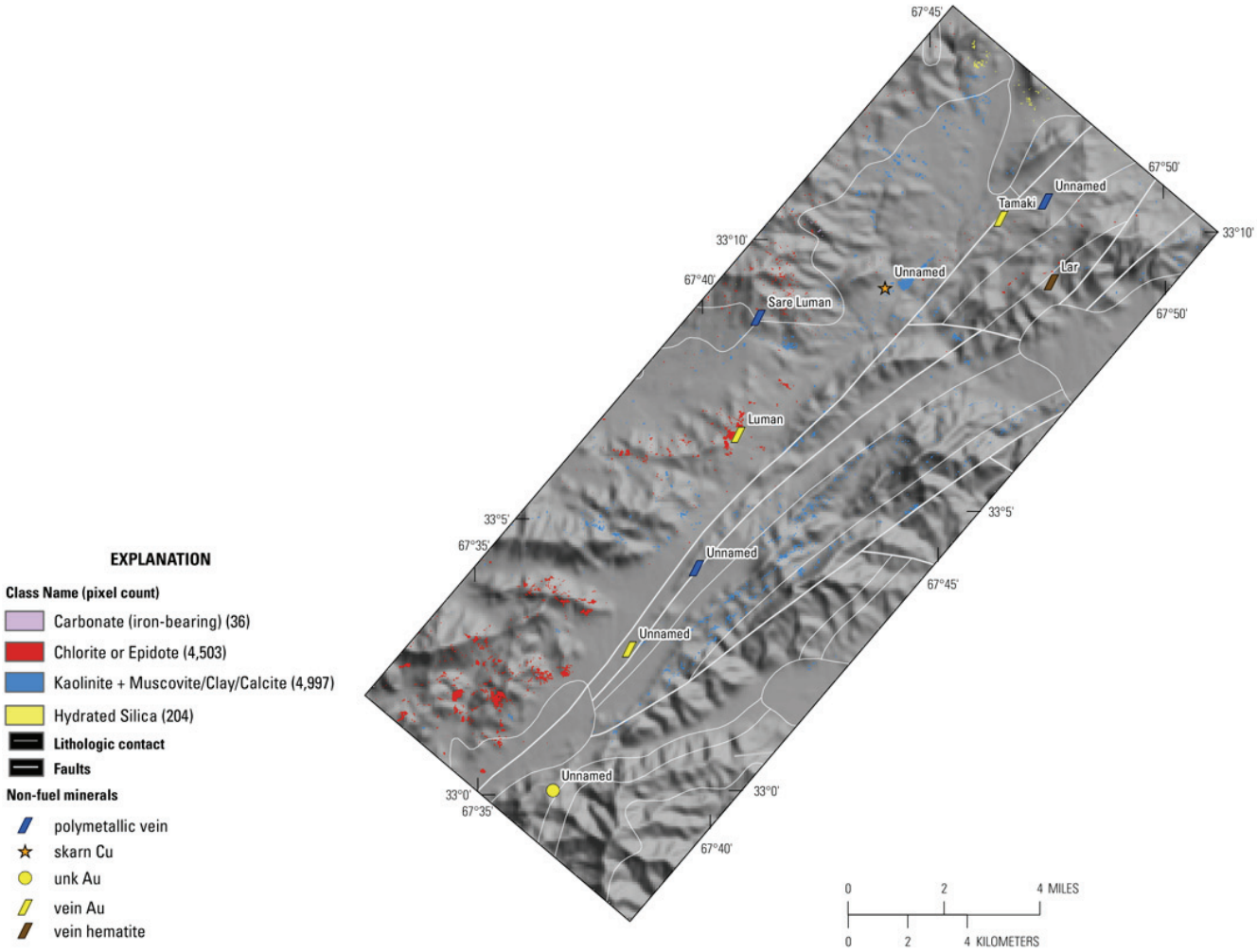

Figure 15B–34. Map showing common alteration materials detected in the HyMap data for the Luman Tamaki subarea. unk, unknown.

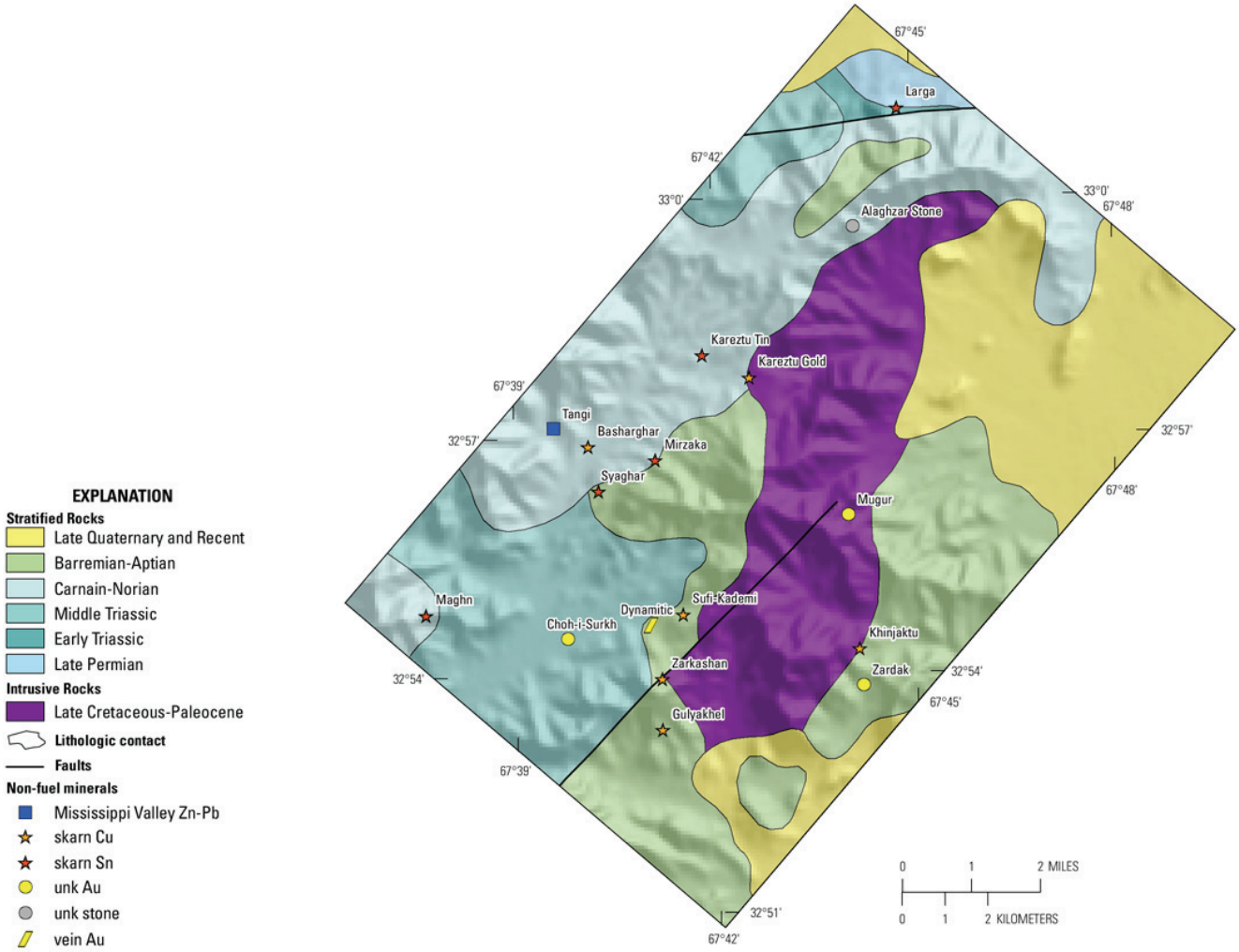

Figure 15B–35. Map showing the known mineral prospects in the Zarkashan mine subarea (Abdullah and Chmyriov, 1977, Doebrich and others, 2006, Peters and others, 2007). unk, unknown.

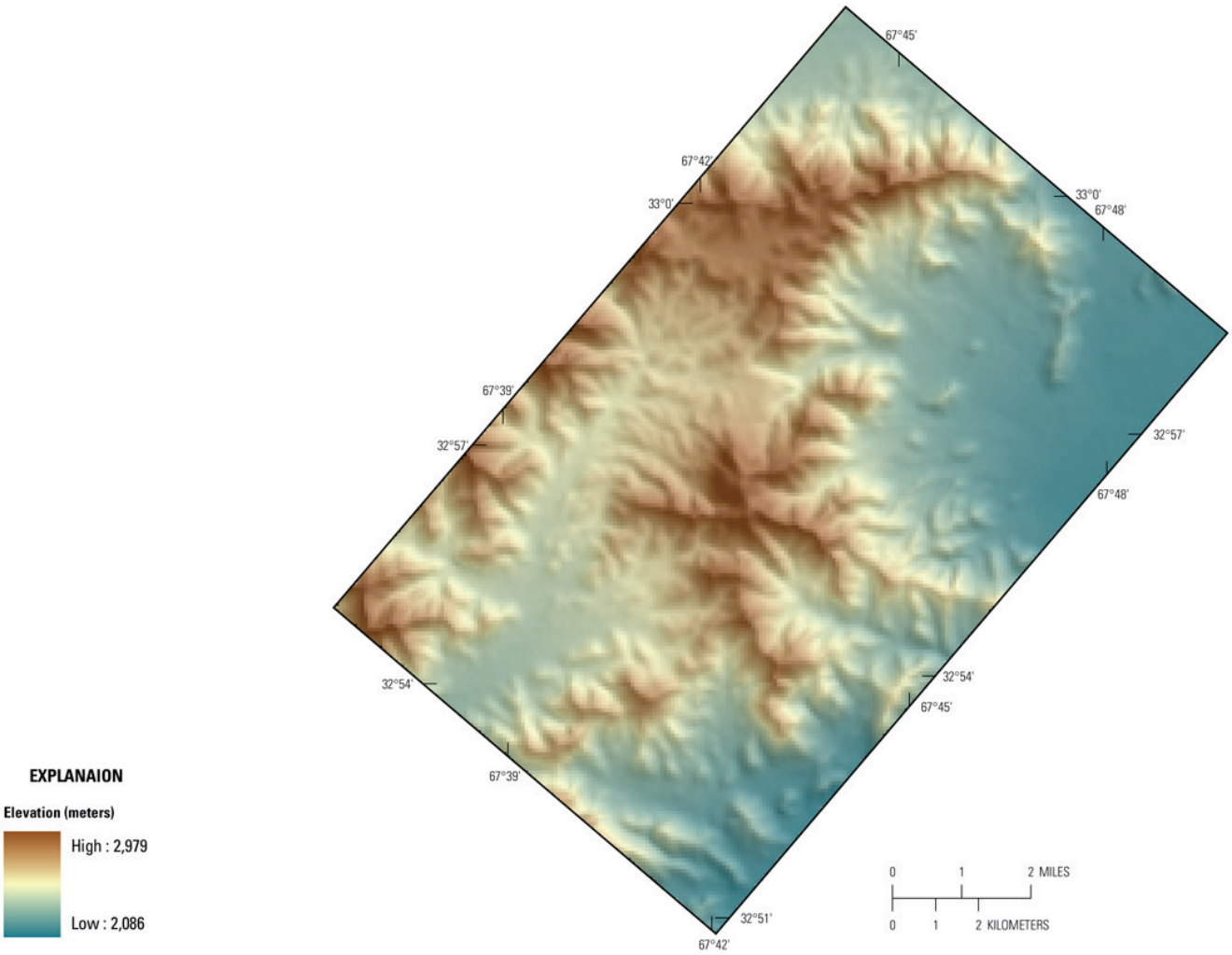

Figure 15B–36. Shaded relief map showing elevations (semi-transparent geologic map overlain on a shaded relief image) in the Zarkashan mine subarea. Dark brown shading indicates higher elevations and blue shading indicates lower elevations.

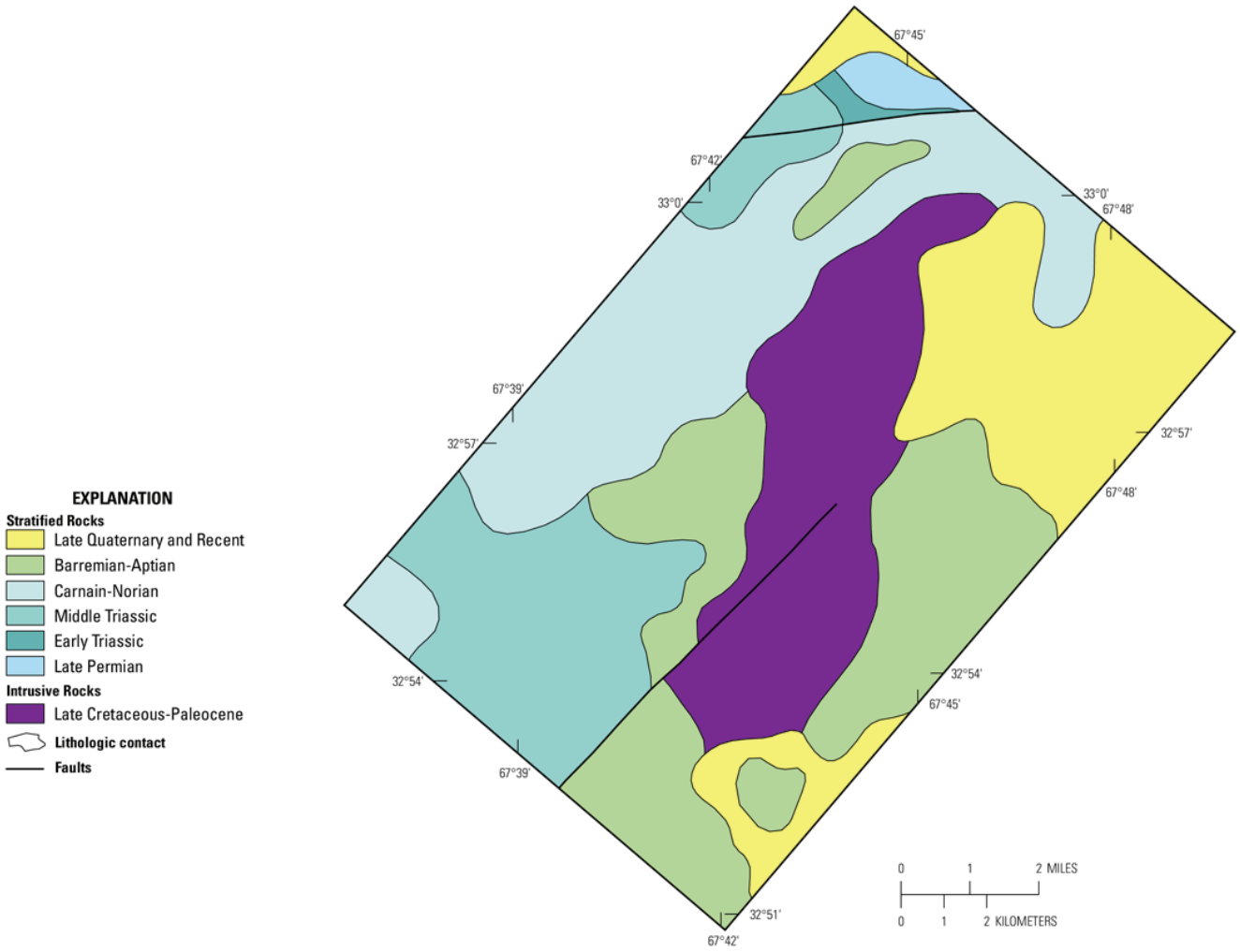

Figure 15B–37. Geologic map of the Zarkashan mine subarea from the digital geologic map of Afghanistan (Abdullah and others, 1977; Doebrich and others, 2006, Peters and others, 2007).

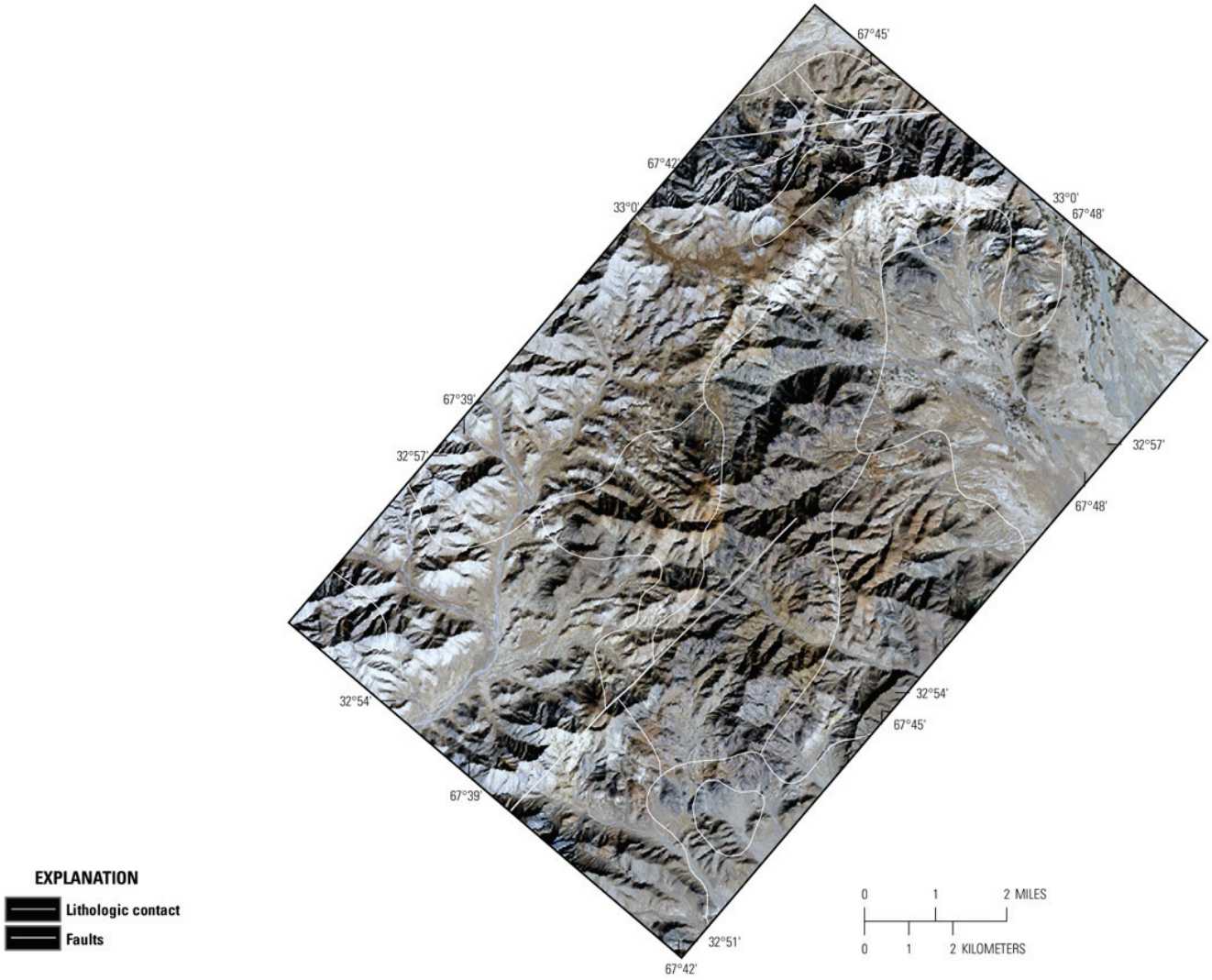

Figure 15B–38. Faults in the Zarkashan mine subarea (from Abdullah and Chmyriov, 1977, and Doebrich and others, 2006) superimposed on Landsat Enhanced Thematic Mapper (TM) data from Davis (2007).

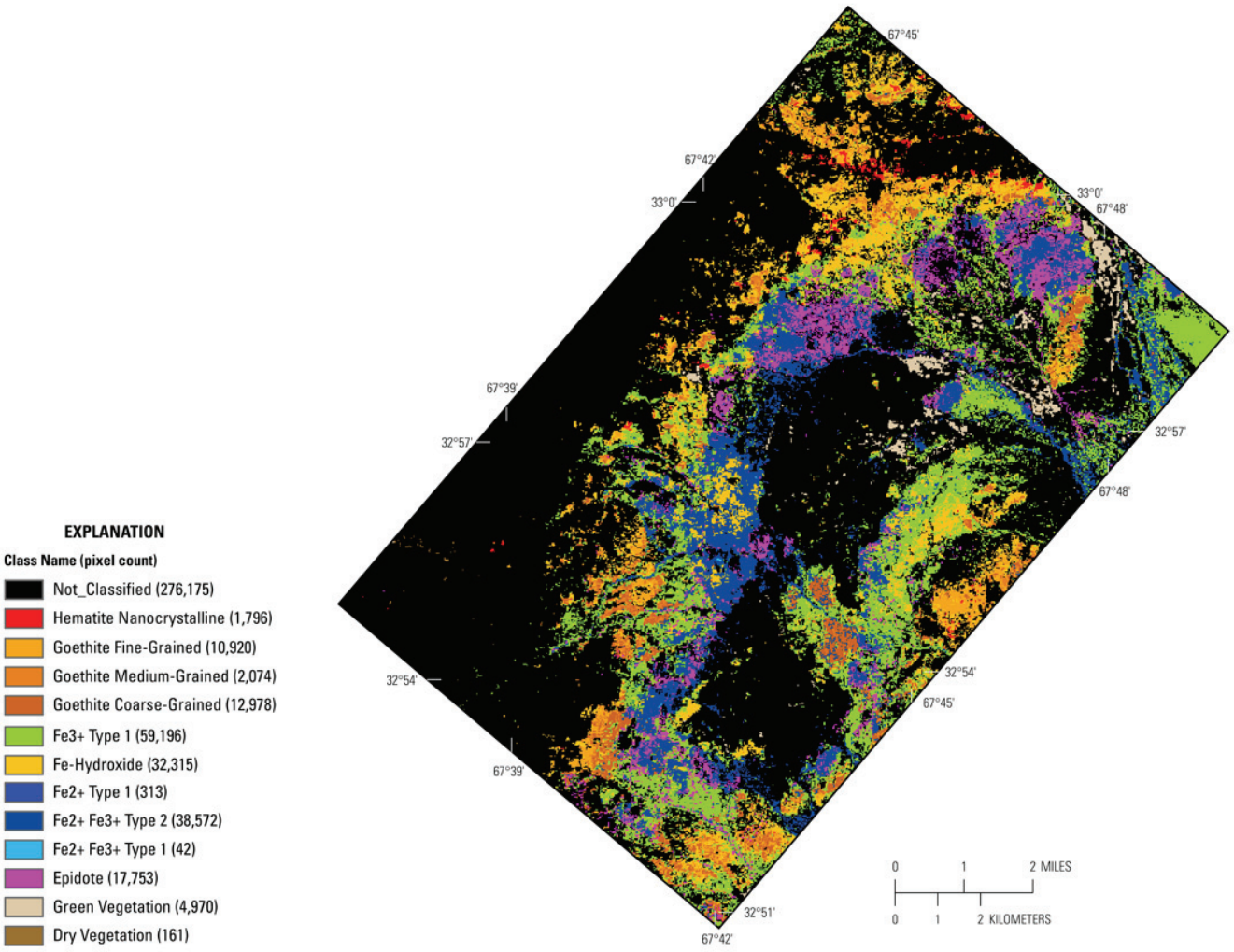

Figure 15B–39. Map showng iron-bearing and other alteration minerals detected in the HyMap data for the Zarkashan mine subarea.

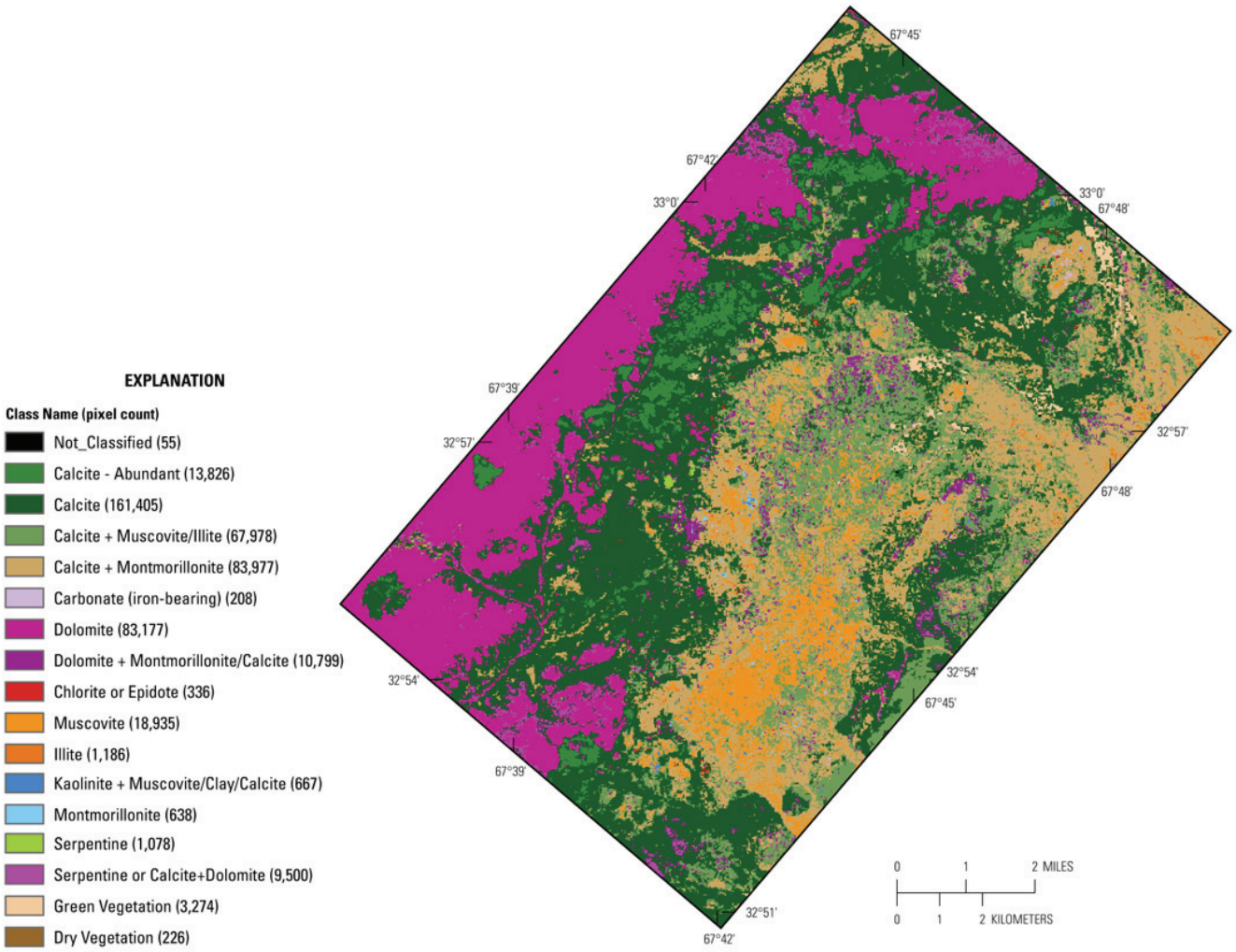

Figure 15B–40. Map showing the distribution of clays, carbonates, phyllosilicates, sulfates, and other alteration minerals in the Zarkashan mine subarea based on the HyMap data.

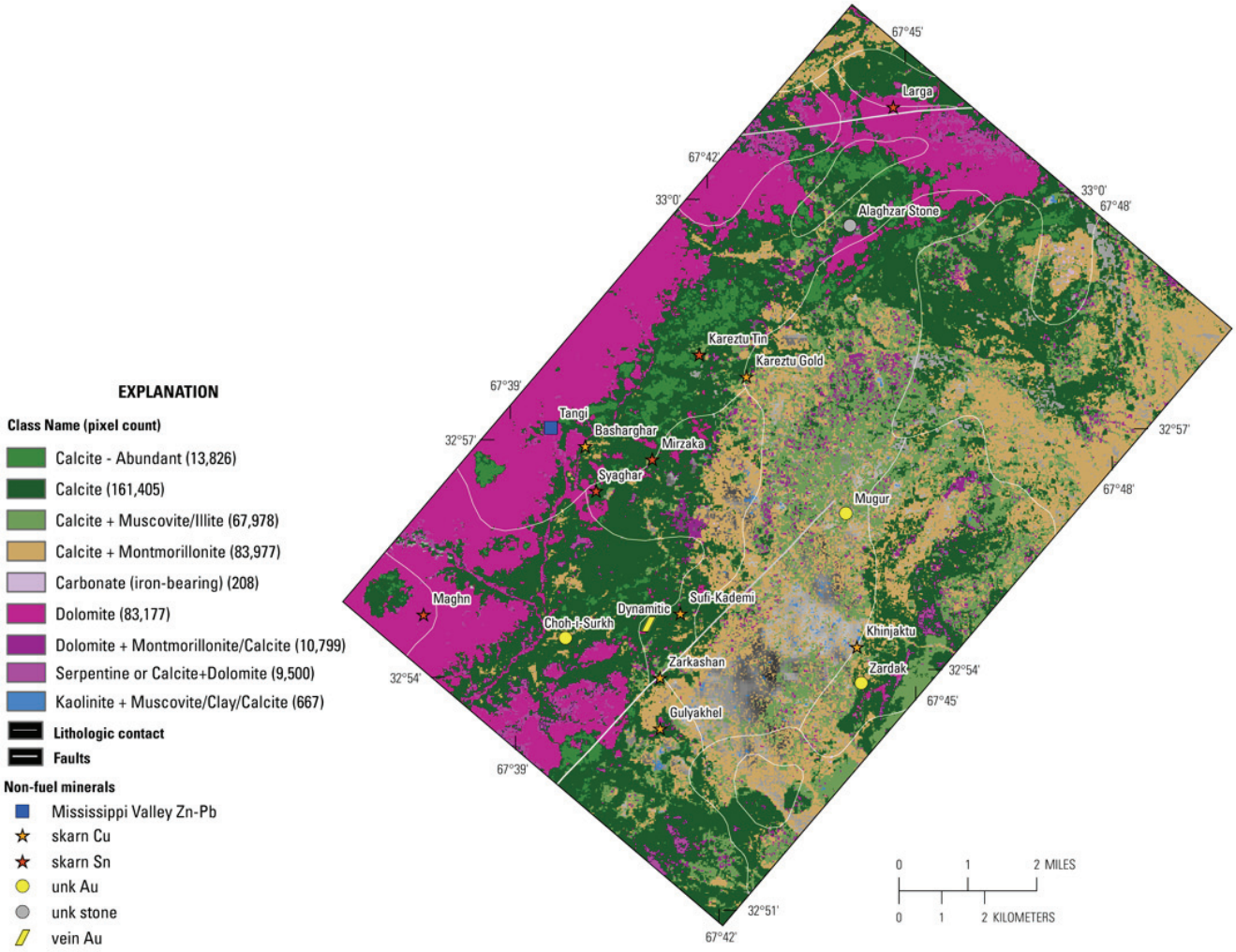

Figure 15B–41. Map showing the distribution of carbonate-bearing minerals in Zarkashan mine subarea based on the HyMap data. unk, unknown.

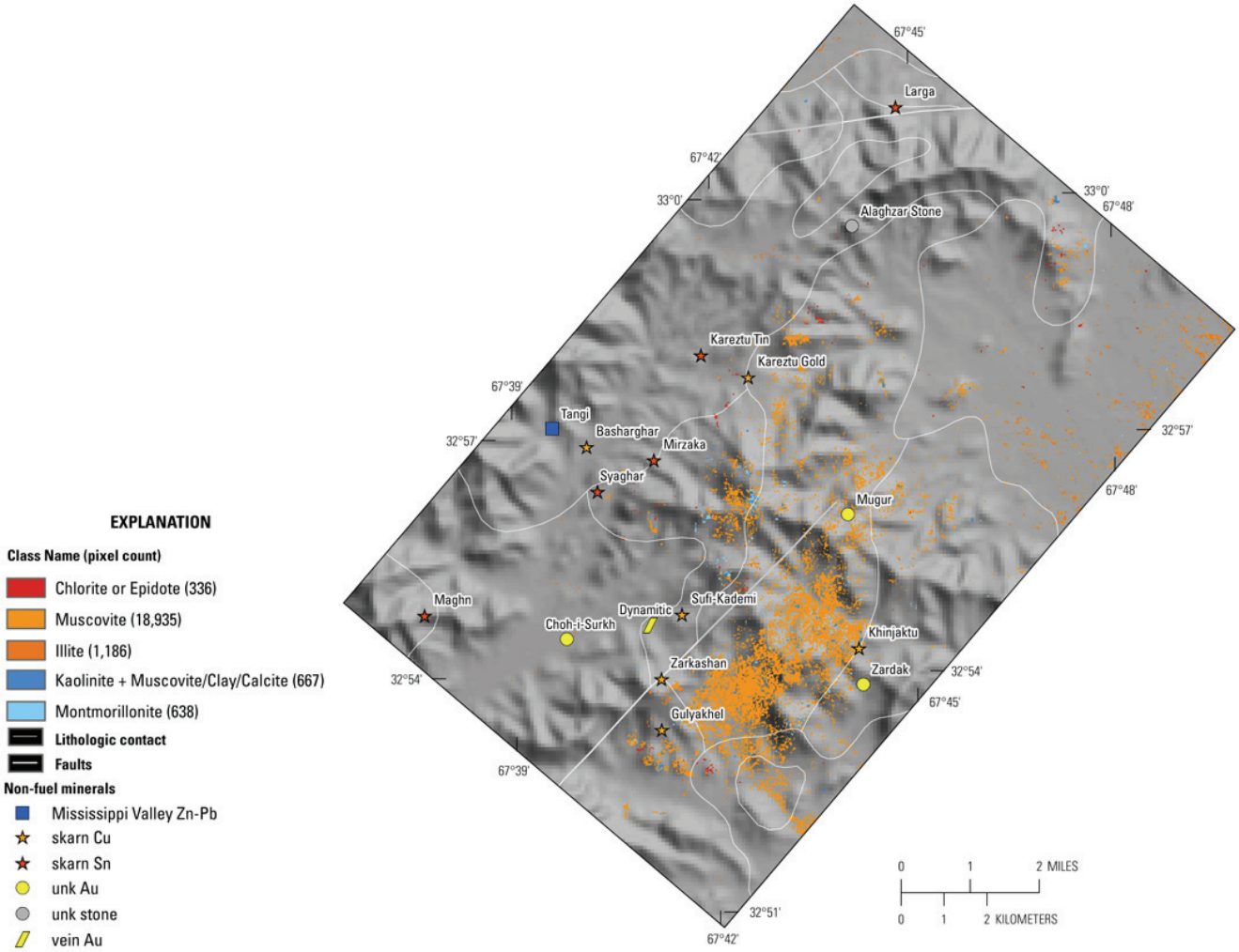

Figure 15B–42. Map showing the distribution of clays and micas in the Zarkashan mine subarea based on the the HyMap data. unk, unknown.

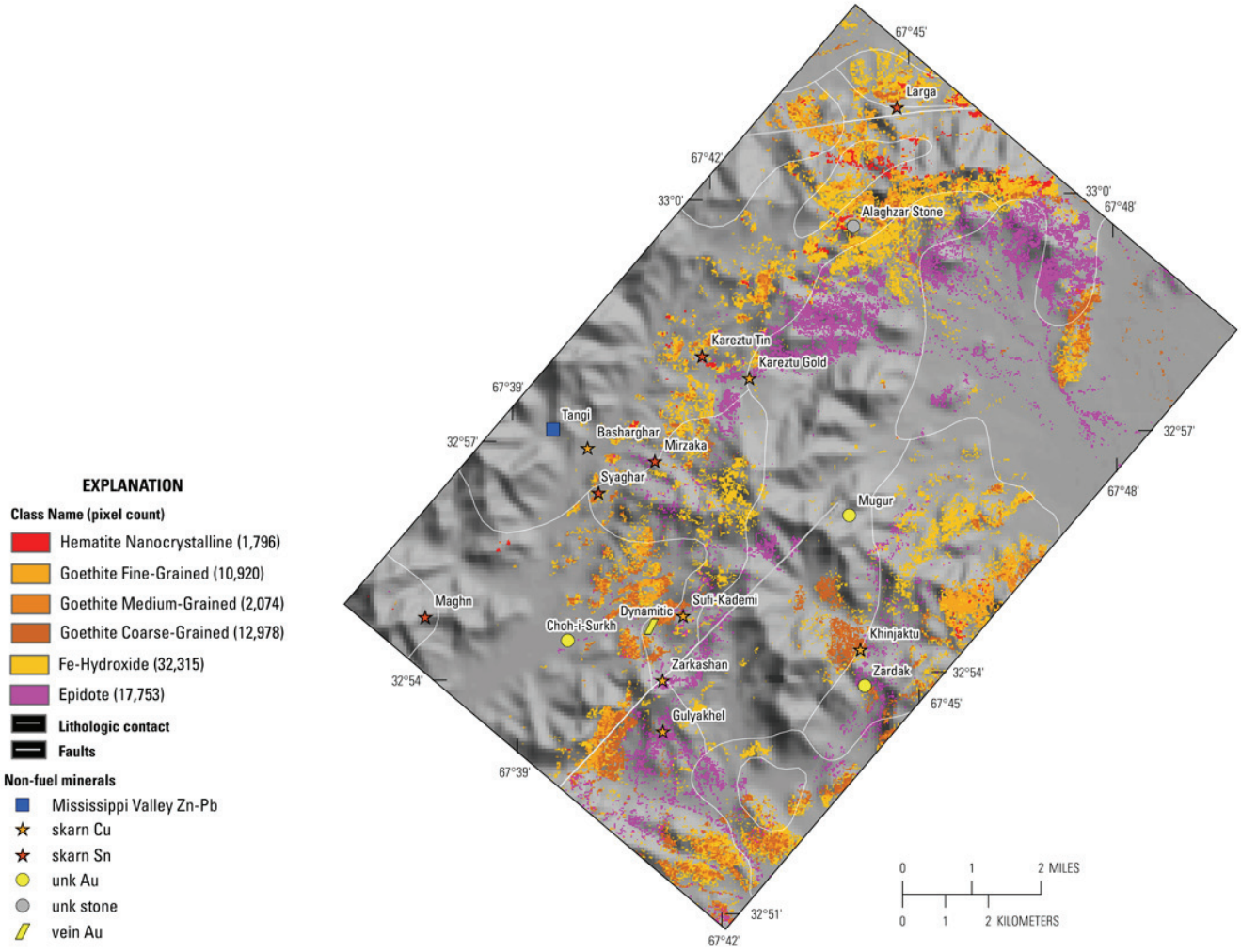

Figure 15B–43. Map showing the distribution of Fe-hydroxides and oxides in the Zarkashan mine subarea based on the HyMap data. unk, unknown.

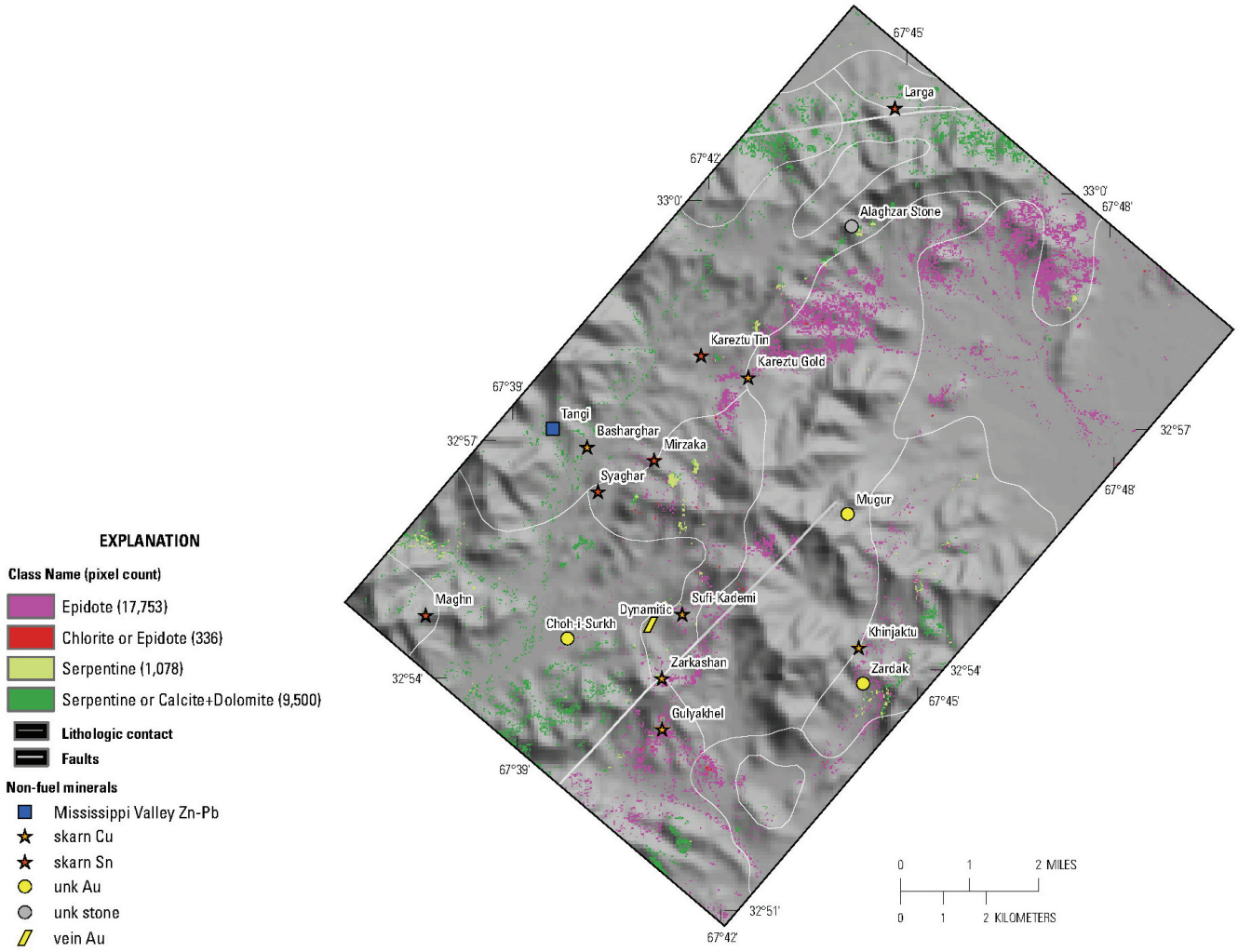

Figure 15B–44. Image showing the occurrence and distribution of common secondary minerals detected in the HyMap data for the Zarkashan mine subarea. unk, unknown.

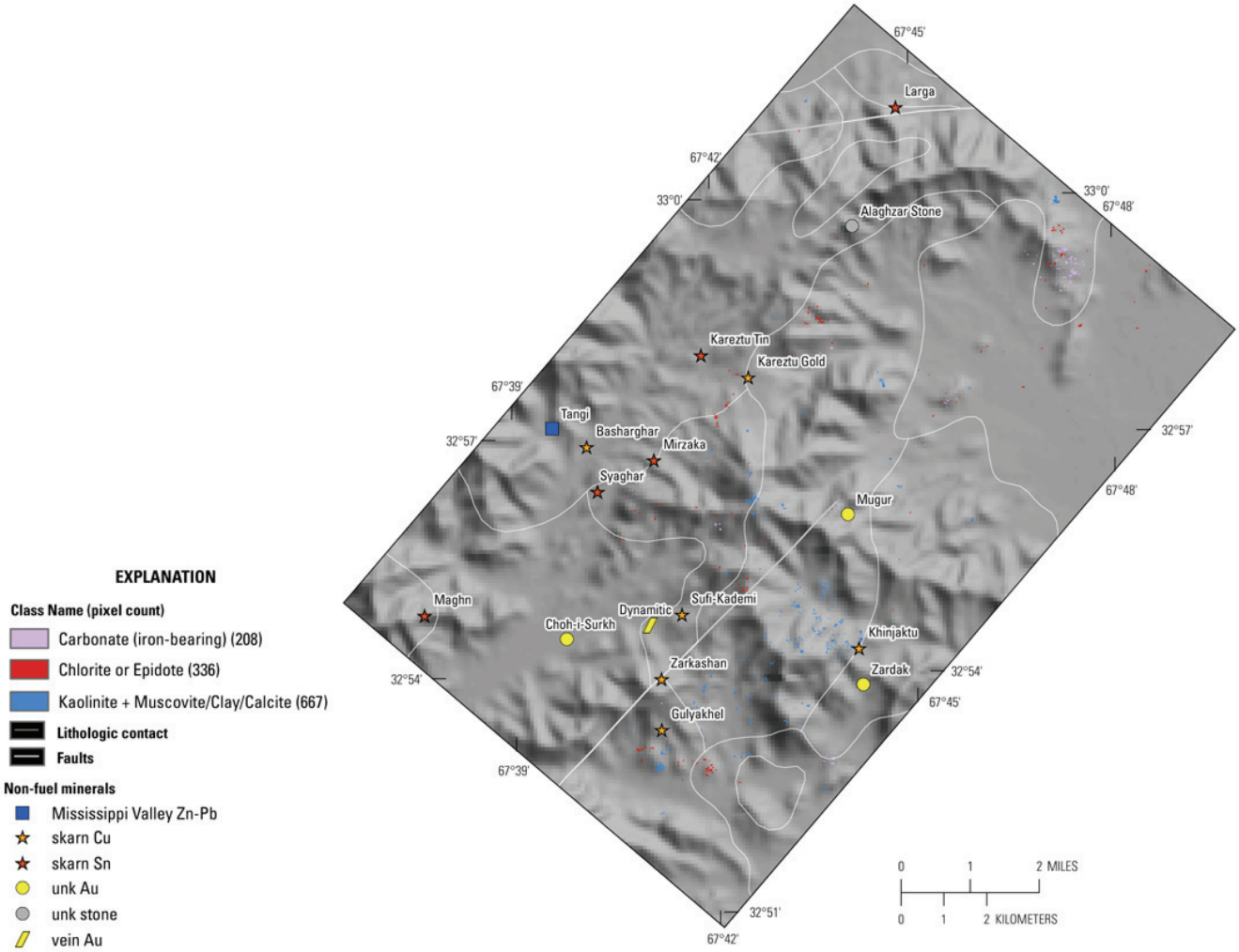

Figure 15B–45. Common alteration materials detected in the HyMap data in the Zarkashan mine subarea. unk, unknown.

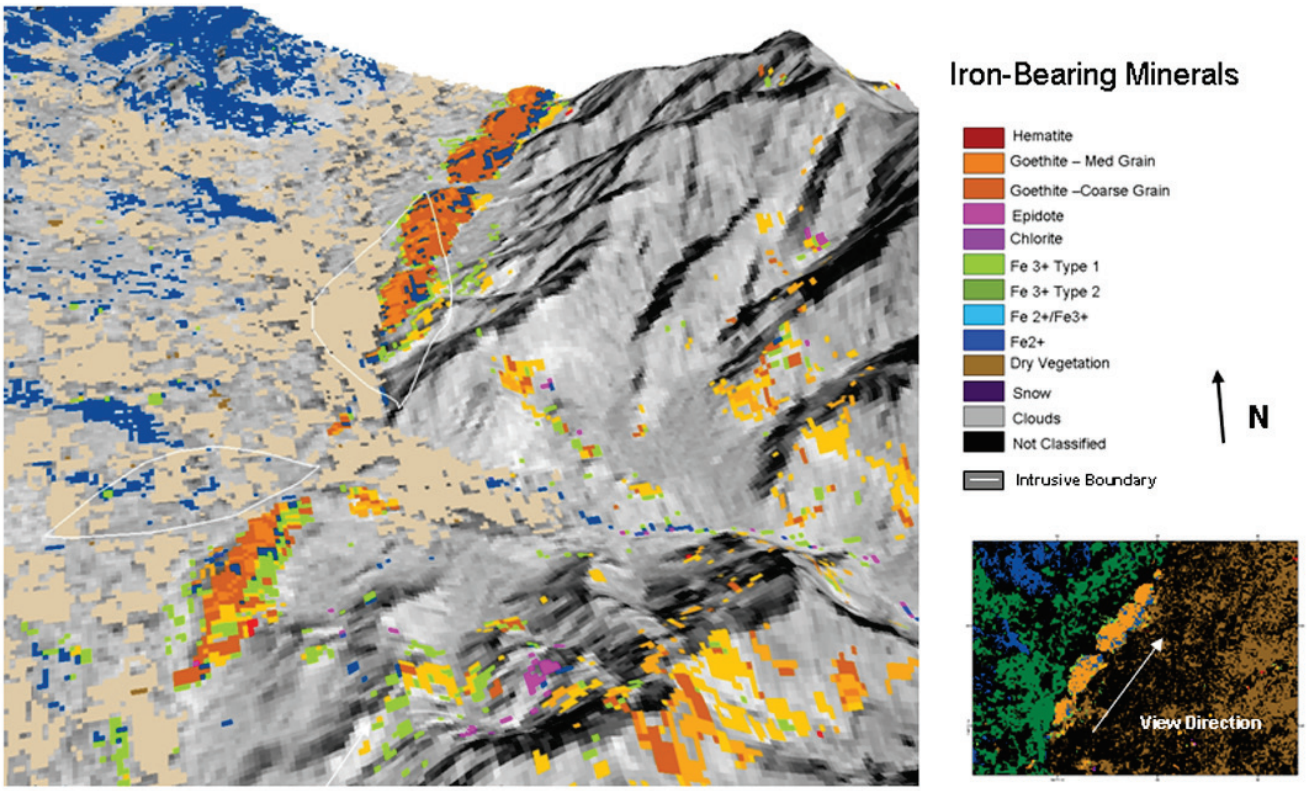

Figure 15B–46. Three-dimensional view of the Bolo subarea created using a portion of figures 15B–6 and 15B–17 overlain on a Digital Elevation Model (DEM). Arrow shows the direction of the view relative to the map view images.

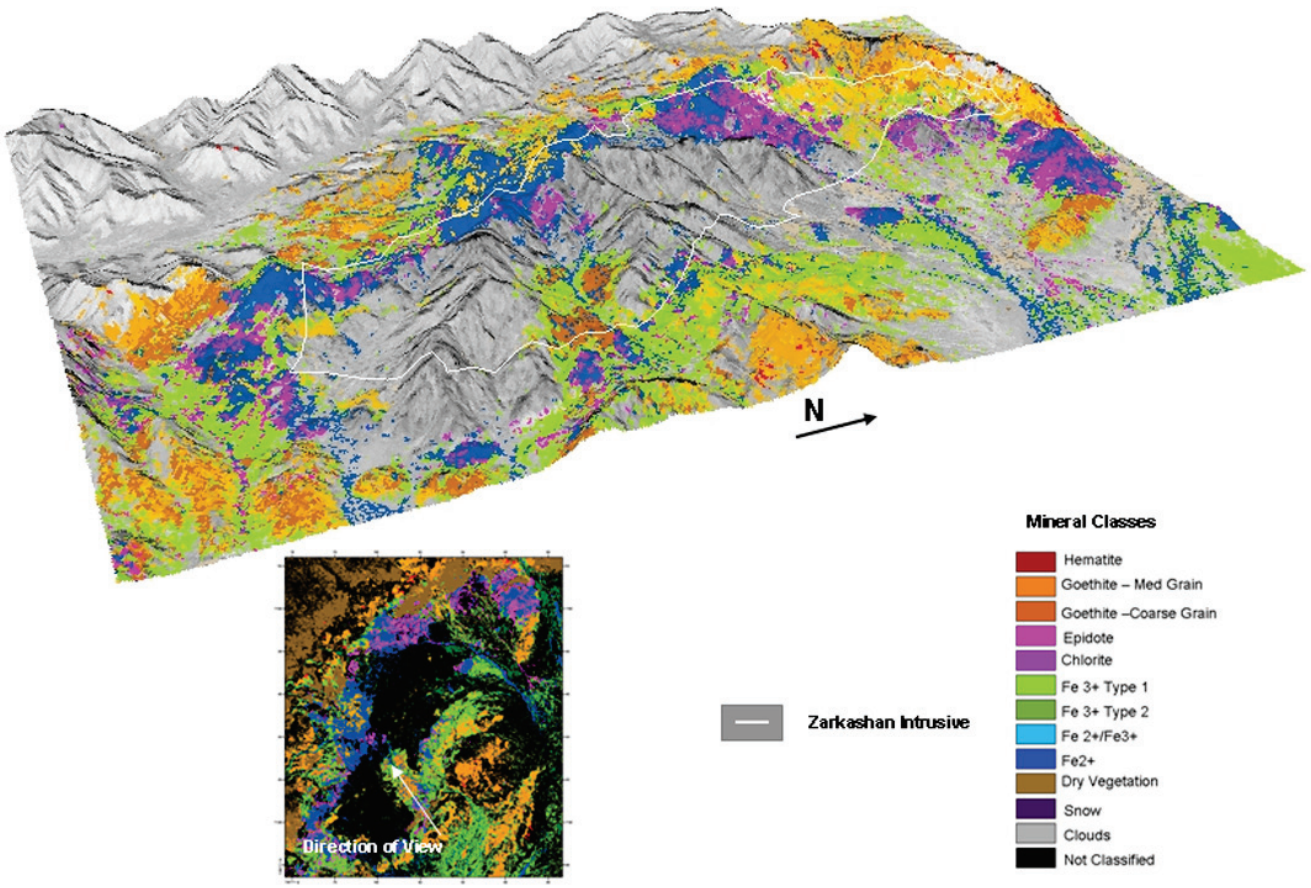

Figure 15B–47. Three-dimensional view of the Zarkashan mine subarea created using a portion of figures 15B–6 and 15B–39 overlain on a Digital Elevation Model (DEM). Arrow shows the direction of view relative to the map view images.

15B.5 References Cited

Abdullah, Sh., and Chmyriov, V.M., 1977, Geological map of Afghanistan: Kabul, Afghanistan, Ministry of Mining and Industry of Democratic Republic of Afghanistan, scale 1:500,000.

Abdullah, Sh., Chmyriov, V.M., Stazhilo-Alekseev, K.F., Dronov, V.I., Gannan, P.J., Rossovskiy, L.N., Kafarskiy, A.Kh., and Malyarov, E.P., 1977, Mineral resources of Afghanistan (2d ed.): Kabul, Afghanistan, Republic of Afghanistan Geological and Mineral Survey, 419 p.

Cocks, T., Jenssen, R., Stewart, A., Wilson, I., and Shields, T., 1998, The HyMap airborne hyperspectral sensor—The system, calibration and performance, *in* Schaepman, M., Schlapfer, D., and Itten, K.I., eds., Proceedings of the 1st EARSeL Workshop on Imaging Spectroscopy, 6–8 October 1998, Zurich: Paris, European Association of Remote Sensing Laboratories, p. 37–43.

Davis, P.A., 2007, Landsat ETM+ false-color image mosaics of Afghanistan: U.S. Geological Survey Open-File Report 2007–1029, 22 p. (Also available at *http://pubs.usgs.gov/of/2007/1029/*.)

Doebrich, J.L., and Wahl, R.R., comps., *with contributions by* Doebrich, J.L., Wahl, R.R., Ludington, S.D., Chirico, P.G., Wandrey, C.J., Bohannon, R.G., Orris, G.J., Bliss, J.D., Wasy, Abdul, and Younusi, M.O., 2006, Geologic and mineral resource map of Afghanistan: U.S. Geological Survey Open File Report 2006–1038, scale 1:850,000, available at *http://pubs.er.usgs.gov/usgspubs/ofr/ofr2005103*.

Doebrich, J.L., and Wahl, R.R., comps., *with contributions by* Doebrich, J.L., Wahl, R.R., Ludington, S.D., Chirico, P.G., Wandrey, C.J., Bohannon, R.G., Orris, G.J., Bliss, J.D., and ____, 2006, Geologic and mineral resource map of Afghanistan: U.S. Geological Survey Open File Report 2006–1038, scale 1:850,000, available at *http://pubs.er.usgs.gov/usgspubs/ofr/ofr2005103*.

Dronov, V.I., Kalimulin, S.M., Sborshchikov, I.M., Svezhentsov, V.P., Chistyakov, A.N., Zelensky, E.D., and Cherepov, P.G., 1972, The geology and minerals of North Afghanistan (parts of map sheets 400-II and 500-I, the Kaysar-Hari Rod Interfluve area): [Afghanistan] Department of Geological and Mineral Survey, 44 p.

Hoefen, T.M., Kokaly, R.F., and King, T.V.V., 2010, Calibration of HyMap data covering the country of Afghanistan, *in* Proceedings of the 15th Australasian Remote Sensing and Photogrammetry Conference, Alice Springs, Australia, September 12–17, 2010, p. 409, available at *http://dl.dropbox.com/u/81114/15ARSPC-Proceedings.zip/*.

King, T.V.V., Johnson, M.R., Hoefen, T.M., Kokaly, R.F., and Livo, K.E., 2011, Mapping potential mineral resource anomalies using HyMap data, *in* King, T.V.V., Johnson, M.R., Hubbard, B.E., and Drenth, B.J., eds, Identification of mineral resources in Afghanistan—Detecting and mapping resource anomalies in prioritized areas using geophysical and remote sensing (ASTER and HyMap) data in Afghanistan: U.S. Geological Survey Open-File Report 2011–1229, available at *http://pubs.usgs.gov/of/2011/1229/*.

King, T.V.V., Kokaly, R.F., Hoefen, T.M., and Knepper, D.H., 2010, Resource mapping in Afghanistan using HyMap data: Proceedings 15th Australasian Remote Sensing and Photogrammetry Conference, Alice Springs, Australia, September 12–17, 2010, p. 500.

King, T.V.V., Kokaly, R.F., Hoefen, T.M., Dudek, K. and Livo, K.E., 2011, Surface materials map of Afghanistan—Iron-bearing minerals and other materials: U.S. Geological Survey Scientific Investigations Map 3152–B.

Kokaly, Ray, 2011, PRISM—Processing routines in IDL for spectroscopic measurements: U.S. Geological Survey Open-File Report 2011–1155, available at *http://pubs.usgs.gov/of/2011/1155/*.

Kokaly, R.F., King, T.V.V., and Livo, K.E., 2008, Airborne hyperspectral survey of Afghanistan 2007: Flight line planning and HyMap data collection, U.S. Geological Survey Open-File Report 2008–1235, 14 p.

Kokaly, R.F., King, T.V.V., Hoefen, T.M., Dudek, K. and Livo, K.E., 2011, Surface materials map of Afghanistan—Carbonates, phyllosilicates, sulfates, altered minerals, and other materials: U.S. Geological Survey Scientific Investigations Map 3152–A.

Mars, J.C., and Rowan, L.C., 2007, Mapping phyllic and argillic-altered rocks in southeastern Afghanistan using advanced spaceborne thermal emission and reflection radiometer (ASTER) data: U.S. Geological Survey Open-File Report 2007–1006, available at *http://pubs.usgs.gov/of/2007/1006/*.

Peters, S.G., Ludington, S.D., Orris, G.J., Sutphin, D.M., Bliss, J.D., and Rytuba, J.J., eds., and the U.S. Geological Survey-Afghanistan Ministry of Mines Joint Mineral Resource Assessment Team, 2007, Preliminary non-fuel mineral resource assessment of Afghanistan: U.S. Geological Survey Open-File Report 2007–1214, 810 p., 1 CD–ROM. (Also available at *http://pubs.usgs.gov/of/2007/1214/*.)

Sweeney, R.E., Kucks, R.P, Hill, P.L., and Finn, C.A., 2006, Aeromagnetic and gravity surveys in Afghanistan—A web site for distribution of data: U.S. Geological Survey Open-File Report 2006–1204, available at *http://pubs.usgs.gov/of/2006/1204/*.